

**UCSF**

**UC San Francisco Electronic Theses and Dissertations**

**Title**

Activation of Specific Apoptotic Caspases with an Engineered Small Molecule-Activated Protease

**Permalink**

<https://escholarship.org/uc/item/1x67310m>

**Author**

Gray, Daniel Christopher

**Publication Date**

2011

Peer reviewed|Thesis/dissertation

**Activation of Specific Apoptotic Caspases with an Engineered Small-Molecule-Activated  
Protease**

by

**Daniel C. Gray**

DISSERTATION

Submitted in partial satisfaction of the requirements for the degree of

DOCTOR OF PHILOSOPHY

in

Chemistry and Chemical Biology

in the

GRADUATE DIVISION

of the

UNIVERSITY OF CALIFORNIA, SAN FRANCISCO

**Copyright 2011  
by  
Daniel C. Gray**

## Acknowledgements

To quote Hillary Clinton and Dr. Charles Craik, founder and head of the Chemistry and Chemical Biology Graduate Group at UCSF, “it takes a village.” First, I thank Dr. James Wells – my mentor, boss and now friend – for inspiring the work that follows in this dissertation. I am honored to have studied and worked in his laboratory for the past four years. I also thank my thesis committee, Dr. Kevan Shokat, Dr. Jonathan Weissman, and Dr. Martin McMahon for their expert advice. Christine Olson and Marja Tarr, my graduate school ‘moms’, always went out of their way to keep me on time, paid and enrolled, and for that (and more) I am grateful. I thank the members of the Wells’ lab, both past and present, and I am especially indebted to Dr. Dennis Wolan, Dr. Sami Mahrus, Julie Zorn and Charles Morgan for their help and collegiality over the years. Big thanks to Andy, Chad and Matt for their patient friendship, help and endless fun.

Most importantly, I dedicate this work to my parents Donna and Christopher and my sister Caitlin. Their endless sacrifice and love make my world go round.

## Chapter Specific Acknowledgements

All of the work herein was conducted under the guidance of Dr. James Wells, and additional contributions are as follows. In section 1.5, I describe my supporting contribution to the following paper: Wolan, D. W., J.A. Zorn, et al. (2009). Small-molecule activators of a proenzyme. *Science*. 326: 853-858. Dr. Dennis Wolan was the first author of this paper, and he is responsible for the majority of the work. Chapter 3 was previously published: Gray, D. C., S. Mahrus, et al. (2010). Activation of specific apoptotic caspases with an engineered small-molecule-activated protease. *Cell*. 142: 637-646. Dr. Sami Mahrus provide the degradomics data demonstrating extensive caspase-mediated processing of the 26S proteasome. Chapter 4 is unpublished. Charles Morgan provided the immunoblotting data for Figure 8 and continues the project independently.

# Activation of Specific Apoptotic Caspases with an Engineered Small Molecule-Activated Protease

Daniel C. Gray

## Abstract

Apoptosis is a conserved cellular pathway that results in the activation of cysteine-aspartyl proteases, or caspases. To dissect the non-redundant roles of the executioner caspases-3, -6 and -7 in orchestrating apoptosis, we have developed an orthogonal protease to selectively activate each isoform in human cells. Our approach uses a split-Tobacco Etch Virus (TEV) protease under small-molecule control, that we call the SNIPer, with caspase alleles containing genetically encoded TEV cleavage sites. These studies reveal that all three caspases are transiently activated but only activation of caspase-3 or -7 is sufficient to induce apoptosis. Proteomic analysis shown here and from others reveals that 20 of the 33 subunits of the 26S proteasome can be cut by caspases, and we demonstrate synergy between proteasome inhibition and dose-dependent caspase activation. We propose a model of proteolytic reciprocal negative regulation with mechanistic implications for the combined clinical use of proteasome inhibitors and proapoptotic drugs.

However, to study *loss of function* proteolysis, we have developed a novel bicistronic viral vector system to knock-in engineered substrates, thus enabling *loss of function* analysis in the cellular context. The targeting vector comprises a microRNA (miRNA) expression cassette directed against the endogenous substrate locus. In this case, we express an engineered caspase substrate with a

miRNA directed against the endogenous copy of the substrate of interest.

Therefore, co-expression of both cassettes on the same transcript results in **(A)** the miRNA-mediated knockdown of the endogenous caspase substrate and **(B)** knock-in of an engineered variant that is susceptible to cleavage by split-TEV, which enables functional analysis of site-specific caspase proteolysis one substrate at a time. This rapid, cell-based engineering of protein alleles we call “Post-Transcriptional Gene Replacement” or *PTGR*.

To faithfully recapitulate ICAD cleavage and CAD activation, PTGR vector technology is applied to replace endogenous ICAD with a TEV-cleavable allele, ICAD-TevS. In principle, this strategy preserves the chaperone function of ICAD, and CAD activation in cells can then be controlled by the SNIPer in a temporal and dose-dependent fashion. Importantly, we induce CAD cleavage in the absence of caspase activation using conventional apoptotic inducers.

## Table of Contents

<b>PRELIMINARY PAGES</b> .....	<b>I</b>
TITLE PAGE .....	I
ACKNOWLEDGEMENTS .....	III
CHAPTER SPECIFIC ACKNOWLEDGEMENTS .....	IV
ABSTRACT .....	V
TABLE OF CONTENTS .....	VII
LIST OF TABLES .....	IX
LIST OF FIGURES .....	X
LIST OF ABBREVIATIONS.....	XI
<b>CHAPTER 1: INTRODUCTION TO CASPASES AND APOPTOSIS</b> .....	<b>1</b>
1.1 INTRODUCTION.....	2
<b>1.2 APOPTOTIC PHENOTYPES AND CASPASE SUBSTRATES</b> .....	<b>3</b>
1.3 CASPASE CLASSIFICATION .....	6
1.4 INTERROGATING THE ROLE OF CASPASES AND THEIR SUBSTRATES IN CELLS .....	8
1.5 <i>Small-Molecule Activators of the Caspases</i> .....	10
1.6 PROTEIN COMPLEMENTATION ASSAY TECHNOLOGY: THE SNIPER .....	12
1.7 NOVEL APPLICATIONS OF THE SNIPER .....	14
1.7.1 <i>Single-cell dynamics of apoptosis</i> .....	14
1.7.2 <i>Probing the role of ATF6 in the UPR</i> .....	16
1.8 REFERENCES.....	23
<b>CHAPTER 2: ACTIVATION OF SPECIFIC APOPTOTIC CASPASES WITH AN ENGINEERED SMALL MOLECULE-ACTIVATED PROTEASE</b> .....	<b>27</b>
2.1 SUMMARY .....	28
2.2 INTRODUCTION.....	29
2.3 RESULTS .....	31
2.3.1 <i>The SNIPer: Design, Optimization, and Characterization in Mammalian Cells</i> .....	31
2.3.2 <i>Engineering Orthogonal Pro-caspase-3 and -7 Alleles for Selective Activation by the SNIPer</i> .....	33
2.3.3 <i>Selective Activation of Orthogonal Pro-caspase-3 and -7 Alleles in Stable Human Cell Lines</i> .....	36
2.3.4 <i>Activated Caspase-3 and -7 are Proteasome Substrates and are Stabilized by a Proteasome Inhibitors</i> .....	38
2.3.5 <i>Activation of Caspase-6 is not Proapoptotic except in Conjunction with Proteasome Inhibition</i> .....	40
2.3.6 <i>Caspases Attack the 26S Proteasome, and Caspase Activation Synergizes with Proteasome Inhibition</i> .....	43
2.4 DISCUSSION.....	46
2.4.1 <i>Design Considerations for SNIPer</i> .....	46
2.4.2 <i>Orthogonal Activation of the Executioner Caspases Reveals Regulation by the UPS</i> .....	47
2.5 EXPERIMENTAL PROCEDURES .....	51
2.5.1 <i>Cell Culture and Transfections</i> .....	51
2.5.2 <i>Phenotypic Analysis of Caspase Activation in Cells</i> .....	51
2.5.3 <i>Vector Construction: the SNIPer, FRET Reporter Plasmids, and Orthogonal Caspase Alleles</i> .....	52
2.5.4 <i>Recombinant Protein Production and Caspase Enzyme Assays</i> .....	54



2.5.5 Immunoblotting and Immunoprecipitation .....	56
2.5.6 Live Cell Imaging of FRET .....	56
2.5.7 Generation of Stable Cell Lines .....	58
2.5.8 Degradomics .....	59
2.6 ACKNOWLEDGEMENTS .....	64
2.7 REFERENCES .....	78
<b>CHAPTER 3: VECTOR SYSTEMS FOR TARGETED GENE REPLACEMENT IN</b>	
<b>CELLS .....</b>	<b>81</b>
3.1 INTRODUCTION.....	82
3.2 RESULTS .....	87
3.2.1 PTGR Vector Design.....	87
3.2.2 miRNA Identification and Intron Characterization .....	88
3.2.3 ICAD TevS-Substrate Engineering and Characterization of PTGR Cell Lines	
.....	90
3.3 DISCUSSION.....	91
3.4 MATERIALS AND METHODS .....	96
3.4.1 Vector Construction (Basic Three-Component Vector System).....	96
3.4.2 Generation of Stable Cell Lines .....	98
3.4.3 Transfection and Fluorescence Microscopy.....	98
3.4.4 Western Blotting.....	99
3.5 REFERENCES.....	110

## List of Tables

Table 2.1: Caspase Substrates of the 26S Proteasome .....	60
Table 2.2 SNIPer DNA Oligonucleotides .....	61
Table 3.1 PTGR DNA Oligonucleotides .....	100

## List of Figures

Figure 1.1. Recent Technology Developments for Apoptosis Research .....	18
Figure 1.2. Caspase Pathways.....	19
Figure 1.3. 1541 activates procaspase-3 and procaspase-6.....	20
Figure 1.4. Genetically-encoded fluorescent reporters for probing single-cell dynamics of apoptosis .....	21
Figure 1.5. SNIPer-mediated cleavage of ATF6.....	22
Figure 2.1. Engineering the SNIPer for Conditional Proteolysis.....	65
Figure 2.2. SNIPer Characterization.....	66
Figure 2.3. Design and In Vitro Characterization of Orthogonal Procaspase-3 and -7 Alleles .....	68
Figure 2.4. In Vitro Characterization of Casp3-TevS Alleles .....	69
Figure 2.5. Phenotypic Analysis of SNIPer-Mediated Activation of Procaspase-3 and -7 in Cells.....	70
Figure 2.6. Casp7 Activation by the SNIPer Yields MOMP .....	71
Figure 2.7. Caspase-3 and -7 Regulation by the Proteasome .....	72
Figure 2.8. Cell-based Analysis of Caspase Activation with Proteasome Inhibition .....	73
Figure 2.9. Proteasome Inhibition Converts Procaspase-6 to an Apoptotic Executioner Caspase Isoform. ....	74
Figure 2.10. Pathway Analysis of Caspase-6 Activity .....	75
Figure 2.11. Reciprocal Negative Regulation between the 26S Proteasome and Executioner Caspases.....	76
Figure 3.1. ICAD:CAD Pathway in Apoptosis.....	102
Figure 3.2. Three-component PTGR system and Workflow .....	103
Figure 3.3 Robust Knockdown of EGFP-ICAD by ICAD-mir#3 .....	104
Figure 3.4. ICAD-mir#3 structure and targeting region within ICAD.....	105
Figure 3.5. Engineering Intron Sequence into pCMV-miR-EV-IVS-GW-L1-L2 and Reverse Configuration of a finalized PTGR Vector .....	106
Figure 3.6. Protein translation from IVS-PTGR vectors is enhanced. ....	107
Figure 3.7. ICAD-L and -S TevS Engineering. ....	108
Figure 3.8. ICAD processing by the SNIPer and PTGR-mediated replacement of ICAD in HEK293 cells.....	109

## List of Abbreviations

AFC	7-Amino-4-(trifluoromethyl)coumarin
CAD	caspase-activated DNase
CARD	Caspase-recruitment domains
ChIP	chromatin immunoprecipitation
cytoC	cytochrome-C
DAMPS	danger-associated molecular patterns
DED	death effector domains
DMSO	Dimethyl sulfoxide
DTT	Dithiothreitol
ECFP	Enhanced Cyan Fluorescent Protein
EGFP	Enhanced Green Fluorescent Protein
FRET	Förster resonance energy transfer
Granzyme-B	Granzyme-B
IAPs	Inhibitor of Apoptosis Proteins
IPTG	isopropyl-B-D-thiogalactoside
IRES	Internal Ribosome Entry Site
LC-MS	Liquid Chromatography-Mass Spectrometry
MEFs	Murine Embryonic Fibroblasts
MOMP	mitochondrial outer-membrane permeabilization
mTOR	Mammalian target of rapamycin
NLS	Nuclear localization signal
PCA	protein complementation assay
PS-SCL	positional scanning synthetic combinatorial libraries
PTGR	post-translational gene replacement
Rap	rapamycin
RFP	Red Fluorescent Protein
RISC	RNA-induced silencing complex
RNAi	RNA interference
siRNA	short-interfering RNAi
SMAC	second-mitochondrial activator of the caspases
SNIPer	Single-Nick in Proteome
STS	Staurosporine
TetR	tetracycline repressor
TEV	Tobacco Etch Virus
TevS	TEV recognition sequence
UPR	unfolded protein response
UPS	ubiquitin-proteasome system



## **Chapter 1: Introduction to Caspases and Apoptosis**

## 1.1 Introduction

Proteases are essential enzymes that catalyze the irreversible cleavage of peptide amide bonds, and protease activity is associated with crucial biological functions including protein homeostasis, signal transduction, and cellular remodeling (Hedstrom 2002). Caspases, or **cysteine-*aspartyl* proteases**, mediate dramatic cellular remodeling events in multiple cell and tissue types. Caspase-mediated cellular remodeling ranges from specific phenotype conversion derived from the proteolysis of *single substrates*, e.g., T-cell anergy; to more extensive processing of *multiple substrates* during profound cellular 'reprogramming,' e.g. cellular differentiation; to the *terminal proteolysis of over 1000 protein substrates* leading to programmed cell death or apoptosis (Mahrus, Trinidad et al. 2008; Taylor, Cullen et al. 2008). In this introduction, I review caspase-mediated proteolysis in mammalian cells, including basic aspects of caspase enzymology and structure, caspase substrate specificity, and the biological regulation of proteases, and I provide detailed examples of caspase substrates in cellular remodeling with an emphasis on programmed cell death or apoptosis.

The Wells lab has made several significant technical contributions to the field of caspase biology: the development of a powerful proteomics technique to identify and sequence caspase substrates (Mahrus, Trinidad et al. 2008) (**Figure 1.1A**), the identification of small-molecule activators of procaspase-3 and -6 (Wolan, Zorn et al. 2009) (**Figure 1.1B**), and **(3)** the engineering of a ligand-inducible protease, based on Tev protease, that we call the SNIPer for **Single Nick in Proteome** (Gray, Mahrus et al. 2010) (**Figure 1.1C**). The application of

these technologies to mammalian systems has yielded several key insights into the biochemical mechanisms of caspase activation, the signaling mechanisms by which caspase activity is restrained or amplified, and the logic of cellular destruction *via* substrate proteolysis.

SNIPer technology enables the selective and site-specific cleavage of specific substrates. This approach was first employed to activate the executioner caspases, and I highlight the major conclusions of this study in terms of split-protein technology development, caspase enzymology *in vitro* and in cells (see Chapter 2) (**Figure 1.2A and 1.2B**). This study has also yielded key observations with respect to the regulation of executioner caspase activity by the *ubiquitin-proteasome system* (UPS). Of course, SNIPer technology could be employed to interrogate caspase substrates beyond the caspases themselves, and I describe a coupled RNAi-protein expression strategy to selectively cleave any substrate by the SNIPer in cells. This gene replacement technique is called *post-translational gene replacement* or PTGR, and all potential outcomes of caspase-mediated proteolysis -- *loss* of function, *gain* of function, *change* of function, and *no apparent* function (or bystander substrates) can now be interrogated in a rapid and dose-dependent fashion (see Chapter 3).

## **1.2 Apoptotic Phenotypes and Caspase Substrates**

The most pronounced morphological hallmarks of apoptosis include cellular rounding, membrane blebbing and retraction from neighboring cells; nuclear condensation and fragmentation leading to a widespread loss of cellular compartmentalization; the dismantling of transcription and translation machinery,



mitochondrial fragmentation, and engulfment of dying cells and apoptotic bodies, the final products of dynamic membrane remodeling, by professional macrophages (Taylor, Cullen et al. 2008). Dynamic membrane remodeling is initiated by the processing of key cytoskeletal substrates including multiple components of actin microfilaments, e.g., actin and gelsolin, microtubules and intermediate filaments including vimentin. Cellular retraction is mediated by the processing of focal adhesion sites and desmosomes, and the activation of membrane-associated flippases catalyze the extracellular presentation of phosphatidylserine to signal phagocytosis. These caspase-mediated membrane remodeling events are in distinct contrast to necrosis, which is characterized by an early and catastrophic loss of plasma membrane integrity. Cytosolic leakage of danger-associated molecular patterns (DAMPs) triggers the immune system, a primary hallmark of necrosis. Apoptosis, however, is thought to evade an immune response where possible.

Although the role of nuclear condensation and fragmentation has been well studied, several important questions remain. Cleavage of lamin-A by caspase-6 leads to the breakdown of the nuclear envelope (Ruchaud, Korfali et al. 2002). Nuclear condensation is also promoted by phosphorylation of histone H2B by the kinases MST1 and PKC $\delta$  in a caspase-dependent fashion (Ura, Masuyama et al. 2001; Hu, Liu et al. 2007), and chromatin-associated genomic DNA is extensively processed by the endonuclease **caspase-activated DNase** (CAD), which is activated by caspase cleavage of **Inhibitor of caspase-activated DNase** (ICAD) (Samejima and Earnshaw 2005). However, CAD-deficient mice

still undergo chromatin condensation, implying that breakdown of the nuclear envelope, histone phosphorylation, or additional CAD-independent endonucleases drive chromatin compaction. Intriguingly, cells enucleated by the natural product cytochalasin B still undergo FAS-induced apoptosis, and this study implies that cleavage of genomic DNA is dispensable for cell autonomous apoptosis (Schulze-Osthoff, Walczak et al. 1994). Genomic DNA cleavage may be required for phagocytosis of apoptotic bodies or to evade immune surveillance, and the latter hypothesis is supported by the prevalence of anti-DNA antibodies in CAD-deficient mice and autoimmune disease patients afflicted with system lupus erythematosus (Napirei, Karsunky et al. 2000; Kawane, Fukuyama et al. 2003). Key questions, therefore, include (1) *can cleavage of single substrates recapitulate nuclear fragmentation and chromatin condensation* and (2) *is cleavage of single substrates in the nucleus sufficient to drive cell-autonomous apoptosis?*

Mid- to late-stage apoptosis is characterized by mitochondrial fragmentation in two phases. In the first phase, mitochondrial fragmentation or **mitochondrial outer-membrane permeabilization** (MOMP), cytochrome-C (cytoC) and **second-mitochondrial activator of the caspases** (SMAC/DIABLO) are released into the cytosol upon oligomerization of Bax and Bak, which occurs in response to intrinsic (DNA damage) or extrinsic (Bid cleavage by caspase-8) death signals (Green 2005). Cytosolic cytoC initiates the formation of the multimeric apoptosome complex containing cytoC, APAF and caspase-9. SMAC/DIABLO functions as a negative regulator of the **Inhibitor of Apoptosis**

**Proteins (IAPs).** MOMP is also associated with acidification of the cytosol, which further promotes the propagation of caspase activity by protonation of the so-called “safety catch” triple Asp motif in procaspase-3 (Roy, Bayly et al. 2001). In the second and more extensive phase of mitochondrial fragmentation, caspase proteolysis of mitochondrial substrates including the p75 subunit of complex I of the electron transport chain results in the abrogation of ATP synthesis and irreversible organelle breakdown (Ricci, Muñoz-Pinedo et al. 2004).

### **1.3 Caspase Classification**

There are 12 caspase isoforms in humans, which are classified as either inflammatory caspases (caspases-1, -4 and -5) or apoptotic caspases (caspases-2, -3, -6, -7, -8, and -9). The apoptotic caspases can be further subdivided into initiator and executioner caspases, the key effector caspases of apoptosis. The initiator and executioner caspases are typically classified according preferred substrate specificity and by sequence homology (Kaufmann, Kottke et al. 2001). Caspase substrate specificity was first defined *in vitro* by using positional scanning synthetic combinatorial libraries (PS-SCL) of fluorogenic peptide substrates in which one residue (P4-P1) is fixed while the remaining positions are randomized (Rano, Timkey et al. 1997; Thornberry, Rano et al. 1997). All mammalian caspases cleave peptide and protein substrates after an Asp residue (termed the P1 residue, which precedes the scissile amide bond), but caspase substrate specificity at P4 through P2 is more variable. The inflammatory and initiator caspases prefer hydrophobic residues at P4, and the

executioner caspases-3 and -7 prefer acidic residues at this position (*DXXD*). Using a global and unbiased N-terminal labeling approach, Mahrus *et al.* identified 292 protein substrates of the caspases in apoptotic Jurkat T-cell lysates (Mahrus, Trinidad et al. 2008). A key advantage of this technique is that the precise location of cleavage is affinity captured and mapped by LC-MS/MS, and caspase substrate selectivity of full-length and folded protein substrates within a complex lysate was determined. Interestingly, optimal peptide substrates in PS-SCL experiments were rarely mapped using N-terminal degradomics in protein substrates (e.g., DEVD was identified in only ~1% of the apoptotic Jurkat dataset). The influence of secondary structure on caspase substrate specificity was also evaluated, with loops and  $\alpha$ -helices preferred to cleavage sites within  $\beta$ -sheets.

Caspases are translated as inactive zymogens that either self-activate or are activated *in trans* as part of hierarchical protease cascades. The initiator caspases possess large autonomously folded prodomains. **Caspase-recruitment domains** (CARD, procaspase-9) or **death effector domains** (DED, procaspase-8) scaffold the initiator caspase activation complexes (Reed, Doctor et al. 2004). The caspase-9 activation complex, or apoptosome, is assembled in a stepwise fashion upon cytoC release during MOMP, which induces APAF oligomerization, and procaspase-9 is then recruited via homotypic interactions with the CARD domain of APAF/cytoC complexes (Riedl and Shi 2004). DED domains, found in caspase-2 and -8 as well as FADD, mediate the formation of the death-inducing signaling complex (caspase-8) formation upon binding of death receptor agonists

such as FAS and TRAIL (Ashkenazi 2008). Inactive initiator caspases are monomeric, and apoptosome/DISC assembly drives initiator caspase dimerization, self-cleavage and activation via induced proximity. In contrast, the executioner caspases-3, -6 and -7 have short prodomains (3kDa) with unknown structure and no annotated function. The executioner caspases also reside as inactive dimers in the cell at normal physiological concentrations (~100nM). Interestingly, procaspase-6, unlike caspase-3 and -7, can self-activate if transiently transfected in 293T cells (Klaiman, Champagne et al. 2009), and procaspase-6 prefers Val or Thr at P4 unlike caspase-3/-7, which prefer acidic residues at this position. Procaspase-6, therefore, shares features with both the executioner and initiator caspases.

#### **1.4 Interrogating the Role of Caspases and Their Substrates in Cells**

Numerous techniques have been developed to study caspase proteolysis in cells, and these techniques have been applied to interrogate caspase function as well as the proteolysis of individual caspase substrates. Several studies have employed conventional 'reverse genetic' methodology, e.g., siRNA and genetically-engineered mice, to interrogate the non-redundant roles of individual caspase isoforms in orchestrating apoptosis. A seminal study utilizing double knockouts of procaspase-3 and procaspase-7 in murine embryonic fibroblasts treated with staurosporine, a standard apoptotic inducer, unexpectedly revealed that caspase-3 and caspase-7 are required for MOMP (Lakhani, Masud et al. 2006). This was a novel result since mitochondrial release of cytoC and

apoptosome formation was previously understood to be upstream of the executioner caspases in the intrinsic pathway. By combining genetically defined cell lines with conventional pharmacological activators of intrinsic apoptosis, this study convincingly implicated a feed-forward loop involving the executioner caspases as necessary for full-blown apoptosis.

Substrate depletion via siRNA is often utilized as a first test of caspase substrate function although drawing firm conclusions can be difficult since siRNA does not necessarily recapitulate proteolysis. Proteolysis may result in substrate degradation, which is approximated by siRNA-mediated depletion, but siRNA is not suited for *gain of function* analysis of caspase substrates. Alternatively, the overexpression of cleavage-resistant alleles may link substrate proteolysis to phenotype in cells and genetically engineered mice. For example, the expression of non-cleavable lamin A alleles rescues the breakdown of the nuclear envelope in cells. To test the role of caspase-6 activity in the development of a neurodegenerative-like phenotype in transgenic mice expressing pathogenic variants of Huntingtin protein (HTT), non-cleavable HTT alleles (TEVA) were shown to be protective in these mice (Graham, Deng et al. 2006). The cleavage products of substrates can also be expressed to assay the function of stable fragments derived from caspase cleavage. It should be noted that expression of COOH-terminal fragments by conventional approaches results in a polypeptide with either an NH<sub>2</sub>-terminal Met, or the expressed polypeptide is processed by aminopeptidases to remove the Met and then acetylated (Brown and Roberts 1976). A recent study showed that expression of a caspase-7 allele without the

prodomain, but with an NH<sub>2</sub>-terminal Met, did not recapitulate the activity of an engineered variant expressed as an in-line fusion to ubiquitin, which is removed by endogenous de-ubiquitinating enzymes to precisely resemble the non-acetylated neo-epitope product of caspase proteolysis.(Choi, Butterworth et al. 2009) In this particular case, a conventional expression approach ‘masked’ the functionally important IAP-binding motif in the large subunit of caspase-7, and a key protein-protein interaction with cIAP-1 was blocked. Caspase function has also been probed by the overexpression of catalytically-inactive caspase variants, which act as dominant negative inhibitors of the endogenous caspases.

### **1.5 Small-Molecule Activators of the Caspases**

Conventional genetic and overexpression approaches often fail to recapitulate the rapid kinetics of caspase activation in cells, and the Wells group recently published the discovery of a small-molecule activators of caspase-3 and -6 (Wolan, Zorn et al. 2009). A potent activator called 1541 was identified in a high-throughput screen, and the rationale for the screen was based on previous work in which covalent inhibitor fragments were disulfide-trapped to a novel and conserved allosteric site in caspase-3 and caspase-7 and later in caspase-1 (Hardy, Lam et al. 2004; Scheer, Romanowski et al. 2006; Datta, Scheer et al. 2008). Crystallographic analysis demonstrated that two distinct caspase conformations could be observed, an “on-state” when bound to irreversible active-site inhibitors and an “off-state” when bound to the covalent inhibitor fragments. Based on these results, it was hypothesized that the “on” and “off” states are in dynamic equilibrium, and it would then be possible to identify small

molecules that promoted procaspase activation by stabilizing the “on” state. *In vitro* enzymatic studies confirmed that 1541 induced a dramatic increase in  $k_{cat}/K_m$  of procaspase-3 against the fluorogenic peptide IETD-AFC ) (**Figure 1.3A**), which corresponds to the sequence of the procaspase intersubunit linker. A second mechanism of action was also demonstrated in which 1541 further promoted activation by *sensitizing* procaspase-3 to upstream proteolysis (**Figure 1.3B**). In structural terms, 1541 may promote an extended conformation in the intersubunit linker that is more accessible to autoproteolysis or to proteolysis *in trans* by upstream proteases. A similar mechanism was previously described by Thornberry and colleagues in which they demonstrated enhanced caspase activation by Granzyme-B (GrB) by disabling the caspase-3 “safety catch” motif via mutagenesis (Roy, Bayly et al. 2001).

1541 rapidly induced apoptosis in multiple cancer cells lines including BT549, MDA-MB361, HEK293, HeLa, and HCC1954 in a dose-dependent manner, and 1541 exceeded the cell-killing kinetics of staurosporine (STS), a broad spectrum kinase inhibitor and apoptotic inducer. To unambiguously confirm caspase-3 and/or caspase-6 as the primary cellular target, a series of genetic experiments were performed in combination with 1541 treatment. As a first test, MEFs deficient in Bax and Bak, proapoptotic BH3 proteins that oligomerize to trigger MOMP and cytoC release, were treated with either 1541 or STS. STS-treated Bax/Bak-knockout MEFs were resistant to apoptosis, but 1541 triggered apoptosis in these cells. As expected, WT MEFs were sensitive to both STS and 1541. A similar experiment was performed using a Jurkat subclone



deficient in caspase-8, which still underwent cell death in the presence of 1541 but not FAS, a proapoptotic death receptor agonist. By utilizing cell lines deficient in key effector proteins for intrinsic apoptosis (Bak / Bak) or extrinsic apoptosis (caspase-8), the 'on-target' activity of 1541 was attributed to direct executioner caspase activation (**Figure 1.3D**). As a second test, three 1541-resistant procaspase-3 variants (S198A, T199A, and S205A) were identified in the intersubunit region of procaspase-3 by alanine-scanning mutagenesis. Each 1541-resistant allele retained activity upon activation of GrB *in vitro*. Five procaspase-3 alleles: WT-caspase-3, S198A, T199A, S205A (**Figure 1.3C**) and catalytically inactive procaspase-3 (C163A) were subcloned into a retroviral expression vector (pQCXIP) and packaged as recombinant retrovirus. MCF-7 cells, derived from a breast adenocarcinoma deficient in procaspase-3, were transduced with the procaspase-3 allele series, and the S198A procaspase-3 mutant was more resistant to 1541-induced apoptosis in comparison to WT (**Figure 1.3E**). Identification of caspase isoform-selective small molecules is ongoing, and 1541 is considered a 'pan-caspase activator.' *In vitro*, enzymatic assays demonstrate that 1541 activates both procaspase-3 and procaspase-6. Preliminary data further suggests that 1541 may activate the initiator caspases as well, and the proposed "sensitizer" mechanism may operate on procaspase-7 as well.

### **1.6 Protein Complementation Assay Technology: The SNIPer**

To address the goal of activating a single executioner caspase isoform in a site-selective manner, we optimized a previously split N1a *Tobacco Etch Virus*

(TEV) protease that is robustly activated to specifically cleave each of the executioner caspase isoforms in human cells (Gray, Mahrus et al. 2010). Our protease engineering strategy utilizes **protein complementation assay** (PCA) technology, which based on the **(1)** strategic dissection and **(2)** inducible re-folding small globular proteins for conditional activation in cells (Michnick, Ear et al. 2007). Upon successful structural dissection of the protein of interest, the protein fails to fold (and is therefore inactive) unless each fragment is fused to autonomously folded protein domains that heterodimerize upon a specific stimulus. PCA technology has been utilized as reporters for protein-protein interactions, and PCA methodology is also an effective strategy to modulate protein activity and/or localization with small molecules. For the SNIPer, our PCA strategy leverages the rapid kinetics of small-molecule pharmacology and the high specificity of TEV protease (7-mer recognition sequence), which can be genetically encoded into specific substrates of interest. I describe the optimization of the SNIPer and TevS-encoded executioner caspase alleles in Chapter 2 and the application of SNIPer technology to the conditional cleavage of individual caspase substrates in Chapter 3. In total, these sections fully describe methods by which to functionally interrogate caspase proteolysis for both *gain of function* and *loss of function* phenotypes. In this section, I discuss novel and unpublished applications of the SNIPer in the following two areas: single-cell dynamics of apoptosis, probing the role of ATF6 in the **unfolded protein response** (UPR).

## 1.7 Novel Applications of the SNIPer

### 1.7.1. Single-cell dynamics of apoptosis

Several groups including the Wells lab have observed that the maximal induction of executioner caspase activity during apoptosis is extremely stochastic when measured at the single-cell level (Albeck, Burke et al. 2008; Gray, Mahrus et al. 2010). A key question, therefore, is *at which apoptotic pathway node(s) does this stochastic behavior originate? Does rapid and/or direct synchronous activation of the executioner caspase alleles result in more homogenous (and less stochastic) caspase activation?* Using activator technology developed in the Wells lab, e.g., 1541 and SNIPer cell lines, in conjunction with genetically-encoded probes for real-time detection of caspase activity (ECFP-YPET), MOMP (SMAC-RFP) and 26S proteasome function (EGFP-CL1), we are well positioned to interrogate the single-cell dynamics of apoptosis with unprecedented detail.

FRET-based caspase reporters have been generated for caspase-3/-7 (DEVD/R), caspase-8 (IETD/G), and caspase-6 (VEID/G) to assay for caspase activity in individual cells (**Figure 1.4A**). Two distinct FRET donor/acceptor pairs have been built and tested. The first generation of caspase activity reporters, based on the established ECFP/EYFP pair, is a modified version of a previously published FRET pair that was optimized by directed evolution (Nguyen and Daugherty 2005). Subsequent studies found that the donor CyPET variant was unsuitable for use in mammalian systems (due to temperature-sensitive folding issues at 37°C). CyPET was replaced with ECFP, and the resulting ECFP-YPET construct was demonstrated to have greatly enhanced FRET (5- to 8-fold) as compared to conventional FRET pairs (Ouyang, Sun et al. 2008). The

development of second-generation FRET-based caspase reporters based on TagBFP-EGFP is currently in progress. Several advantages of this FRET pair exist. First, TagBFP is derived from a distinct coral species as EGFP, and spurious recombination between donor and acceptor proteins is prevented. Second, this pair demonstrated enhanced FRET efficiency as compared to other monomeric donor/acceptor pairs, and TagBFP is compatible with DAPI filter sets present in most fluorescent microscopes (Subach, Gundorov et al. 2008). SMAC-RFP is the fusion of a bright monomeric red fluorescent protein (from sea anemone *Entacmaea quadricolor*) to the 59-residue NH<sub>2</sub>-terminal SMAC mitochondrial transit peptide (**Figure 1.4B**), which targets SMAC-RFP to the intermembrane space of mitochondria in resting cells (Albeck, Burke et al. 2008). The precise time point of MOMP is determined by measuring RFP translocation from the mitochondria to the cytosol during apoptosis. Furthermore, SMAC-RFP does not any possess functional SMAC sequence, i.e., AKPD, to disrupt IAP-caspase interactions. EGFP-CL1, with a 16-residue degron fused to the COOH-terminus of EGFP, serves as a single-cell proteasome reporter (**Figure 1.4C**). The synthetic CL1 degron sequence was first identified in yeast (Gilon, Chomsky et al. 1998), and similar constructs have been used in several mammalian systems to assay for proteasome activity by FACS or by fluorescent microscopy. EGFP-CL1 is rapidly polyubiquitinated and degraded in a proteasome-dependent fashion with a half-life of <8 min (Bence, Bennett et al. 2005). However, in the presence of proteasome inhibitors, a rapid increase in the cellular concentration of EGFP is observed by a dramatic increase in fluorescence, and this technique

has been employed to study proteasome function in cells expressing mutant alleles of CFTR (Bence, Sampat et al. 2001). Importantly, both first and second-generation caspase activity FRET reporters can be multiplexed with the SMAC-RFP MOMP reporter, thus enabling multiplexed detection executioner and initiator caspase activity and MOMP in the same cell. Alternatively, EGFP-CL1 proteasome reporter can be combined with SMAC-RFP to correlate 26S proteasome function and MOMP.

### 1.7.2 Probing the role of ATF6 in the UPR

Protease activity is central to numerous signaling pathways beyond apoptosis, and we are extending our approach of engineering protease substrates for conditional processing by the SNIPer. In the endoplasmic reticulum (ER), disruption of homeostatic balance of folded to unfolded proteins in the secretory pathway triggers the *unfolded protein response* (UPR), and the three key 'sentinel' proteins, PERK, Ire1 and ATF6, control the UPR (Schröder and Kaufman 2005). Unlike PERK and Ire1, which are kinases, ATF6 encodes a transcription factor, which is sequestered in the ER by the chaperone BiP, and ATF6 translocates to the Golgi during acute ER stress (**Figure 1.5A**). The cytosolic-facing zinc-finger domain is processed by S1P/S2P family proteases at the Golgi to release a functional transcription factor that translocates to the nucleus.

An important question is to identify and validate the key transcriptional targets of ATF6. In collaboration with the Walter lab, TevS-alleles of ATF6 were generated and rapamycin-inducible cleavage was demonstrated in transient

transfection assays by western blotting. In principle, this strategy allows ATF6 activation without inducing Ire1 or PERK activity. The UPR is subject to multiple levels of positive feedback, and ATF6 overexpression is sufficient to induce a significant UPR response. To address this concern, stable cell lines were prepared in the 293 TREX cell line, which harbors the tetracycline repressor (TetR) and a defined locus for integration flanked by FRT recombination sites. These cells, therefore, are capable of expressing transgenes with tetracycline-inducible transcriptional control. A single-vector SNIPer construct in which of both SNIPer halves are expressed on the same transcript was also developed in the following configuration: mCherry-T2A-Frb-N-TEV-IRES(WT)-FKBP-C-TEV. mCherry is the selectable marker (stably expressing cells were enriched by FACS), and the COOH-terminal half of the SNIPer is expressed via the wild-type ECMV IRES (**Figure 5B and 5C**). Our approach affords multiple layers of orthogonal control for ATF6 expression and cleavage, both transcriptional (via TetR) and post-translational (via the SNIPer). We will first define the transcriptional targets by treating SNIPer TevS-ATF6 cells  $\pm$ Rap at various time points, harvest RNA, and perform microarray analysis. We will then globally identify ATF6 binding sites by chromatin immunoprecipitation (ChIP) and deep sequencing.

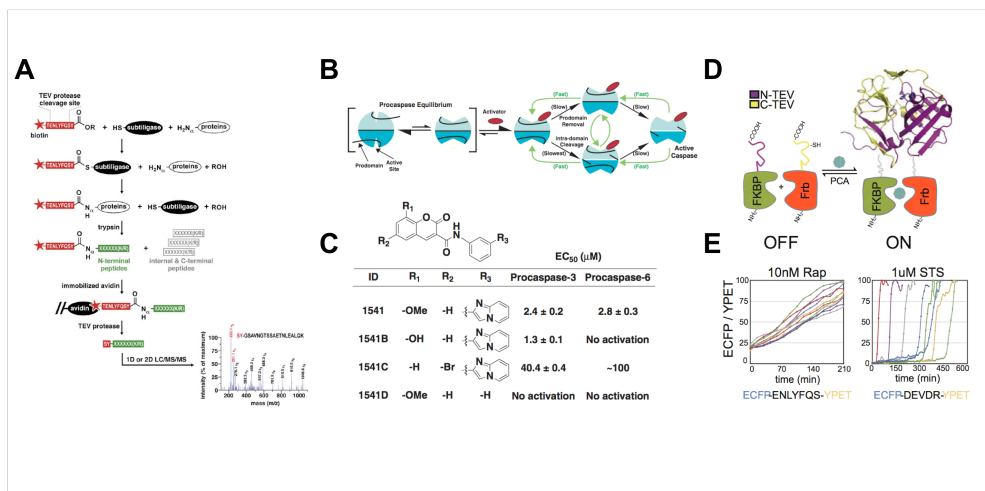


**Figure 1.1. Recent Technology Developments for Apoptosis Research**

**(A)** Degradomics work flow. Neo-termini derived from caspase proteolysis are ligated to a biotinylated ester by subtiligase. After streptavidin capture, on-bead trypsin digestion and release by Tev protease, caspase cleavage sites are sequenced by 1D or 2D LC-MS/MS (Mahrus, Trinidad et al. 2008). **(B)** Model for 1541-mediated activation of procaspase-3 in which 1541 stabilizes the ‘active’ procaspase conformer and **(C)** structure of 1541 and EC<sub>50</sub> data for procaspase-3 and procaspase-6 (including analogs) (Wolan, Zorn et al. 2009). **(D)** Model for SNIPer PCA activation by rapamycin and **(E)** synchronous activation of SNIPer activity as compared to caspase-3 activity during STS-induced intrinsic apoptosis (Gray, Mahrus et al. 2010).

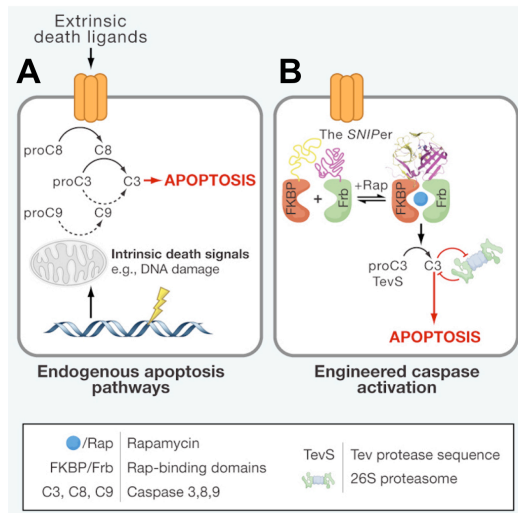


**Figure 1.2. Caspase Pathways**

**(A)** Extrinsic and intrinsic apoptosis pathways converge on the activation of the executioner caspases. **(B)** Executioner caspase activation by the SNIPer and a model for reciprocal negative regulation by the 26S proteasome (Gray, Mahrus et al. 2010).



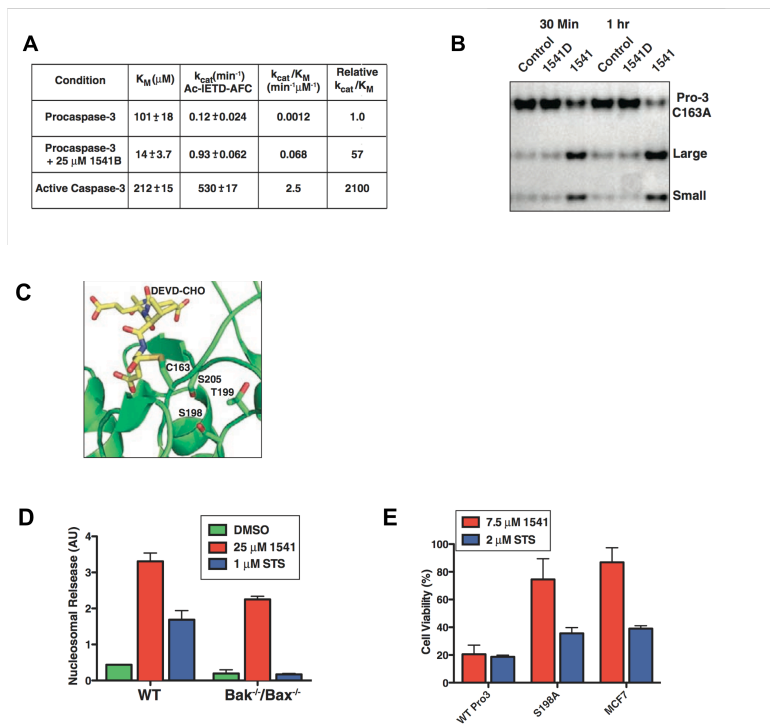


**Figure 1.3. 1541 activates procaspase-3 and procaspase-6**

**(A)** Kinetic data for 1541-induced Ac-IETD-AFC cleavage for procaspase-3 and active caspase-3. **(B)** 1541 'sensitive' processing of procaspase-3 by upstream proteases such as Granzyme-B. **(C)** Structure of caspase-3 with 1541-resistant mutations highlighted (S198A, T199A and S205A). **(D)** 1541 activates procaspase-3 to result in apoptosis in Bak/Bax deficient MEFs and **(E)** procaspase-3 (S198A) is as resistant to 1541-induced apoptosis as WT MCF-7 cells, which lack endogenous procaspase-3 (Wolan, Zorn et al. 2009).

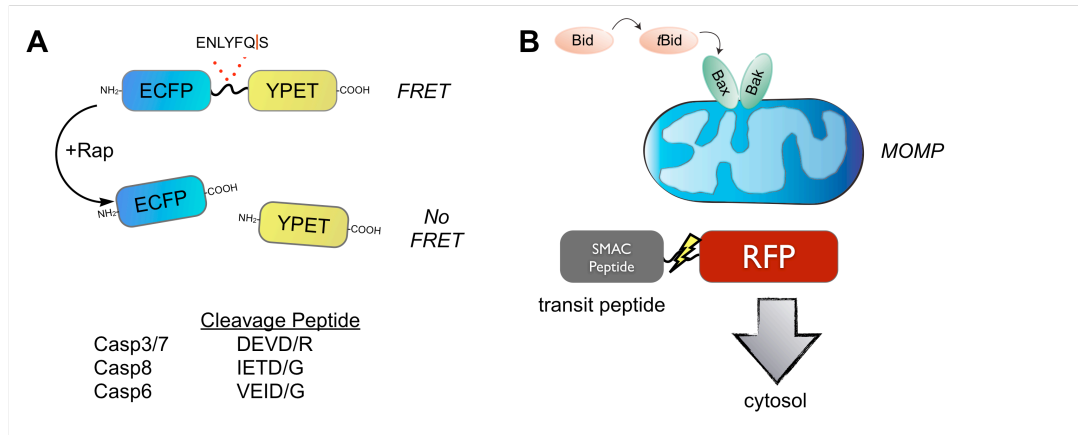


**Figure 1.4. Genetically-encoded fluorescent reporters for probing single-cell dynamics of apoptosis**

**(A)** Cyan-yellow fluorescent protein FRET reporter for Tev protease, caspase-3/-7, caspase-8 and caspase-6 activity **(B)** SMAC-RFP reporter for MOMP and **(C)** EGFP-CL1 degron fusion for measuring proteasome activity in cells.

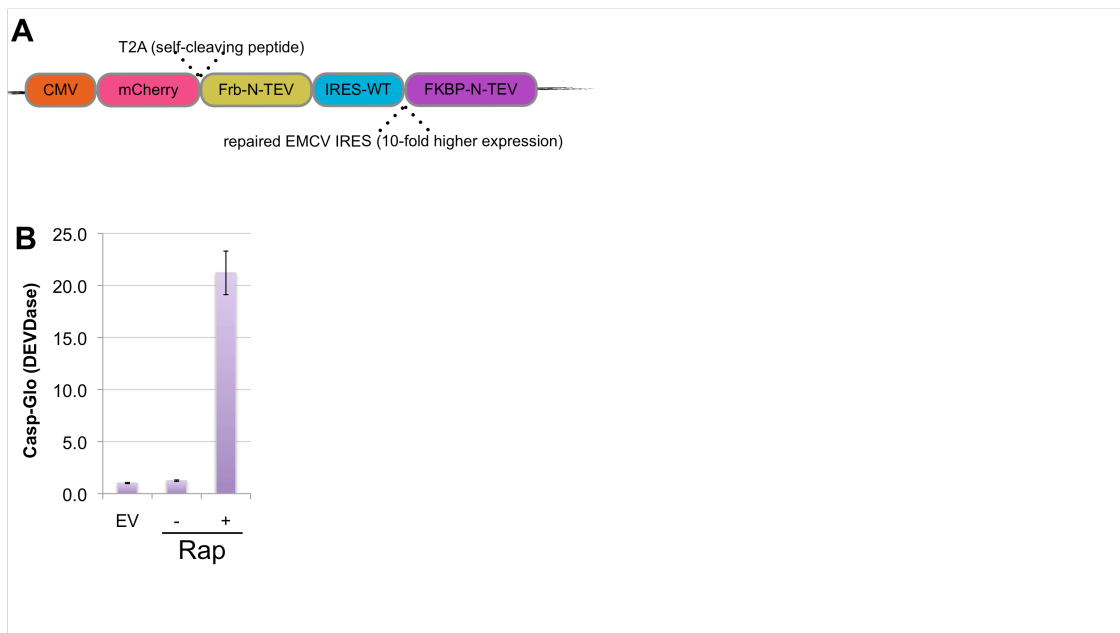


**Figure 1.5. SNIPer-mediated cleavage of ATF6**

**(A)** Domain organization of single-vector split-TEV construct and **(B)** transient transfection of the single-vector split-TEV construct plus casp3-TevS with 8nM Rap induces a 20-fold increase in cellular DEVDase activity in 293T cells.

## 1.8 References

- Albeck, J. G., J. M. Burke, et al. (2008). Quantitative analysis of pathways controlling extrinsic apoptosis in single cells. Mol Cell. **30**: 11-25.
- Ashkenazi (2008). Directing cancer cells to self-destruct with pro-apoptotic receptor agonists. Nature reviews Drug discovery.
- Bence, N. F., E. J. Bennett, et al. (2005). Application and analysis of the GFPu family of ubiquitin-proteasome system reporters. Meth Enzymol. **399**: 481-490.
- Bence, N. F., R. M. Sampat, et al. (2001). Impairment of the ubiquitin-proteasome system by protein aggregation. Science. **292**: 1552-1555.
- Brown, J. L. and W. K. Roberts (1976). Evidence that approximately eighty per cent of the soluble proteins from Ehrlich ascites cells are Nalpha-acetylated. J Biol Chem. **251**: 1009-1014.
- Choi, Y. E., M. Butterworth, et al. (2009). The E3 Ubiquitin Ligase cIAP1 Binds and Ubiquitinates Caspase-3 and -7 via Unique Mechanisms at Distinct Steps in Their Processing. J Biol Chem. **284**: 12772-12782.
- Datta, D., J. M. Scheer, et al. (2008). An allosteric circuit in caspase-1. J Mol Biol. **381**: 1157-1167.
- Gilon, T., O. Chomsky, et al. (1998). Degradation signals for ubiquitin system proteolysis in *Saccharomyces cerevisiae*. EMBO J. **17**: 2759-2766.
- Graham, R. K., Y. Deng, et al. (2006). Cleavage at the caspase-6 site is required for neuronal dysfunction and degeneration due to mutant huntingtin. Cell. **125**: 1179-1191.
- Gray, D. C., S. Mahrus, et al. (2010). Activation of specific apoptotic caspases with an engineered small-molecule-activated protease. Cell. **142**: 637-646.
- Green, D. R. (2005). Apoptotic pathways: ten minutes to dead. Cell. **121**: 671-674.
- Hardy, J. A., J. Lam, et al. (2004). Discovery of an allosteric site in the caspases. Proc Natl Acad Sci USA. **101**: 12461-12466.
- Hedstrom, L. (2002). Serine protease mechanism and specificity. Chem Rev. **102**: 4501-4524.

Hu, Y., Z. Liu, et al. (2007). Acinus-provoked protein kinase C delta isoform activation is essential for apoptotic chromatin condensation. Cell Death Differ. **14**: 2035-2046.

Kaufmann, S. H., T. J. Kottke, et al. (2001). Analysis of caspase activation during apoptosis. Curr Protoc Cell Biol. **Chapter 18**: Unit 18.12.

Kawane, K., H. Fukuyama, et al. (2003). Impaired thymic development in mouse embryos deficient in apoptotic DNA degradation. Nat Immunol. **4**: 138-144.

Klaiman, G., N. Champagne, et al. (2009). Self-activation of Caspase-6 in vitro and in vivo: Caspase-6 activation does not induce cell death in HEK293T cells. Biochim Biophys Acta. **1793**: 592-601.

Lakhani, S. A., A. Masud, et al. (2006). Caspases 3 and 7: key mediators of mitochondrial events of apoptosis. Science. **311**: 847-851.

Mahrus, S., J. C. Trinidad, et al. (2008). Global sequencing of proteolytic cleavage sites in apoptosis by specific labeling of protein N termini. Cell. **134**: 866-876.

Michnick, S. W., P. H. Ear, et al. (2007). Universal strategies in research and drug discovery based on protein-fragment complementation assays. Nature reviews Drug discovery. **6**: 569-582.

Napirei, M., H. Karsunky, et al. (2000). Features of systemic lupus erythematosus in Dnase1-deficient mice. Nat Genet. **25**: 177-181.

Nguyen, A. W. and P. S. Daugherty (2005). Evolutionary optimization of fluorescent proteins for intracellular FRET. Nat Biotechnol. **23**: 355-360.

Ouyang, M., J. Sun, et al. (2008). Determination of hierarchical relationship of Src and Rac at subcellular locations with FRET biosensors. Proc Natl Acad Sci USA. **105**: 14353-14358.

Rano, T. A., T. Timkey, et al. (1997). A combinatorial approach for determining protease specificities: application to interleukin-1beta converting enzyme (ICE). Chem Biol. **4**: 149-155.

Reed, J. C., K. S. Doctor, et al. (2004). The domains of apoptosis: a genomics perspective. Sci STKE. **2004**: re9.

Ricci, J.-E., C. Muñoz-Pinedo, et al. (2004). Disruption of mitochondrial function during apoptosis is mediated by caspase cleavage of the p75 subunit of complex I of the electron transport chain. Cell. **117**: 773-786.

Riedl, S. J. and Y. Shi (2004). Molecular mechanisms of caspase regulation during apoptosis. Nat Rev Mol Cell Biol. **5**: 897-907.

Roy, S., C. I. Bayly, et al. (2001). Maintenance of caspase-3 proenzyme dormancy by an intrinsic "safety catch" regulatory tripeptide. Proc Natl Acad Sci USA. **98**: 6132-6137.

Ruchaud, S., N. Korfali, et al. (2002). Caspase-6 gene disruption reveals a requirement for lamin A cleavage in apoptotic chromatin condensation. EMBO J. **21**: 1967-1977.

Samejima, K. and W. C. Earnshaw (2005). Trashing the genome: the role of nucleases during apoptosis. Nat Rev Mol Cell Biol. **6**: 677-688.

Scheer, J. M., M. J. Romanowski, et al. (2006). A common allosteric site and mechanism in caspases. Proc Natl Acad Sci USA. **103**: 7595-7600.

Schröder, M. and R. J. Kaufman (2005). The mammalian unfolded protein response. Annu Rev Biochem. **74**: 739-789.

Schulze-Osthoff, K., H. Walczak, et al. (1994). Cell nucleus and DNA fragmentation are not required for apoptosis. J Cell Biol. **127**: 15-20.

Subach, O. M., I. S. Gundorov, et al. (2008). Conversion of red fluorescent protein into a bright blue probe. Chem Biol. **15**: 1116-1124.

Taylor, R. C., S. P. Cullen, et al. (2008). Apoptosis: controlled demolition at the cellular level. Nat Rev Mol Cell Biol. **9**: 231-241.

Thornberry, N. A., T. A. Rano, et al. (1997). A combinatorial approach defines specificities of members of the caspase family and granzyme B. Functional relationships established for key mediators of apoptosis. J Biol Chem. **272**: 17907-17911.

Ura, S., N. Masuyama, et al. (2001). Caspase cleavage of MST1 promotes nuclear translocation and chromatin condensation. Proc Natl Acad Sci USA. **98**: 10148-10153.

Wolan, D. W., J. A. Zorn, et al. (2009). Small-molecule activators of a proenzyme. Science. **326**: 853-858.

## **Chapter 2: Activation of Specific Apoptotic Caspases with an Engineered Small Molecule-Activated Protease**



## 2.1 Summary

Apoptosis is a conserved cellular pathway that results in the activation of cysteine-aspartyl proteases, or caspases. To dissect the non-redundant roles of the executioner caspases-3, -6 and -7 in orchestrating apoptosis, we have developed an orthogonal protease to selectively activate each isoform in human cells. Our approach uses a split-Tobacco Etch Virus (TEV) protease under small-molecule control, that we call the SNIPer, with caspase alleles containing genetically encoded TEV cleavage sites. These studies reveal that all three caspases are transiently activated but only activation of caspase-3 or -7 is sufficient to induce apoptosis. Proteomic analysis shown here and from others reveals that 20 of the 33 subunits of the 26S proteasome can be cut by caspases, and we demonstrate synergy between proteasome inhibition and dose-dependent caspase activation. We propose a model of proteolytic reciprocal negative regulation with mechanistic implications for the combined clinical use of proteasome inhibitors and proapoptotic drugs.

## 2.2 Introduction

Apoptosis, or programmed cell death, is a ubiquitous and conserved cellular pathway required for development, immune cell maturation and to prevent oncogenesis (Taylor, Cullen et al. 2008). Apoptosis is triggered by signaling events involving a diverse array of protein networks, organelles, and macromolecular complexes that converge upon the activation of caspases (Fuentes-Prior and Salvesen 2004). The executioner caspases are the final proteases to be activated in apoptosis. This leads to cleavage of upwards of 1000 (Dix, Simon et al. 2008; Mahrus, Trinidad et al. 2008) to produce the characteristic apoptotic phenotypes of membrane blebbing, nuclear condensation, DNA fragmentation, and ultimately phagocytosis by immune cells. Executioner caspases have been recently linked to non-apoptotic phenotypes such as axonal pruning, stem cell differentiation, and red blood cell enucleation (Yi and Yuan 2009). The cellular processes that stop caspases short of inducing apoptosis in these diverse biological settings remain a mystery.

There are 12 caspase isoforms in humans but their precise and non-redundant roles for mediating apoptosis, non-apoptotic phenotypes, and innate immunity are only beginning to be fully elucidated. Extensive biochemical and structural analyses indicate that the inflammatory and initiator caspases are recruited to larger complexes that induce caspase dimerization, auto-proteolysis, and protease activation. Upon activation, the apoptotic initiator caspases-8 and -9 cleave the executioner procaspases-3, -6 and -7. The executioner caspases are translated as inactive dimers; there are at least two sites of processing in the executioner caspases; and the specific role of each proteolytic event in regulating

executioner caspase activity is still unclear, both *in vitro* and in cells, as is the role of the prodomain in executioner caspase function.

Gene knockout studies in murine embryonic fibroblasts demonstrate that cells deficient in both caspase-3 and -7 are more resistant to a variety of apoptotic stimuli as compared to single knockouts, suggesting functional redundancy in these two executioner isoforms (Lakhani, Masud et al. 2006). Furthermore, single-cell studies reveal that the induction of executioner caspase activity is highly stochastic. To further probe the function of each caspase with sharp temporal resolution, we needed to activate an individual isoform selectively and synchronously. Recent progress was reported toward building small molecule activators of the procaspases (Wolan, Zorn et al. 2009), but these compounds are not yet selective enough to trigger each one of the caspases individually.

To address the goal of activating a single executioner caspase isoform in a site-selective manner, we describe the optimization of a previously split Nla Tobacco Etch Virus (TEV) protease (Wehr, Laage et al. 2006; Wehr, Reinecke et al. 2008). We demonstrate that an engineered variant of split-TEV can be robustly activated in cells to specifically cleave each of the executioner caspase isoforms. These studies reveal that activation of caspase-3 or -7, but not caspase-6, is sufficient to induce apoptosis. Remarkably, the activation is transient for each isoform. These data support a model of antagonistic proteolysis between the executioner caspases and the proteasome.

## 2.3 Results

### 2.3.1 The SNIPer: Design, Optimization, and Characterization in Mammalian Cells

Our initial split-TEV construct was based on a previous design developed for protein-complementation assays (Wehr et al., 2006) (**Figure 2.1A**). The full-length TEV variant S219V was split into two component fragments: N-TEV (residues 1-118) and C-TEV (residues 119-242). This design inactivates TEV protease by separating the catalytic triad residues His46 and Asp81 from the Cys151 nucleophile. N-TEV was fused to the C-terminus of FKBP with a 10-amino acid (GGGGS)<sub>2x</sub> linker between the two domains, and C-TEV was fused to the C-terminus of Frb (the rapamycin-binding domain of mTOR kinase). Therefore, protease activity is conditionally restored by the addition of rapamycin, which promotes split-TEV fragment association and ligand-dependent protein folding.

We assayed for reconstituted protease activity in 293T cells by co-transfecting both N- and C-TEV halves and a FRET-based ECFP-YPET reporter that is cleaved by TEV. In the presence of rapamycin (Rap), the split-TEV construct extending to residue 242 cleaved the protease reporter as compared to an empty vector control (**Figure 2.1B**). However, significant processing also occurred in the absence of Rap, suggesting the two halves can associate and reconstitute activity in the absence of a small molecule dimerizer. Another group recently implemented the published N-TEV and C-TEV design in mammalian cells and similarly observed leaky TEV protease activity in the absence of Rap (Williams, Puhl et al. 2009). They reduced Rap-independent activation by

lowering the amount of split-TEV DNA that was transiently transfected or by targeting one fragment to the cell membrane via a genetically encoded myristoylation tag. However, our goal was to engineer cell death pathways using stable cell lines, which requires a split-TEV design with no background activity. We hypothesized that the C-terminus of the TEV was causing spontaneous refolding of the fragments in the absence of Rap (**Figure 2.2A for a model**). A systematic set of deletion mutants was created from the C-TEV<sup>119-242</sup> fragment to generate four truncated C-TEV constructs. Co-expression of FKBP-N-TEV and Frb-C-TEV-219 yielded inducible proteolysis upon addition of Rap with reduced leaky proteolytic activity in mock-treated cells as confirmed by the FRET assay (**Figure 2.1B**) and immunoblot analysis (**Figure 2.2B, top panel**).

Further optimization was required due to detectable TEV activity for FKBP-N-TEV and Frb-C-TEV-219 in the absence of Rap (**Figure 2.1C and Figure 2.2B, bottom panel**). We tested the opposite FKBP and Frb protein fusions to N-TEV and to the enhanced C-TEV-219 fragment, and we observed that Frb-N-TEV(1-118) and FKBP-C-TEV(119-219) maintained robust TEV activity in the presence of Rap with little background. As an initial test of split-TEV stability, we found that proteolysis of the FRET reporter was not enhanced after treatment with Rap and 500nM PS-341 (Bortezomib), a clinically available proteasome inhibitor (**Figure 2.2C**), indicating that a proteasome inhibition was not sufficient to promote increased split-TEV activity in cells. Each split-TEV protein fragment was also detected by immunoblotting after blocking protein translation with cyclohexamide for 8hr, suggesting both were stable in cells (**Figure 2.2D**). Both

removal of the C-terminal end of the C-TEV fragment and fusion pair optimization to FKBP and Frb were necessary to generate a rapamycin-inducible split-TEV protease for mammalian cells. We refer to this optimized construct pair as the SNIPer (Single Nick in Proteome) since there are no known natural TEV cleavage sites in the human proteome except for those we introduce.

We observed rapid activation of the SNIPer in individual cells (**Figure 2.1D, left panel**) using the TevS-FRET reporter in transiently transfected HEK293 cells. Cells were monitored over a 3 hr time frame over which a linear increase in TEV activity was measured by single-cell fluorescent microscopy. Approximately 50% of the ECFP-YPET<sup>ENLYFQIS</sup> substrate was cleaved by  $100 \pm 20$  min. Importantly, activation of the SNIPer at the single-cell level was more synchronous than endogenous caspase pathways during experiments in which SNIPer-expressing cells were directly compared to HEK293 cells transfected with ECFP-YPET<sup>DEVDIR</sup>, a reporter for caspase-3 and -7 activity (Albeck, Burke et al. 2008) (**Figure 2.1D, right panel**), and treated with 1uM staurosporine (STS). We conclude that SNIPer activation kinetics matches or exceeds endogenous DEVDase activation kinetics during apoptosis, which prompted its further use to probe executioner caspase signaling in cells.

### **2.3.2 Engineering Orthogonal Procaspace-3 and -7 Alleles for Selective Activation by the SNIPer**

The executioner caspases are translated as inactive zymogens that are cleaved by initiator caspases, by other executioner caspases *in trans*, or by auto-activation. Two sites of processing exist in procaspase-3 and -7: one at the

junction of the prodomain and large subunit (site-1) and the second between the large and small subunits in the intersubunit linker (site-2) (Earnshaw, Martins et al. 1999). To date, there are no reported crystal structures of procaspase-3 or procaspase-7 with defined electron density in the intersubunit linker or the prodomain. However, previous studies have shown that mutation of several residues within the “loop bundle” of the intersubunit linker of caspase-3 influences the activity of the protease (Feeney, Pop et al. 2006). Therefore, we inserted a TEV recognition sequence (TevS) into the P1 position at site-2 on procaspase-3, replacing the P1 Asp of the endogenous caspase site, P5-IETD-P1' with the preferred P6 Glu for the Tev cleavage site (TevS), P7-ENLFYQ-P1'. This resulted in a chimeric substrate at site-2 (IETENLYFQ) that maintained the integrity of the caspase cleavage site from P4-P2 while eliminating the aspartic acid critical for cutting by the caspases themselves (**Figure 2.3A, top panel**). In principle, this approach would render the sites cleavable by the SNIPer only. Since caspases and TEV protease share similar preference for the small P1' residues (Gly, Ser and Ala), the wild-type peptide sequence after the scissile bond was also maintained. Once the TevS is cleaved, a small peptide 'scar' is left behind with an ENLYFQ sequence on the C-terminus.

With this insertion strategy we generated four alleles in both procaspase-3 and -7: one where TevS was inserted between the pro-domain and the large subunit (TevS-1), one where the TevS was inserted between the large and small domain (TevS-2), one where two insertions were made (TevS-1,2) and one that contained the TevS inserted between the large and small subunits but that also

contained a mutation of Asp to Ala mutation at site-1 to prevent prodomain cleavage (D2A-TevS-2) (**Figure 2.3A, bottom panel**). To begin to test the impact of these mutations on processing and activity, a His-tagged version of the Casp3-D2A-TevS-2 protein was over-expressed in *E. coli* and purified by Ni-NTA affinity chromatography. Casp3-D2A-TevS-2 was co-incubated with recombinant TEV protease, and the processed samples were analyzed by SDS-PAGE to confirm that the engineered caspase construct was indeed cleaved at the expected single site (**Figure S.4A**). Furthermore, the measured catalytic efficiency ( $k_{cat} / K_M$ ) for the engineered caspase was in good agreement with the value for wild-type active caspase-3 produced in our lab (**Figure 2.4B**).

To further probe the functional consequence of processing at site-1 and site-2 *in vitro*, we constructed a matrix of the three procaspase-3 and -7 alleles harboring TevS sites that replace one or both endogenous caspase processing. Granzyme-B (GrB), a serine protease secreted by cytotoxic T-lymphocytes, is capable of cleaving procaspase-3 at site-2 (Casciola-Rosen, Garcia-Calvo et al. 2007), but it does not process Casp3-TevS-2 since that cleavage site is mutated. Incubation of Casp3-WT and Casp3-TevS alleles with active GrB or Tev confirmed Casp3-TevS-2 is an orthogonal caspase; it is activated by TEV protease but not by GrB (**Figure 2.3B**).

Each procaspase-3 and -7 allele was expressed as a proenzyme in *E. coli*, treated with GrB or TevS for 1 hr, and relative caspase activity was measured with Ac-DEVD-AFC (**Figure 2.3C**). Immunoblots confirmed the predicted cleavage patterns for TEV protease or GrB for procaspase-3 allele series (**Figure**



**2.4C).** Cleavage by GrB at IETD<sup>175</sup> at site-2 was sufficient to activate WT and TevS-1 procaspases variants, both of which are WT for site-2. TEV processing at TevS-2 was sufficient to activate both caspase-3 and -7-TevS-2, regardless if the prodomain is cleavable. TEV protease processing at TevS-1 was not sufficient to induce activity for either isoform. Together, these results confirm that processing at site-2 is both necessary and sufficient for activation *in vitro* by either TEV protease or GrB. Processing of the prodomain is neither sufficient for activation nor necessary for full levels of activation in conjunction with processing at the inter-subunit linker.

### **2.3.3 Selective Activation of Orthogonal Procaspase-3 and -7 Alleles in Stable Human Cell Lines**

The matrix of caspase-TevS alleles was stably engineered as single-copy integrants into HEK293 cells in order to minimize the over-expression phenotypes associated with transient transfection. HEK293 SNIPer cell lines expressing Casp3-WT, Casp3-TevS-1 or Casp3-TevS-2 were induced for 6 hr with 10nM Rap and assayed for DEVDase activity. Addition of Rap induced a 8-fold increase in caspase-3 activity in the Casp3-TevS-2 line as compared to the same cells treated with DMSO only (**Figure 2.5A, left top and bottom panels**). After 8 hr, the Casp3-TevS-2 cells showed robust GFP-Annexin-V staining (Ernst, 1998), a hallmark of apoptosis involved in the recruitment of macrophages for engulfment and clearance of apoptotic cells. By 16 hr, only 25% of the cells remained viable. In contrast, no increase in DEVDase activity, Annexin-V staining or cell death was observed with the Casp3-WT or Casp3-

TevS-1 lines treated with Rap. Similar functional results were obtained for the Casp7-TevS-2 line, which showed a 6-fold induction of DEVDase activity by 6 hr, an increase Annexin-V staining by 8 hr, and a large decrease in cellular viability by 16 hr (**Figure 2.5A**). Overall, the relative phenotypic consequences of the WT, TevS-1 and TevS-2 lines were similar for procaspase-3 and procaspase-7, although total DEVDase activity and Annexin-V staining were less for activated Casp7-TevS-2 as compared to the corresponding procaspase-3 allele. These data establish that SNIPer-mediated cleavage and activation of either procaspase-3 or -7 at site-2 *alone* is sufficient to induce robust caspase activation and rapid apoptosis in human cells.

To further understand the functional consequences of prodomain cleavage in cells, we compared the D2A-TevS-2 and TevS-(1,2) alleles (**Figure 2.5B**). In parallel to the *in vitro* results, prodomain removal is neither necessary nor sufficient for caspase activation and apoptosis in cells. A comparison of the lines expressing TevS-2, D2A-TevS-2 and TevS-(1,2)-Casp7 suggested that prodomain removal results in modestly lower DEVDase activity at 6 hr (~40%) and reduced Annexin-V staining.

It has been proposed that the executioner caspases may amplify apoptotic pathways via cleavage of Bid to generate tBid, which induces mitochondrial outer membrane permeability (MOMP), cytochrome-C release and activation of caspase-9 (Green 2005) (**Figure 2.6A**). To examine if executioner caspase activation can 'feedback' and result in the activation of initiator caspases, we tested whether SNIPer-mediated activation of the Casp-7-TevS-2 allele was

sufficient to promote MOMP. We observed several biochemical hallmarks of MOMP after 4 hr of Rap induction, including Bid cleavage and cleavage of procaspase-9 (**Figure 2.6B**). As expected, extensive PARP processing was also detected. These results further confirm the existence of positive feedback signaling between the executioner caspases and upstream apoptotic pathways.

#### **2.3.4 Activated Caspase-3 and -7 are Proteasome Substrates and are Stabilized by a Proteasome Inhibitors**

Processing of engineered procaspase alleles by the SNIPer was examined in cells by immunoblotting with an anti-FLAG antibody that detects the C-terminal His/FLAG epitope tag on both Casp3-TevS-2 and Casp7-TevS-2 constructs. The anti-FLAG antibody detects the full-length proenzyme (32 kDa), a processed form cleaved only at site-1 (29 kDa), and the form cleaved at site-2 to generate the small subunit (12 kDa). We also used a polyclonal caspase-3 antibody that recognizes both caspase-3 subunits. After the addition of Rap to the Casp3-TevS-2 cell line for 6hr, which correlates with the induction of DEVDase activity and apoptosis, the small subunit (~12kDa) of cleaved caspase-3 could not be readily detected by immunoblot. Similar results were observed for Casp7-Tevs-2 (**Figure 2.7A**).

Recent studies have suggested that caspase-3 is ubiquitinated and degraded by the proteasome (Suzuki, Nakabayashi et al. 2001; Choi, Butterworth et al. 2009). To address the role of the Ubiquitin-Proteasome System (UPS) in mediating turnover of SNIPer-activated caspases, we added one of two different proteasome inhibitors, MG-132 or PS-341, in combination with Rap, which

stabilized the cleaved caspase subunits for both caspase-3 and caspase-7, respectively (**Figure 2.7A**). Furthermore, Rap and PS-341 treatment promoted the accumulation of polyubiquitinated caspase-3 detected by immunoblotting as compared to Rap alone (**Figure 2.7B**). To evaluate the effects of the proteasome inhibition on the induction of caspase activity, a time course of Rap-induced processing of the procaspase-3 and -7 allele series was performed  $\pm 5\mu\text{M}$  MG-132. Addition of MG-132 resulted in a 6- to 8-fold enhancement in Rap-induced DEVDase activity for those caspase-3 and -7 alleles that were active in cells (TevS-2, D2A-TevS-2 and TevS-1,2 variants) (**Figure 2.7C**; **Figure 2.8A**).

An increase in caspase activity induced by MG-132 directly correlated to the severity and kinetics of the apoptotic phenotype (**Figure 2.7D**). For example, at 4h, MG-132 increased Annexin-V staining to 60% of cells compared to 25% with Rap alone. By 8 hr, almost 50% of the cells were double positive for Annexin-V and propidium iodide, a marker for the loss of cell membrane integrity. Thus, selective activation of either caspase-3 or -7 in combination with MG-132 robustly increased the level of DEVDase activity, accelerated apoptotic hallmarks such as Annexin-V staining and, by 8 hr, resulted in a large fraction of late-stage apoptotic cells. A minor population of cells were PI positive only, excluding necrotic cell death as the primary response to proteasome inhibitors. The addition of both Rap and MG-132 for as long as 8 hr to Casp-3-WT or Casp7-WT control lines did not induce a increase in caspase activity (**Figure 2.7C**), which further established a direct relationship between the UPS and the *activated forms* of caspase-3 and -7 generated by the SNIPer. We also tested the possibility that

proteasome inhibitors stabilized the SNIPer itself. However, HEK293 cells stably expressing both SNIPer and the TevS-FRET reporter showed no detectable proteasome inhibitor-dependent enhancement of TEV activity by the FRET assay, which was further confirmed by immunoblotting to assess FRET reporter cleavage.

We observed similar levels of Casp7-TevS-2 activation in experiments in which MG-132 or the more potent and selective PS-341 was directly compared (**Figure 2.8B**). To determine if proteasome inhibition promoted executioner caspases in a second cell line, we co-expressed the SNIPer in HeLa cells with retroviruses expressing the Casp3-WT and Casp3-TevS-2 alleles, and we successfully activated the SNIPer and Casp3-TevS-2 in a Rap-dependent fashion (**Figure 2.8C**). Moreover, the level of caspase-3 induction was potently enhanced by MG-132.

### **2.3.5 Activation of Caspase-6 is not Proapoptotic except in Conjunction with Proteasome Inhibition**

Procaspase-6 activation was tested *in vitro* and in cells with the SNIPer. Although procaspase-6 is defined as an executioner caspase and is closely related to caspase-3 and -7 by sequence homology, several distinct features have been observed for this isoform. First, procaspase-6, unlike procaspase-3 and -7, has been reported to self-activate when over-expressed in 293T cells (Klaiman, Champagne et al. 2009). There is an additional loop in the intersubunit linker that bisects a region known as the “safety catch” at the homologous site in procaspase-3. Second, procaspase-6 prefers Val or Thr at P4

unlike caspase-3/-7, which prefer acidic residues at this position (Thornberry, Rano et al. 1997). Procaspase-6, therefore, resembles the initiator caspases by a tendency to self-activate and by similar substrate preferences at P4.

To probe caspase-6 signaling in apoptosis, we applied the TevS insertion strategy to engineer a series of orthogonal procaspase-6 alleles. In addition to site-1 at the junction of the prodomain and the large subunit, there are two reported cleavage sites in the intersubunit linker of procaspase-6 (**Figure 2.9A**): DVVD|N, which we refer to as site-2a, and TEVD|A, or site-2b. Although TEV protease can process sites with a P1' Asn with reduced efficiency, an Ala was substituted at P1' to enhance proteolysis at Site 2a. Thus, three TevS alleles were engineered by insertion at each of the three reported sites (site-1, site-2a with a P1' Ala, and site 2b).

Each construct was expressed in *E. coli* and processed *in vitro* with recombinant TEV protease or recombinant active caspase-3, which is capable of activating WT procaspase-6. A fluorogenic Ac-VEID-AFC peptide substrate, the preferred substrate for caspase-6, was used in these experiments (**Figure 2.9B**). TEV protease could process and activate the TevS-2 variants (2a and 2b), whereas recombinant caspase-3 activated Casp6-WT, and, unexpectedly, Casp6-TevS-2b. Because this allele is WT at site-2a, and caspase-3 was not able to activate the TevS variants at site-2a, we infer that site-2a is a functional caspase-3 processing site (**Figure 2.9B**). TEV protease did activate Casp6-TevS-2a with an Asn at P1' (data not shown), but total VEIDase activity was less than that of the Ala mutant.

Casp6-TevS variants were transduced into HEK293 cells with the SNIPer, and cell-based assays were employed to measure caspase-6 activity in cells. Casp6-TevS-2a was nearly fully processed by the SNIPer by 6 hr (**Figure 2.10A**), but induced VEIDase activity was only 2.4-fold above the control (**Figure 2.9C, left panels**). Cellular viability was not significantly affected by caspase-6 activation at 16 or 24 hours post-Rap for the Casp6-TevS-2a line as compared to Casp6-WT or to an empty vector control (**Figure 2.9D**), and we did not observe a significant apoptotic response by Annexin-V staining (**Figure 2.9C, right panels**).

We hypothesized that the UPS may negatively regulate caspase-6 activity as well. Cells harboring the SNIPer and the Casp6-TevS-2a allele were treated with Rap±MG-132. Remarkably, VEIDase activity with Rap and MG-132 was elevated 14-fold at 4hr compared to Rap alone or to Casp6-WT or Casp6-TevS-1 control lines (**Figure 2.9C, left panels**). Amplification of VEIDase activity was accompanied by a dramatic increase (50%) in Annexin-V positive cells (**Figure 2.9C, right panels**). To further probe the mechanism by which MG-132 promotes caspase-6 activity and apoptosis, we immunoblotted for caspase-6 before and after SNIPer-mediated cleavage. Surprisingly, MG-132 stabilized the unprocessed Casp6-TevS-2a zymogen (**Figure 2.10A, lanes 1 and 2**). This result was independent of SNIPer-induced cleavage and in stark contrast to the mode of caspase-3 and -7 regulation by proteasome. When Casp6-TevS-2a cells were treated with Rap±MG132 (**Figure 2.10A, lanes 3 and 4**), the small subunit was also stabilized with MG-132. Similar results were obtained with PS-341. We

next tested if caspase-6 activation induced MOMP, and after 8hr of sustained Casp6-TevS-2a activation with Rap only, we observed no evidence for MOMP. However, addition of PS-341 and Rap caused a large increase in Bid cleavage, procaspase-9 and PARP (**Figure 2.10B**). These results suggest that both procaspase-6 and activated caspase-6 are targets for negative regulation by the UPS, and caspase-6 is only proapoptotic in the presence of proteasome inhibitors. The severity of the apoptotic phenotype directly correlates with increased VEIDase activity in cells, stabilization of both the pro- and active forms (unlike casase-3 and -7), and recruitment of the endogenous apoptotic machinery via MOMP.

### **2.3.6 Caspases Attack the 26S Proteasome, and Caspase Activation Synergizes with Proteasome Inhibition**

Recently gel-based proteomic data from several other laboratories have identified 10 proteins from the 26S proteasome, mostly in the 19S cap, that are cleaved during apoptosis(Adrain, Creagh et al. 2004; Sun, Butterworth et al. 2004). We have described a new proteomics strategy for the global identification of protease substrates in mammalian cells (Mahrus, Trinidad et al. 2008). This method utilizes an engineered protein ligase called subtiligase to biotin-tag and enrich for nascent N-termini produced during proteolysis, which are then sequenced by LC/MS/MS. A distinct advantage to this technology is that the exact site of proteolysis is identified. Our group has identified >1000 caspase substrates in several cell lines induced by a variety of apoptotic drug stimuli (S. Mahrus, H. Nguyen, and J. Wells, manuscript in preparation). Within this data



set, we found 12 caspase substrates in the 26S proteasome and defined their cleavage sites from MS/MS data (**Table S1**). Ten of these are novel.

Surprisingly, the substrate list included two additional  $\alpha$ -subunit sites and three  $\beta$ -subunit sites of the 20S catalytic core particle. One of the three  $\beta$ -subunit cleavage sites identified by our degradomics experiments, PSB7\_HUMAN or  $\beta$ 2, is a *bona fide* proteasome catalytic subunit, providing trypsin-like hydrolase activity to the complex. The site of caspase proteolysis in the  $\beta$ 2 subunit is only 10 residues from the catalytic N-terminal nucleophile and was likely missed in previous gel-based studies. These mass spectrometry data do not address the extent of cutting for each of these subunits by caspases, nor their functional impact. Nonetheless, the aggregate of our data plus previous publications show that 20 of 33 of the subunits in the 26S proteasome can be cleaved in a cellular context by caspases (**Figure 2.11A**). Further studies will be required to assess the functional impact and timing of these individual cuts on proteasome function.

We then assayed for proteasome function during apoptosis in our system. As caspase activity increased upon activation of the Casp3-TevS-2 allele by the SNIPer, proteasome activity decreased coincidentally (**Figure 2.11B**). These data lead us to hypothesize that there is a negative feedback loop between the executioner caspases and the proteasome (**Figure 2.11C**). This model predicts that caspase activation should synergize with proteasome inhibition. To test this prediction, we modulated the activation of Casp3-TevS-2 by the SNIPer by titrating Rap ( $EC_{50}$  of  $\sim 4$  nM for SNIPer activation of the caspases) in combination with titration of MG-132 to achieve a range of proteasome inhibition

(IC<sub>50</sub> of 0.8  $\mu$ M). We observed dramatic synergy between caspase-3 activation and inhibition of the proteasome (**Figure 2.11D**). For example, at the EC<sub>50</sub> for SNIPer activation by Rap (~2 nM), the addition of saturating MG-132 (5 $\mu$ M) yielded a 7.7-fold induction of caspase activity as compared to 1.6-fold induction with Rap only. Similarly, at the EC<sub>50</sub> for MG-132 (0.8  $\mu$ M), addition of saturating amounts of Rap (8nM) induced a 8.9-fold increase in caspase activity as compared to 2.8-fold with Rap alone.

## 2.4 Discussion

### 2.4.1 Design Considerations for SNIPer

We envisioned an inducible orthogonal protease and substrate system with the following design principles: (1) the orthogonal protease should have no reported substrates in the human or mouse proteome (2) expression and activation must be well tolerated in mammalian cell lines that stably express the protease (3) the time-course of induced protease activity should match or exceed the expected time-course of apoptosis (4) the cognate protease substrate sequence must be tolerated within the context of the target protein and (5) there can be no 'leaky' protease activity when the orthogonal protease and an engineered caspase isoform are co-expressed in living cells.

The remarkable specificity of TEV protease is attributed to the 7-mer cleavage sequence ENLYFQ/S (Parks, Leuther et al. 1994). Although TEV is most often used as recombinant protein *in vitro*, the Naysmith group demonstrated that TEV protease is well tolerated when expressed in *S. cerevisiae* or *D. melanogaster* (Uhlmann, Wernic et al. 2000; Pauli, Althoff et al. 2008), and that ectopic TEV protease expression was capable of cleaving specific protein targets with genetically encoded TevS sequences. Wehr and co-workers elegantly expanded upon this approach by engineering a split-TEV construct based on protein complementation assay technology, and they demonstrated regulated TEV protease activity in several diverse cell-culture systems (Wehr, Laage et al. 2006). However, when we implemented this design as fusions to the ligand-binding domains FKBP and Frb, there was only modest control of activity upon addition of Rap, especially at higher expression levels, and Williams and

colleagues recently observed a similar phenomenon(Williams, Puhl et al. 2009).

We made two essential changes to the previous split-TEV construct: (1) removal of the C-terminal peptide from the C-domain in order to prevent the spontaneous association between N- and C-TEV fragments in the absence of Rap and (2) optimization of the fusion domain partners such that Frb is fused to N-TEV and FKBP to the truncated C-TEV variant. We detect little to no background caspase activity for TevS-caspase alleles in the absence of Rap, and stable cell lines harboring these alleles and the SNIPer were readily produced and showed no impairment of growth (data not shown). Both fragments of the SNIPer exhibited reasonable post-translational stability in cells, and Rap-induced activation was rapid and synchronous as compared endogenous caspase pathways.

#### **2.4.2 Orthogonal Activation of the Executioner Caspases Reveals Regulation by the UPS**

The SNIPer can be used to synchronize populations of cells expressing caspase alleles that mimic discrete states of caspase activation, and this approach has revealed the specific processing requirements for executioner caspase activation and maturation, which are difficult to deconvolute in cells(Pop and Salvesen 2009). Targeted and synchronous caspase activation may facilitate additional functional studies to understand how cell-to-cell variability, pathway redundancy and multiple levels of positive and negative feedback regulate cell death processes.

The constructs presented here should also serve as important tools for

further studying the role of the UPS in restraining caspase activity. A recent study demonstrated that prodomain release was necessary for cIAP-1 binding to caspase-7, which is then polyubiquitinated *in vitro* upon binding cIAP-1 (Choi, Butterworth et al. 2009). Our TevS insertion strategy maintains the native P1' residue, and cIAP-1 binding to cleaved caspase-7 explicitly depends the presence of the N-terminal Ala of the large subunit. We have conducted preliminary studies showing that RNAi-mediated knockdown of cIAP-1, cIAP-2 or XIAP has a modest effect (1.5-2 fold) on enhancing caspase-3 or -7 activity induced by the SNIPer (data not shown). Nevertheless, depletion of individual IAPs did not phenocopy pharmacological inhibition of the proteasome. Several factors could explain this result, including redundancy between the IAPs, different cellular compartment(s) where the SNIPer is activating caspases as compared to DISC or the apoptosome, the stoichiometry of orthogonal caspase to IAP expression, and the kinetics of the SNIPer relative to endogenous initiator caspases. Alternatively, additional E3-ligases may mediate caspase degradation.

Orthogonal caspase activation by the SNIPer revealed synergy between caspase activation and pharmacological inhibition of the proteasome, and these data are consistent with a model in which the UPS potentially restricts executioner caspase activity while the caspases disable the proteasome via subunit proteolysis during apoptosis. Our new proteomics data reveals that caspase proteolysis of the proteasome subunits is more extensive than previously reported. Strikingly, caspase-6 can induce apoptosis only when activated in

combination with proteasome inhibitors, and in this context the UPS appears to control the propagation of positive feedback from SNIPer-induced caspase activation to MOMP.

This is the first example of reciprocal negative regulation between proteases that we are aware of. Mutual antagonism between signaling molecules is metabolically 'expensive,' but it is a common regulatory motif that allows for rapid pulses of activity (Rosenfeld, Elowitz et al. 2002), and we believe that proteasome may also constrain homeostatic (non-apoptotic) caspase activity in this fashion. Our data also provide an additional mechanism for bistability in apoptotic signaling. There are additional feedback loops between the executioner caspases and their substrates in apoptosis pathways, including caspase proteolysis of substrates yielding neo-epitopes that mimic SMAC/Diablo, an IAP inhibitor (Hell, Saleh et al. 2003).

The caspase-6 zymogen is essentially converted to an apoptotic effector caspase by MG-132. Recently, a targeted knockout of PSMC1 (a 19S proteasome subunit) in the mouse neuron results in the depletion of the 26S proteasome and yielded a neurodegenerative-like phenotype including the presence of cleaved caspases (Bedford, Hay et al. 2008). Similarly, genetically encoded proteasome reporters are potently induced in the presence of pathogenic Huntington's Disease (HD) alleles (Wang, Wang et al. 2008). Caspase-6 has already been implicated in the pathogenesis of the disease, but in the context of the present data, a second proteasome-caspase axis of mutual antagonism could exist in which HD patients could have impaired neuronal UPS

function, stabilizing and potentially activating procaspase-6, which has been implicated in cleaving Htt (Graham, Deng et al. 2006), a crucial event in the etiology of the disease.

The proteasome inhibitor Bortezomib (PS-341) is approved as first-line therapy for treating multiple myeloma (MM), a severe hematopoietic malignancy caused the clonal proliferation of plasma cells. Proteasome inhibitors induce apoptosis in these cell types, which can be blocked by caspase inhibitors. Much research has focused on Bortezomib's therapeutic effect on NF- $\kappa$ B signaling, although recent evidence has also pointed to down-regulation of MAPK signaling, p53 activation and stabilization of p27, a cell-cycle inhibitor. Our model implies an additional mechanism: stabilization of the executioner caspases. As a single agent in MM, Bortezomib-mediated caspase stabilization may reduce the apoptotic threshold in these cells. Our data further suggest that combinations of proapoptotic agents to activate the caspases and proteasome inhibitors may synergize to induce apoptosis in additional cancer types.

## **2.5 Experimental Procedures**

### **2.5.1 Cell Culture and Transfections**

The 293T (ATCC#CRL-11268) and HEK293 (ATCC#CRL-1573) cell lines were obtained from the UCSF Cell Culture Facility, and the HeLa (ATCC#CCL-2) cell line was obtained from ATCC. Cells were passaged in MEM with Earle's Balanced Salt Solution supplemented 10% FBS (Invitrogen), 1mM Sodium Pyruvate, 2mM L-Glutamine, 1x Non-Essential Amino Acids and 100ug/mL Normocin (Invivogen).

Transient transfection of plasmids was performed at the 12- or 6-well plates scale. Wells were coated with poly-*d*-lysine prior to plating target cells. Cells were plated to reach ~90% confluence the following day, and transfection mixes were prepared according to the standard Lipofectamine 2000 protocol. For FRET studies, N- and C-TEV fragments were co-transfected over a range of 3:1 to 12:1 molar excess to the TEV-FRET reporter. Rap (Calbiochem) and MG-132 (Sigma) were dissolved in DMSO and were stored as aliquots at -20°C.

### **2.5.2 Phenotypic Analysis of Caspase Activation in Cells**

Caspase-Glo-3/-7, Proteasome-Glo (Chymotrypsin-like activity) and CellTiter-Glo Assays (Promega) were performed according to the manufacture's protocol. Replicate wells in a 96-well plate were mock-treated or with 10nM Rap. At defined endpoints, equal volume of either reagent was added to cells. Cellular lysis proceeded at room temperature for 30 minutes, and luciferase activity was recorded in the SpectraMax M5 plate reader with an integration time of 500 ms. To measure caspase-6 activity, a VEID-R110 (rhodamine 110-based caspase-6



substrate) was used. VEID-R110 was added to a final concentration of 50uM. To assay for PS exposure and membrane integrity, 1uL GFP-Annexin-V, a gift of Dr. Joel Ernst (New York University), and 5ug/mL propidium iodide were added to cells with Annexin-V assay buffer (1x final concentration 10uM HEPES, pH 7.4; 140 uM NaCl; and 2.5 mM CaCl<sub>2</sub>). After 10 minutes at 37°C, fluorescent imaging was performed in the Incell Analyzer 1000 (GE Healthcare).

### **2.5.3 Vector Construction: the SNIPer, FRET Reporter Plasmids, and Orthogonal Caspase Alleles**

We synthesized codon-optimized FKBP-N-TEV (residues 1-118) and Frb-C-TEV S219V (residues 119-242) with a 2x-(GGGGS) 10-residue linker by a synthetic gene construction procedure. Oligonucleotide sequences were designed using the DNABWorks (NIH) web server and assembled into two rounds of PCR during which a Kozak sequence and *NotI* and *Bam*HI restriction sites were added for subcloning into retroviral vectors pQCXIP and pQCXIH (Clontech). pQCXIH-Frb-C-TEV was used as a PCR template to generate a truncation series ending at residues 219, 224, 229 and 234 by incorporating stop codons following the intended residues and these PCR products were re-ligated back into pQCXIH using *NotI* and *Bam*HI sites. A two-round overlapping PCR strategy was employed to swap FKBP and Frb domain fusions between N-TEV and C-TEV-219, and PCR products were ligated into modified pQCXIP and pQCXIH vectors as in-frame fusions to an initiator Met and Myc epitope tag (MEQKLISEEDL) using *Xho*I and *Eco*RI restriction sites (the *Eco*RI site the

pQCXIH vector backbone was removed by site-directed mutagenesis prior to this cloning step).

To generate the FRET reporter plasmid, a two-round, overlapping PCR approach was used to fuse ECFP (a gift from Orion Weiner, UCSF) and YPET (Addgene) with a TevS cleavage site embedded within a flexible linker GGSGSEENLYFQSGSGG between proteins (TevS is underlined). *Bgl*III and *Spe*I sites were added for ligation to *Bam*HI and *Xba*I sites of the expression vector pcDNA3.1-Myc/His (Invitrogen). We used a partially overlapping primer design for inverse PCR to add the DEVDR cleavage peptide to pcDNA3.1-ECFP-TevS-YPET.

Procaspase-3 and procaspase-7, a gift from Dr. Dennis Wolan (UCSF), were PCR amplified and subcloned into the *Nde*I and *Xho*I sites as in-frame fusions to a 6xHis-FLAG epitope tag of a modified pET23B *E. coli* expression vector. Procaspase-6 was also cloned into the same expression vector, but *Xba*I and *Xho*I sites were used because human procaspase-3 encodes an *Nde*I in the open reading frame. The resulting vectors, e.g. casp3-pET23B-6xHis-FLAG, were subjected to single or double rounds of site-directed mutagenesis in order to insert TevS-1 and -2 sites and/or the D2A mutation. As before, we used a partially overlapping primer design to add the TevS cleavage peptide ENLYFQS (DNA sequence 5'-GAAAATCTCTACTTCCAG-3'). The resulting matrix of wild-type and orthogonal caspase alleles was PCR amplified, adding a Kozak and *Not*I and *Eco*RI sites and ligated into a modified pQCXIN (Clontech) vector

backbone with the 6xHis-FLAG epitope tag for retroviral packaging. All constructs were exhaustively DNA sequenced before actual experiments.

#### **2.5.4 Recombinant Protein Production and Caspase Enzyme Assays**

BL21(DE3)-pLysS cells (Stratagene) were transformed with Casp-pET23B-6xHis-FLAG plasmids, and Casp3-D2A-TevS cells were grown in 2xYT media supplemented with 200 µg/ml ampicillin and 50 µg/ml chloramphenicol at 37°C to an OD600 of ~.6. Protein expression was induced with 0.2 mM isopropyl-B-D-thiogalactoside (IPTG) at 30°C for 3 hr. Cells were immediately harvested on ice, resuspended in 100 mM Tris, pH 8.0, 100 mM NaCl (Buffer A) and lysed by microfluidization (Microfluidics). The lysate was cleared by centrifugation at 45,000 x g for 30 minutes at 4 °C and loaded onto HP Ni-NTA affinity column (GE Healthcare). After elution with 200 mM Imidazole, purified fractions were pooled and dialyzed, and protein concentration was determined by the Edelhoch Method.

15 µg of purified Casp3-D2A-TevS-2 was incubated with 1.5µg of recombinant TEV protease in caspase-3 activity buffer (50 mM HEPES, pH 7.4, 0.01% Triton X-100, 50 mM KCl, 0.1 mM EDTA, and 1 mM DTT) and cleaved for 12h at room temperature. Cleaved caspase-3 was diluted to 200nM for kinetic analysis over a range of substrate peptide concentrations (.25µM to 125µM of Ac-DEVD-AFC, Axxora) and the liberation of AFC was monitored by an increase in 365/495 Ex/Em fluorescence over 15 minutes. Michaelis-Menton parameters were fit in Prism 4.0 (Graph Pad Software).

Procaspase-3, -6 and -7 alleles were expressed as described (Roy, Bayly et al. 2001). Small volumes (25-50mL) of M9 media supplemented with 200 µg/ml ampicillin and 50 µg/ml chloramphenicol were induced with .2mM IPTG at OD600. Optimal induction times were previously established for each of the procaspases to prevent autoactivation of wild-type: procaspase-3 (30 minutes), procaspase-7 (45 minutes) and procaspase-6 (90 minutes). At the indicated times, cultures were immediately placed on ice, sonicated in 50 mM Tris-HCl, pH 8.0, .5 mM EDTA and cleared by centrifugation at 20,000 x g for 15 minutes at 4°C. Lysates were normalized for total protein by the BCA assay (Pierce) and were split in triplicate for no treatment, for treatment with rat Granzyme-B (20nM, for casp3 and -7) or active caspase-3 (2nM, for casp6) in caspase-3 activity buffer (50 mM HEPES, pH 7.4, 0.01% TritonX-100, 50 mM KCl, 0.1 mM EDTA, and 1 mM DTT), or for treatment with Tev Protease (1.1uM) with 1mM DTT for 1 hr. To assay for induced activity, the Ac-DEVD-AFC peptide was added to caspase-3 and -7 lists to a final concentration of 10uM in caspase activity buffer and cleavage was monitored as before in a fluorescent microplate reader. To compare between different activated forms and control for variable processing by TEV or GrB, active-site titrations with VAD-FMK were performed to measure the concentration of active caspase-3 or -7. Procaspase-6 lysates were incubated in caspase activity buffer supplemented with 30uM Ac-VEID-AFC and 5mM DTT. Caspase-3 processing of Ac-VEID-AFC was observed and accounted for by measuring VEIDase activity of caspase-3 alone and subtracting this value in caspase-6 samples treated with caspase-3.

### **2.5.5 Immunoblotting and Immunoprecipitation**

For immunoblotting, cells were lysed in 1% SDS in PBS, pH-7.4 supplemented with protease inhibitors (Halt, Pierce), 20uM DEVD-FMK and 20uM MG-132 and sonicated. Lysates were fractionated by SDS-PAGE, blotted to PVDF membranes and probed with the following primary antibodies: anti-FLAG-M2-HRP (Sigma), anti-V5 (Bethyl Laboratories#A190-120P), anti-Myc (Cell Signaling Technology#2278), anti-Casp-3 (CST#9662), anti-casp-3 (Biomol#SA-320), anti-Bid (CST#2002), anti-Casp-9 (CST#9508), anti-PARP (BD#4C10-5), anti-GAPDH (CST#2118), and anti-GFP (A.V. Polyclonal, Clontech). To detect covalent ubiquitination, Casp3-TevS-2 cells were transfected with pcDNA3.1-Ub-V5 for 24 hr and treated with 10nM rapamycin ± 500nM PS-341. Cells were lysed in M-PER lysis buffer (ThermoPierce) with protease inhibitors (Halt, Pierce), 20uM DEVD-FMK, 20uM MG-132 and N-Ethyl-Maleamide. Casp-3-TevS-2 was immunoprecipitated with pre-washed anti-FLAG-M2-agarose beads (Sigma). After elution with 3x-FLAG peptide, immunoprecipitated Casp-3 was blotted as above.

### **2.5.6 Live Cell Imaging of FRET**

Transfected cells were plated at  $2 \times 10^4$  per 96-well in black clear-bottom microplates (Greiner) in quadruplicate. After treating cells with rapamycin for a specified time period, media was removed from the wells, and the plate was analyzed with a SpectraMax M5 (Molecular Devices) plate reader in well-scan

mode at three excitation / emission (Ex/Em) wavelengths using an automatic cut-off filter: 420/485 nm for ECFP, 485/535 nm for YPET and 420/535 nm for FRET. After background correction of mock-transfected cells, ECFP and YPET bleedthrough were calculated for each experiment by measuring the apparent FRET (420/535 nm) signal generated from cells transfected with ECFP or YPET only. Corrected FRET values were internally normalized by dividing by ECFP to control for variation in reporter expression levels between wells: normalized FRET = [FRET (420/535nm) - ECFP (420/485nm) x ECFP\_bleed - YPET (485/535nm) x YPET\_bleed]/ECFP.

SNIPer and TEV-FRET and DEVDR-FRET transfected cells were plated on #1.5 coverslips (Lab-Tek) coated with poly-*d*-lysine for live-cell imaging of FRET protease reporters in phenol-free CO<sub>2</sub>-independent media (Invitrogen) supplemented with 2.5% FBS and 2mM L-Glutamine. Images were taken at 37°C on a Nikon Eclipse TE2000-E inverted microscope with a Plan Apo 20x/0.75 objective and CoolSNAP HQ2 CCD camera (Photometrics) with Perfect Focus (Nikon). Nikon Elements software version 3.0 was used for image acquisition, and images were further processed in ImageJ. Fluorescent images were background corrected, and ratiometric ECFP / YPET values were analyzed using the custom plug-ins Ratio\_Plus and Movie\_Explorer, a kind gift from Dr. Peter Sorger and Dr. John Albeck (Harvard Medical School)(Albeck, Burke et al. 2008).

### 2.5.7 Generation of Stable Cell Lines

Retroviral supernatants were generated by transfecting SNIPer plasmids (Frb-N-TEV and FKBP-C-TEV-219) or engineered caspase alleles into the GPG packaging cell line, a gift of Orion Weiner (UCSF), using the standard Lipofectamine 2000 protocol. GPG cells were cultured in DMEM supplemented with 10% FBS, 100ug/uL Normocin, 2ug/mL puromycin (Invivogen), 300ng/uL G418 (Invitrogen) and 1ug/mL Doxycycline (Dox) (Sigma) and, 24 hr prior to transfection, GPG cells were set in poly-*d*-lysine coated wells 1 x 10<sup>6</sup> per 6-well or 4 x 10<sup>6</sup> per 10cm dish. Retroviral supernatants were harvested 4-5 days after transfection without Dox, contaminating cellular debris was removed by centrifugation at 2000 rpm x 10 min or by filtration with a .4uM filter, and clarified media with retrovirus was added to HEK293 cells for 8-20 hrs with 8ug/mL polybrene (Sigma).

The two halves of the SNIPer were packaged as retroviruses. Viral supernatants were used to serially-transduce HEK293 or HeLa cells. Since each SNIPer open-reading frame and selectable marker is encoded on the same mRNA transcript in these vectors, maximal expression of the SNIPer components was enforced by selecting only those clones that survived the highest concentrations of puromycin and hygromycin tolerated during selection. Up to 3ug/mL puromycin and 350ug/mL hygromycin (Roche) were added 24 h post-transduction to select for double-positive cells (3-5 days). Stable clones were then pooled and transduced for a second time with the panel of engineered procaspase-3 and -7 alleles in a third bicistronic vector, pQCXINeo with a COOH-terminal His/FLAG epitope tag. This transduction was performed at a

multiplicity of infection (MOI) of ~0.2 to ensure single-copy integration. Stable pools of each procaspase allele were then selected and maintained at an intermediate G418 concentration. Once selected, stable SNIPer-HEK293-Casp lines were propagated in media with 1.5ug/mL puromycin, 150ug/mL hygromycin and 300ug/mL G418.

### **2.5.8 Degradomics**

Jurkat, DB and HEK293 cells were induced by a variety of apoptotic inducers and cell lysates were subjected to the previously described N-terminal Degradomics workflow (Mahrus, Trinidad et al. 2008). Non-acetylated N-termini (including products of caspase proteolysis) were labeled with a biotinylated peptide ester by subtiligase and subjected to gel-filtration. Labeled proteins were captured by avidin-agarose and released by on-bead digest with Tev Protease. After trypsin digest, tryptic peptides were desalted and subjected to off-line ion-exchange chromatograph and reverse-phase liquid chromatography and tandem mass spectrometry. MS spectra were searched against the Swiss-Prot database to identify putative substrates.



**Table 2.1: Caspase Substrates of the 26S Proteasome**

	Subunit Class	Subunit	Uniprot	Gene	Cleavage Site		
20S	alpha	$\alpha$ 1	PSA6_HUMAN	PSMA6			
		$\alpha$ 2	PSA2_HUMAN	PSMA2			
		$\alpha$ 4	PSA7_HUMAN	PSMA7	TVFSPD GHLFQV		
		$\alpha$ 5	PSA5_HUMAN	PSMA5	KIVEID AHIGC		
		$\alpha$ 6	PSA1_HUMAN	PSMA1			
		$\alpha$ 7	PSA3_HUMAN	PSMA3			
		beta	$\beta$ 2	PSB7_HUMAN	PSMB7	GVVYKD GIVLGA	
	$\beta$ 6		PSB1_HUMAN	PSMB1	AIAGED FAIVAS		
	$\beta$ 7		PSB4_HUMAN	PSMB4	IPSTPD SFMDPA		
	19S	ATPase	Rpt1	PRS2_HUMAN	PSMC2		
			Rpt2	PRS1_HUMAN	PSMC1		
			Rpt3	PRS6B_HUMAN	PSMC4	LNQMD GFDQNV	
			Rpt4	PRS10_HUMAN	PSMC6	LLNQMD GFDTLH	
			Rpt5	PRS6A_HUMAN	PSMC3	DEAEQD GIGEEV	
Non-ATPase						LLNQLD GFQPNT	
			Rpt6	PRS8_HUMAN	PSMC5	FMDEID SIGSSR	
			Rpn1	PSMD2_HUMAN	PSMD2		
			Rpn2	PSMD1_HUMAN	PSMD1		
			Rpn3	PSMD3_HUMAN	PSMD3	STGEAD GKTAAA	
			Rpn6	PSD11_HUMAN	PSMD11	VKMEVD YSATVD	
			Rpn10	PSMD4_HUMAN	PSMD4		
		11S		PA28 $\alpha$	PSME1_HUMAN	PSME1	KISELD AFLKEP
				PA28 $\gamma$	PSME3_HUMAN	PSME3	

Caspase substrates identified in this study or in previous published studies. Subunit nomenclature according to Baumeister (Baumeister et al., 1998). The site of cleavage listed if identified with a line to denote the location of the scissile bond.

**Table 2.2 SNIPer DNA Oligonucleotides**

<b>DNA Oligonucleotides</b>	
<b>Original TEV constructs</b>	<b>DNA Sequence (5'-3')</b>
Fwd_FKBP_N_TEV_NotI	AAA GGG AAA GCG GCC GCC CAC CAT GGG TGT GCA GGT AGA AAC AA
Rev_FKBP_N_TEV_BamHI	AAA GGG AAA GGA TCC TCA GGT CTG GAA GTT GGT GGT CAC CAG GCA GAT T
Fwd_Frb_C_TEV_NotI	AAA GGG AAA GCG GCC GCC CAC CAT GGA GAT GTG GCA CGA GGG ACT CGA A
Rev_Frb_C_TEV_BamHI	AAA GGG AAA GGA TCC TCA CTG GCT ATA CAC CAG CTC GTT CAT AA
<b>Truncation of Frb-C-TEV-FL</b>	
R_Oligo_C_TEV_219_BamHI	AAA GGG AAA GGA TCC TCA CAT GAA CAC CTT ATG TCC GCC CCA AA
R_Oligo_C_TEV_224_BamHI	AAA GGG AAA GGA TCC TCA TTC CTC GGG CTT GAC CAT GAA CAC CTT A
R_Oligo_C_TEV_229_BamHI	AAA GGG AAA GGA TCC TCA AAC GGG CTG GAA GGG TTC CTC GGG CTT GA
R_Oligo_C_TEV_234_BamHI	AAA GGG AAA GGA TCC TCA CTG AGT GGC TTC CTT AAC GGG CTG GAA
<b>FKBP / Frb Swap</b>	
Fwd_Outer_Frb_N_TEV_XhoI	AAA GGG AAA CTC GAG ATG GAG ATG TGG CAC GAG GGA CTC GAA
Rev_Inner_Frb_N_TEV	CCC CCA CCG CCG CTT CCG CCA CCT CCC TGC TTG CTG ATC CTC CTG AAC A
Fwd_Inner_Frb_N_TEV	GGC GGA AGC GGC GGT GGG GGA AGC GGC GAG AGC CTT TTC AAG GGC CCG AGG GAC TA
Rev_Outer_Frb_N_TEV_EcoRI	AAA GGG AAA GAA TTC TCA GGT CTG GAA GTT GGT GGT CAC CAG GCA GAT T
Fwd_Outer_FKBP_C_TEV_XhoI	AAA GGG AAA CTC GAG GGT GTG CAG GTA GAA ACA ATC TCC CCG GGA GAT
Rev_Inner_FKBP_C_TEV	CCT CCC CCG CTG CCA CCA CCG CCT TCC AGC TTG AGC AGC TCC ACA TCA A
Fwd_Inner_FKBP_C_TEV	GGT GGT GGC AGC GGG GGA GGT GGT TCC AAG TCC ATG AGC AGC ATG GTC TCT GAT A
Rev_Outer_FKBP_C_TEV_EcoRI	AAA GGG AAA GAA TTC TCA CAT GAA CAC CTT ATG TCC GCC CCA AAG AA
<b>Construction of FRET Vectors</b>	
Fwd_Outer_FRET_TevS_BglII	AAA GGG AAA AGA TCT CCA CCA TGG GAG GCT CCC TCG AGG GAG GCT CCG GAT CCG TGA GCA AGG GCG AGG AGC TGT TCA
Rev_Inner_FRET_TevS	CTG GAA GTA GAG ATT TTC GGA GCC GGA GCC CCC CTT GTA CAG TTC GTC CAT GCC GAG AGT GAT
Fwd_Inner_FRET_TevS	CCG GCT CCG AAA ATC TCT ACT TCC AGA GTG GCA GCG GAG GCT CCG TGA GCA AAG GCG AAG AGC TGT T

Rev_Outer_FRET_TevS_Spel	AAA GGG AAA CTA GTT TAC GTA GAA TCG AGA CCG AGG AGA GGG TTA GGG ATA GGC TTA CCC TTA TAG AGC TCG TTC ATG CCC TCG GTG AT
FRET_DEVD_R_top	CGG CGA TGA AGT GGA CAG GGG TAC CAT GGT GAG CAA AGG CGA AGA GCT GTT CAC C
FRET_DEVD_R_bottom	GCT CAC CAT GGT ACC CCT GTC CAC TTC ATC GCC GAG AGT GAT CCC GGC G
<b>Construction of Orthogonal Caspase Constructs</b>	
Fwd_Casp3_NotI	AAA GGG AAA GCG GCC GCC ACC ATG GAG AAC ACT GAA AAC TCA GTG
Fwd_Casp3_NdeI	AAA GGG AAA CAT ATG GAG AAC ACT GAA AAC TCA GTG GAT TCA A
Rev_Casp3_EcoRI	AAA GGG AAA GAA TTC GTG ATA AAA ATA GAG TTC TTT TGT GAG CAT GGA AA
TevS-1 Top	CAA TGG AAA ATC TCT ACT TCC AGT CTG GAA TAT CCC TGG ACA ACA G
TevS-1 Bottom	CCA GAC TGG AAG TAG AGA TTT TCC ATT GAT TCG CTT CCA TGT ATG ATC
TevS-1 D_A Top	CAA TGG CCT CTG GAA TAT CCC TGG ACA ACA GTT ATA AAA TGG
TevS-1 D_A Bottom	CCA GAG GCC ATT GAT TCG CTT CCA TGT ATG ATC TTT GGT TCC
TevS-2 Top	GAG ACA GAA AAT CTC TAC TTC CAG AGT GGT GTT GAT GAT GAC ATG G
TevS-2 Bottom	CCA CTC TGG AAG TAG AGA TTT TCT GTC TCA ATG CCA CAG TCC AGT TCT GTA CC
Fwd_Casp6_NotI	AAA GGG AAA GCG GCC GCC ACC ATG AGC TCG GCC TCG GGG CTC CGC A
Fwd_Casp6_XbaI	AAA GGG AAA TCT AGA AAT AAT TTT GTT TAA CTT TAA GAA GGA GAT ATA CAT ATG AGC TCG GCC TCG GGG CTC CGC AGG GGG
Rev_Casp6_EcoRI	AAA GGG AAA GAA TTC ATT AGA TTT TGG AAA GAA ATG CAG CTT TTT AGT TA
TevS-1 Top	GAA ACA GAA AAT CTC TAC TTC CAG GCC TTC TAT AAA AGA GAA ATG TTT GAT CC
TevS-1 Bottom	GAA GGC CTG GAA GTA GAG ATT TTC TGT TTC TGT CAT GTT TTC TTC C
TevS-2 Top_DVVD_N	GTA GTA GAA AAT CTC TAC TTC CAG AAT CAG ACA GAG AAG TTG GAC ACC
TevS-2 Bottom_DVVD_N	CTG ATT CTG GAA GTA GAG ATT TTC TAC TAC ATC CAA AGG AAT GAC TGG
TevS-2 Top_DVVD_A	GTA GTA GAA AAT CTC TAC TTC CAG GCA CAG ACA GAG AAG TTG GAC ACC
TevS-2 Bottom_DVVD_A	CTG TGC CTG GAA GTA GAG ATT TTC TAC TAC ATC CAA AGG AAT GAC TGG
TevS-2_Top_TEVD	GAG GTG GAA AAT CTC TAC TTC CAG GCA GCC TCC GTT TAC ACG CTG CCT GC
TevS-2_Bottom_TEVD	GCT GCC TGG AAG TAG AGA TTT TCC ACC TCA GTT ATG TTG GTG TCC AAC

Fwd_Casp7_NotI	AAA GGG AAA GCG GCC GCC CAC CAT GGC AGA TGA TCA GGG CTG TAT TGA A
Fwd_Casp7_NdeI	AAA GGG AAA CAT ATG GCA GAT GAT CAG GGC TGT ATT GAA
Rev_Casp7_EcoRI	AAA GGG AAA GAA TTC TTG ACT GAA GTA GAG TTC CTT GGT GAG CAT
TevS-1 Top	CAG TGG AAA ATC TCT ACT TCC AGG CTA AGC CAG ACC GGT CCT CGT TTG TAC C
TevS-1 Bottom	CTT AGC CTG GAA GTA GAG ATT TTC CAC TGA ATC TTC ATT TGC TGA ATC C
TevS-1 D_A Top	GAT TCA GTG GCA GCT AAG CCA GAC CGG TCC TCG
TevS-1 D_A Bottom	GCT TAG CTG CCA CTG AAT CTT CAT TTG CTG AAT CC
TevS-2 Top	GGC CGA AAA TCT CTA CTT CCA GTC GGG GCC CAT CAA TGA CAC AGA TGC TAA TCC
TevS-2 Bottom	CCG ACT GGA AGT AGA GAT TTT CGG CCT GGA TGC CAT CAT CAA GCT CGG TCC CTC GG

## **2.6 ACKNOWLEDGEMENTS**

We are grateful to members of the Wells lab for useful discussions and to Emily Crawford for curation of the laboratory caspase substrate database. We also thank the UCSF NIKON Imaging Center and Dr. Kurt Thorn for assistance with live cell imaging. We also thank Drs. Al Burlingame, David Maltby, and Jon Trinidad for use of the Mass Spectrometry Facility at the Mission Bay Campus of UCSF. This work was supported by NIH R01 GM081051 and CA136779 (JAW), The Hartwell Foundation (JAW) and the University of California Systemwide Biotechnology Research & Education Program GREAT Training Grant 2008-23 (DG).

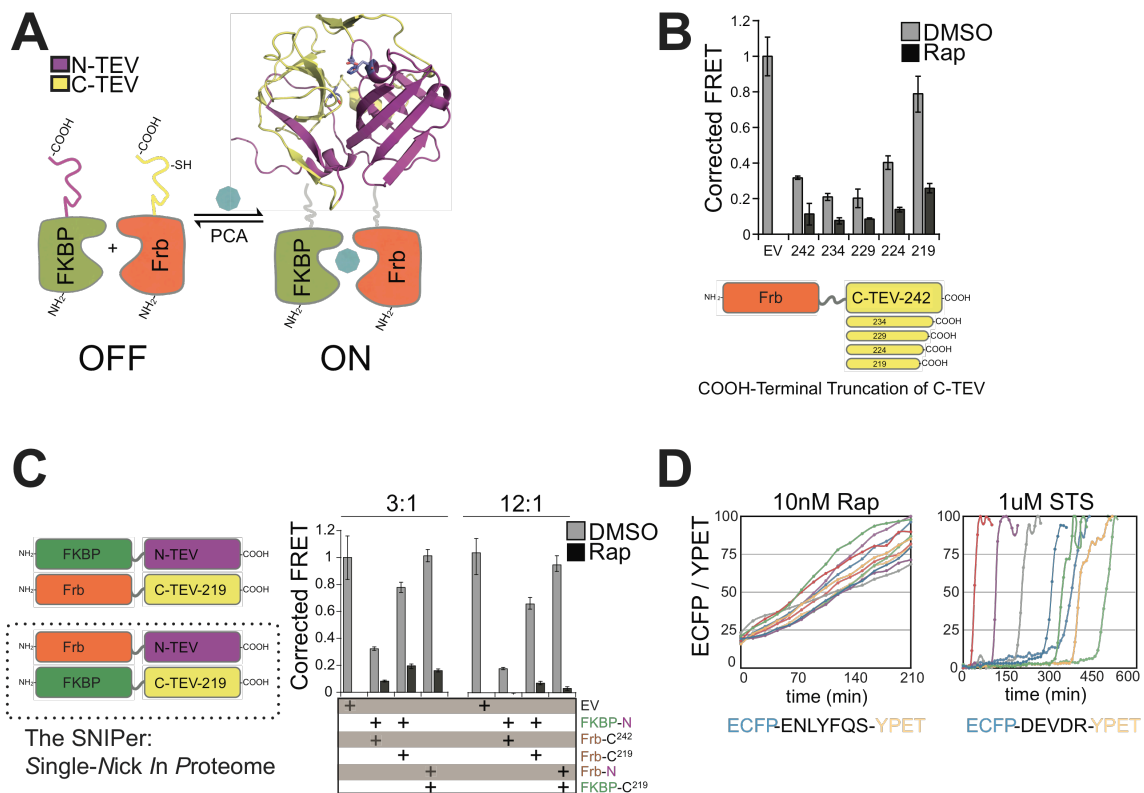


**Figure 2.1. Engineering the SNIPer for Conditional Proteolysis**

(A) Generalized scheme for a ligand-inducible orthogonal protease based on the protein complementation system. (B) Plasmids with deletions at the C-terminus of Frb-C-TEV or empty vector (EV) were co-transfected with FKBP-N-TEV and ECFP-TevS-YPET in 293T cells. 10nM Rap was added for 12h and FRET measurements were recorded using a fluorescent microplate reader. Data are presented as corrected averages of FRET / ECFP from an experiment performed in quadruplicate (Error Bars $\pm$ SD). (C) N-TEV and C-TEV-219 were fused to either FKBP or Frb and assayed by FRET in quadruplicate as above. Transfections were performed with 3x or 12x molar excess of Tev constructs to reporter plasmid (Error Bars $\pm$ SD). (D) The kinetics and cell-to-cell heterogeneity of SNIPer-mediated protease activity were compared to endogenous caspase activation by live-cell fluorescent imaging. HEK293 cells were transfected with the SNIPer and ECFP-TevS-YPET or ECFP-DEVDR-YPET, a reporter for caspase-3/-7 activity in cells, and treated with 10nM Rap or 1uM staurosporine. Live-cell FRET measurements were recorded every 15 minutes.

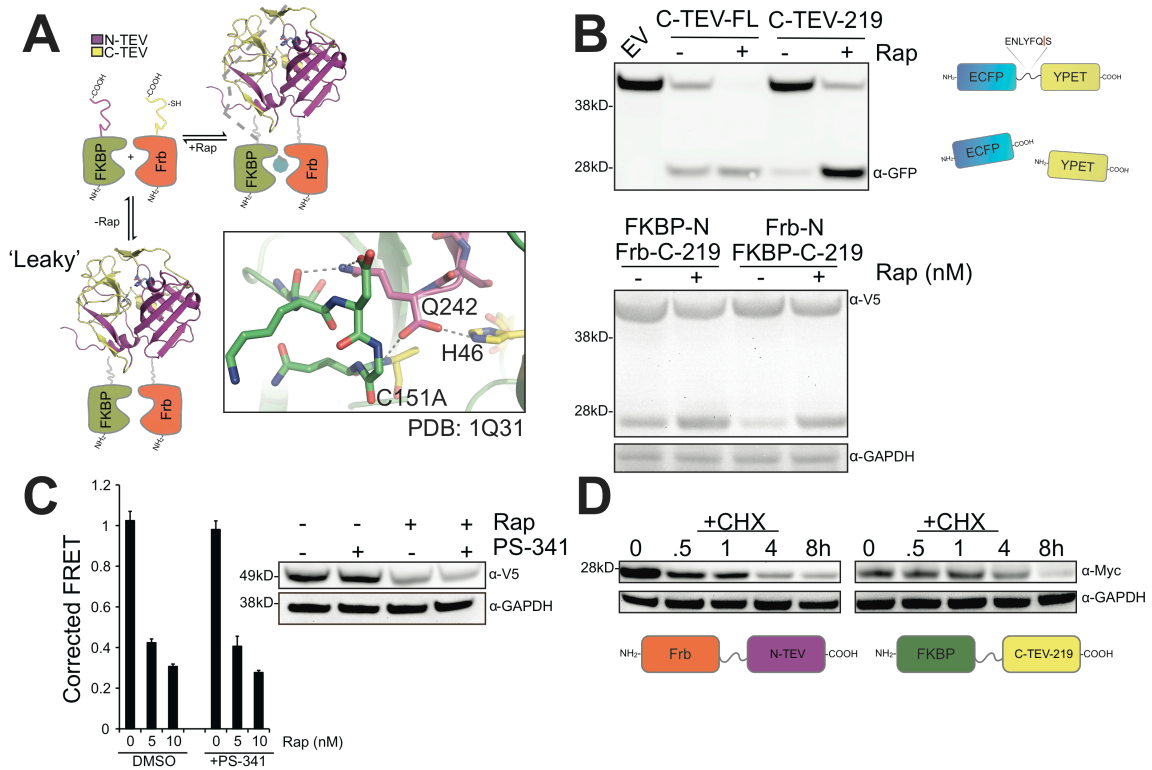


**Figure 2.2. SNIPer Characterization**

(A) Scheme for regulated split-TEV folding and activation (+Rap) or unregulated split-TEV activity (-Rap). The crystal structure of inactive (C151A) TEV protease (PDB Code: 1Q31) reveals that the C-terminal tail (residues 234-242) of the full-length (FL) protease binds to the active site, and thus may act as an intramolecular competitive inhibitor for substrate binding. The C-terminal sequence, ELVYSQ, closely resembles the P6-P1 residues of the canonical substrate sequence. Furthermore, the  $\alpha$ -carboxylate of Glu242 potentially makes critical hydrogen bonds to the oxyanion hole and to the catalytic His81. Because the C-terminal peptide bridges the interface of the N-TEV and C-TEV protein complementation fragments, it is possible that the C-terminus of FL TEV promotes the assembly of the split-TEV constructs in the absence of rapamycin and contributes to the leaky activity.

(B) 10ug of lysate from 293T cells transfected with the indicated plasmids were fractionated by SDS-PAGE and immunoblotted with an anti-GFP antibody (top panel). 50ug of lysate from 293T cells transfected with the indicated plasmids were fractionated by SDS-PAGE and immunoblotted with an anti-V5 antibody, which recognizes the COOH-terminus of the FRET construct (bottom panel).

(C) HEK293 cells stably-expressing the optimized SNIPer constructs and the ECFP-TevS-YPET construct were treated with 0, 5 or 10nM Rap ±PS-341 and FRET measurements were performed on a fluorescent microplate reader. Data are presented as corrected averages of FRET / ECFP from an experiment performed in quadruplicate (Error Bars±SD). Lysates (10ug per lane) for this experiment were immunoblotted for anti-V5 and anti-GAPDH. (D) 293T cells were transfected with myc-tagged Frb-N-TEV (left panel) and FKBP-C-TEV (right panel) and treated with 10ug/mL cyclohexamide for the indicated times. Lysates were immunoblotted with anti-Myc and anti-GAPDH.



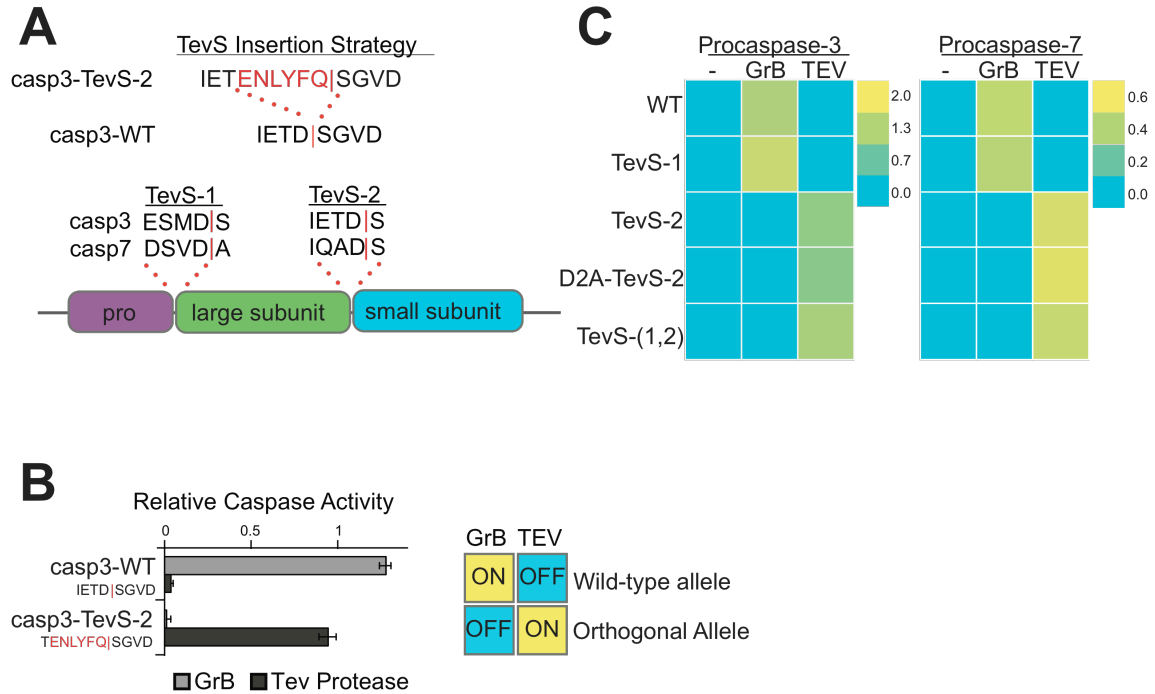


**Figure 2.3. Design and In Vitro Characterization of Orthogonal Procaspase-3 and -7 Alleles**

(A) We employed the indicated TevS insertion strategy to convert caspase sites into SNIPer-cleavage sites as shown for caspase-3. The sequences (P4-P1' with a red bar to denote the scissile bond) and location of site-1 and site-2 are shown in the context of executioner caspase domain structure below. (B) *In vitro* activation of wild-type procaspase-3 (Casp3-WT) or Casp3-TevS was assayed by expressing each allele in *E. coli*, treating with either rat Granzyme-B (20nM) or TEV Protease (1.1uM) for 1h, and measuring caspase activity with 10uM Ac-DEVD-AFC. Data are presented as the average rate of substrate cleavage (RFU s<sup>-1</sup>) from an experiment performed in triplicate (Error Bars±SD). (C) Caspase activity of the procaspase-3 and -7 matrix of orthogonal alleles was performed as above and is presented as a heat map. Abbreviations: WT, wild-type; TevS-1, TevS insertion at site-1; TevS-2, TevS insertion at site-2; D2A-TevS-2, TevS insertion at site-2 with a non-cleavable site-1; and TevS-(1,2), TevS insertions at site-1 and site-2.

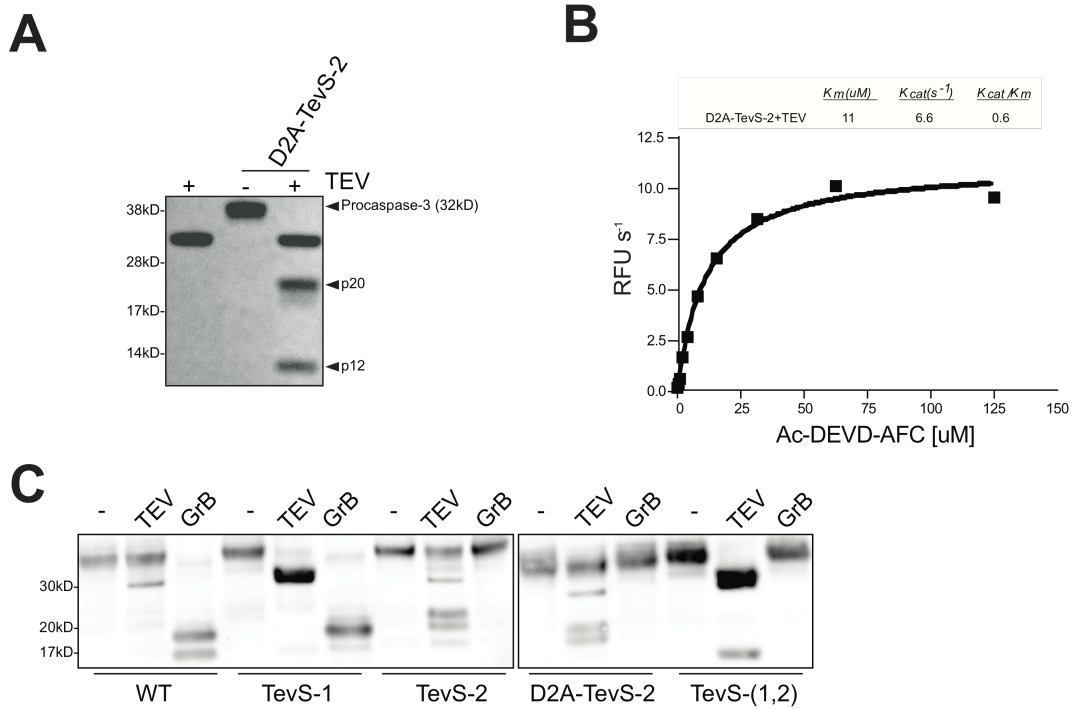
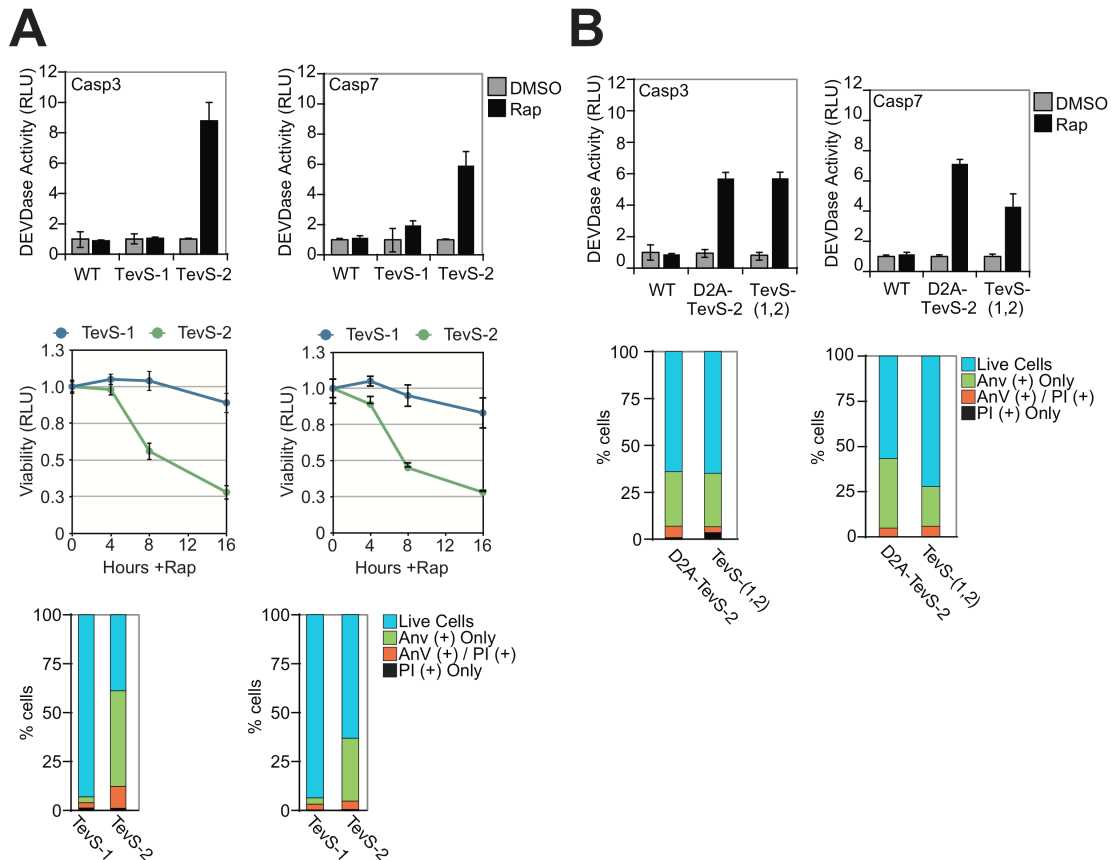


## Figure 2.4. In Vitro Characterization of Casp3-TevS Alleles

(A) Casp3-D2A-TevS was expressed in *E. coli*, purified by Ni-NTA chromatography and cleavage  $\pm$ TeV protease overnight at 4°C was analyzed by SDS-PAGE (Lane 1: Tev only, Lane 2: Casp3-D2A-Tev-2 only, Lane 3: Tev+Casp3-D2A-Tev-2)

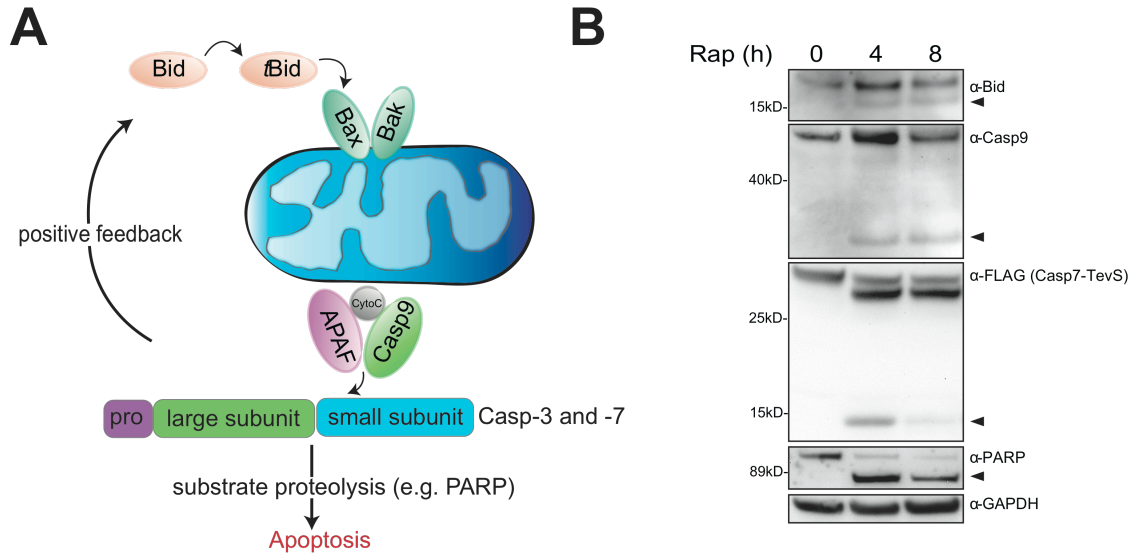
(B) Michaelis-Menton parameters were measured with 10nM Casp3-D2A-TevS and Ac-DEVD-AFC.

(C) The orthogonal procaspase-3 panel was expressed in *E. coli*, treated with GrB (20nM) or Tev Protease (1.1 $\mu M$ ) for 1 hr, fractionated by SDS-PAGE and immunoblotted. Cleavage of the zymogen is partially incomplete for the TevS-2 and D2A-TevS-2 alleles.



**Figure 2.5. Phenotypic Analysis of SNIPer-Mediated Activation of Procaspase-3 and -7 in Cells**

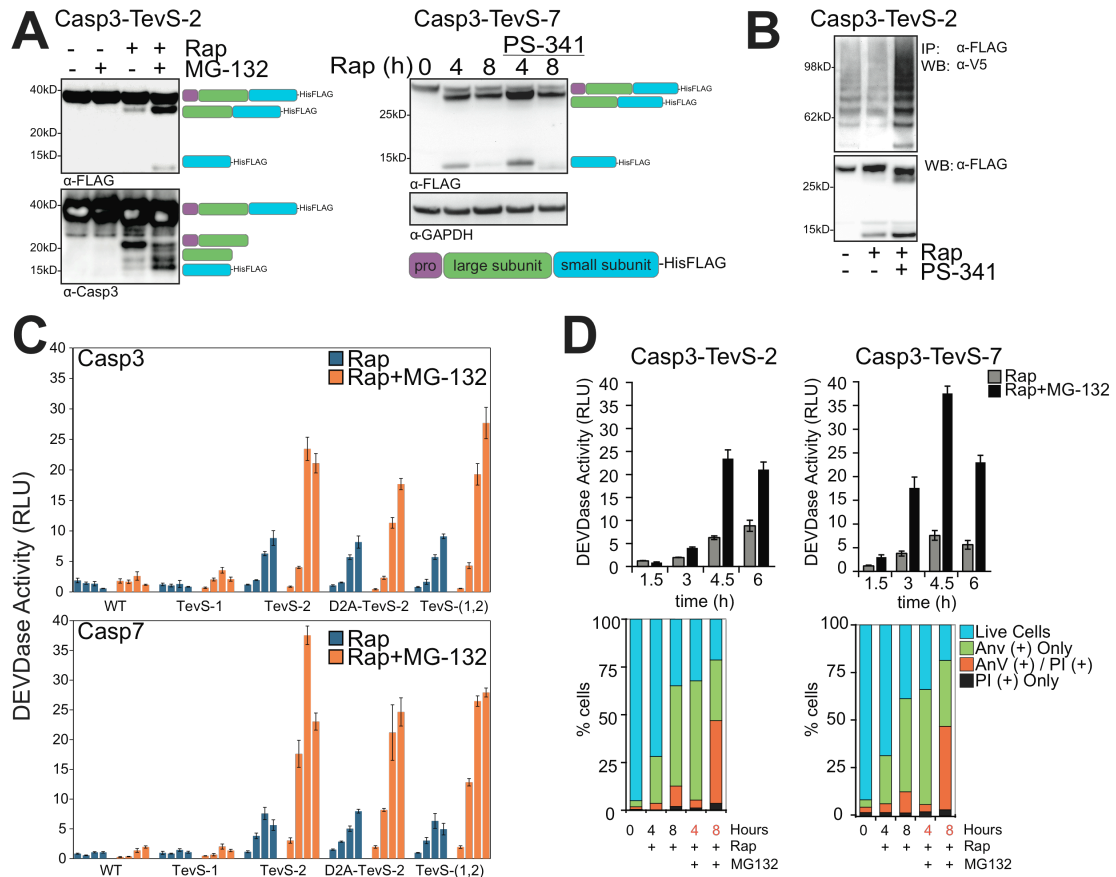
(A) HEK293 cells stably expressing the SNIPer and indicated procaspase-3/-7 alleles were treated with DMSO or 10nM Rap over the course of 16 hr. The indicated cells lines were assayed for caspase activity using the Caspase-Glo-3/-7 assay at 6 hr (top row), for total cellular viability using the Cell-Titer-Glo assay the indicated times (line graph, bottom row), and for phosphatidylserine (PS) exposure/membrane integrity by staining with GFP-Annexin-V and propidium iodide (PI) and imaging by fluorescent microscopy at 8 hr. Each data point is presented as an average of triplicate experiments (Error Bars $\pm$ SD). (B) HEK293 stably expressing procaspase-3/-7 D2A-TevS and TevS-(1,2) alleles were analyzed for caspase activity and for GFP-Annexin-V / PI staining exactly as above.



**Figure 2.6. Casp7 Activation by the SNIPer Yields MOMP**

(A) Model for positive feedback from executioner caspase activation by split-TEV resulting in MOMP.

(B) The Casp7-TevS-2 line was treated with 10nM rapamycin for 0, 4 or 8 hr and blotted for critical apoptotic pathway components: Bid, caspase-9, the engineered Casp7 allele (FLAG epitope tag), PARP and GAPDH.

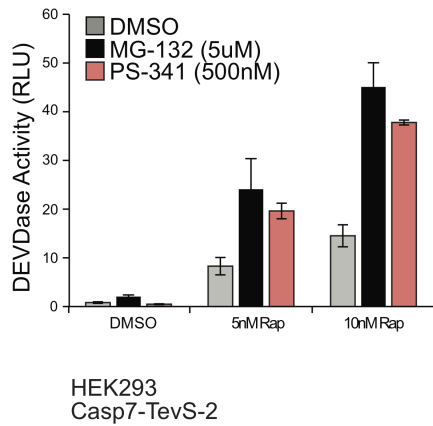
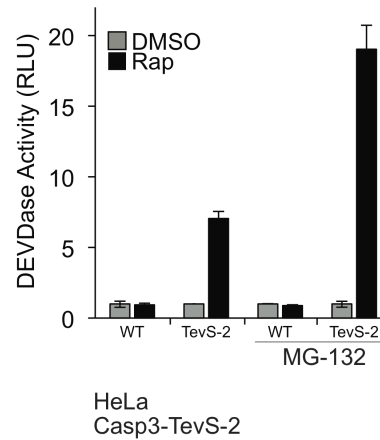


**Figure 2.7. Caspase-3 and -7 Regulation by the Proteasome**

(A) The Casp3-TevS-2 line was treated with DMSO or 10nM Rap  $\pm$ 5 $\mu$ M MG-132 for 6 hr and cell lysates were blotted with anti-FLAG M2 (left panel, top) or anti-caspase-3 (left panel, bottom) antibodies. The expected processing intermediates detected by each antibody are shown to the right of the immunoblots. The Casp7-TevS-2 line was treated with 10nM Rap for 4 or 8 hr  $\pm$ 500nM PS-341 and immunoblotted with anti-FLAG M2 (right panel) and anti-GAPDH. (B) The Casp3-TevS-2 line was transfected with pcDNA3.1-V5-Ubiquitin for 24 hr and treated with DMSO, 10nM Rap or 10nM Rap + 500nM PS-341 for 4 hr. Cell lysates were immunoprecipitated with anti-FLAG M2 agarose and immunoblotted for covalent ubiquitin with an anti-V5 antibody or with anti-flag to assess caspase-3 recovery. (C) The Casp3-TevS-2 and Casp7-TevS-2 lines were treated with 10nM Rap (blue bars) or 10nM Rap and 5 $\mu$ M MG-132 (orange bars). Caspase activity was measured every 1.5 hr in triplicate (Error Bars  $\pm$ SD). (D) Casp3-TevS-2 and Casp7-TevS-7 cell lines were treated with 10nM Rap  $\pm$ 5 $\mu$ M MG-132 and assayed for caspase activity as above (top) or by staining with GFP-Annexin-V and PI and imaging with fluorescent microscopy (bottom) for indicated time courses in triplicate (Error Bars  $\pm$ SD).

**A**

		+ Rap (RLU / h)	+ Rap + MG-132 (RLU / h)	Fold MG-132 Enhancement
Caspase-3	TevS-2	2.1±.3	11.5±.54	5.4
	D2A-TevS-2	1.42±.06	5.4±.21	3.8
	2x-TevS	1.8±.43	8.2±.26	4.6
Caspase-7	TevS-2	1.7±.14	7.5±.66	4.4
	D2A-TevS-2	2.1±.18	4±.21	2.3
	2x-TevS	1.9±.07	6.4±.60	3.2

**B****C**

### Figure 2.8. Cell-based Analysis of Caspase Activation with Proteasome Inhibition

(A) Table summarizing the rates of caspase activity in response to proteasome inhibition from 1.5 to 6 hr post-SNIPer induction. Replicate data points of caspase activity at 1.5 hr intervals were measured to calculate the rate of DEVDase activation in cells.

(B) Casp3-TevS-2 cells were treated with 0, 5 or 10nM rapamycin with DMSO, 5uM MG-132 or 500nM PS-341 and assayed 4hr later with Casp-Glo-3/-7. (Error Bars±SD for an experiment in quadruplicate).

(C) HeLa cells stably expressing the SNIPer and Casp3-WT or Casp3-TevS-2 alleles were treated with DMSO or 10nM rapamycin ±5uM MG-132 for 6 hr and assayed with CaspaseGlo-3/-7 in triplicate (Error Bars±SD).

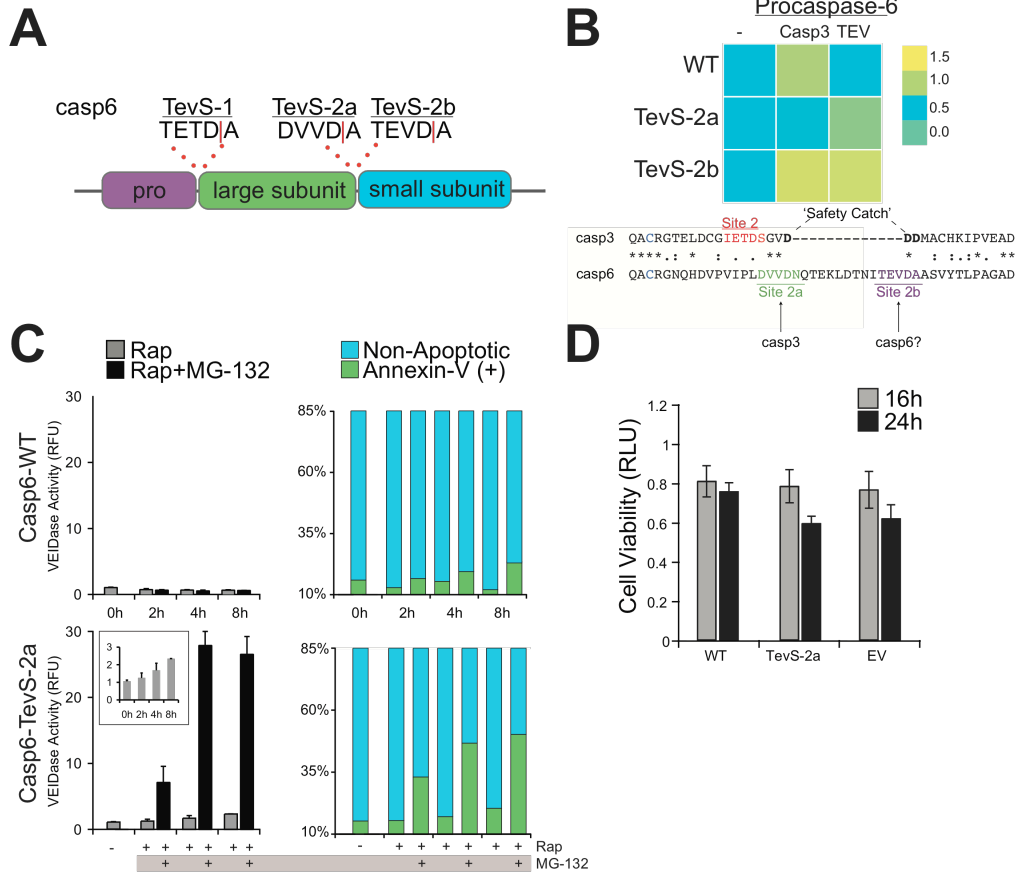


**Figure 2.9. Proteasome Inhibition Converts Procaspase-6 to an Apoptotic Executioner Caspase Isoform.**

(A) Sites for which the TevS insertion was applied for caspase-6. (B) *In vitro* caspase activity of the procaspase-6 matrix of orthogonal alleles is presented as a heat map (top). Caspase activity was measured by expressing each allele in *E. coli*, treating with active caspase-3 (2nM) or Tev Protease(1.1uM) for 1h with 30uM Ac-VEID-AFC in triplicate, correcting for caspase-3 VEIDase activity where appropriate. Abbreviations: WT, wild-type; TevS-2a, TevS insertion at site-2a with P1' Ala; TevS-2b, TevS insertion at site-2b. Alignment of the protein sequences of procaspase-3 (CASP3\_HUMAN) and procaspase-6 (CASP6\_HUMAN) indicates an extra loop region in caspase-6 that harbors site-2a and -2b. (C) The Casp6-WT (top) line was treated with 10nM Rap  $\pm$ 5uM MG-132 over a course of 8h and assayed for caspase-6 activity with 50uM VEID-R110 (left) or by staining with GFP-Annexin-V imaging with fluorescent microscopy. Casp6-TevS-2 (bottom) was treated identically. The inset is the same assay in the range of 0-3 RFU. Data are presented as the average from an experiment performed in quadruplicate (Error Bars $\pm$ SD). (D) The Casp3-TevS-2 line was treated with 10nM Rap for 16 or 24 hr and cell viability was measured with Cell Titer-Glo (Promega, WI).

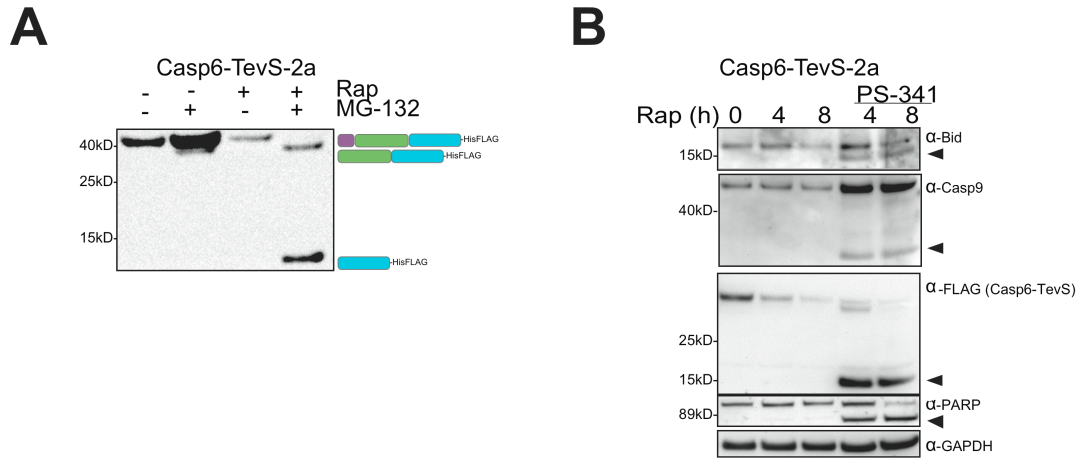


### Figure 2.10. Pathway Analysis of Caspase-6 Activity

(A) The Casp6-TevS-2 line was treated with DMSO or 10nM rapamycin  $\pm$ 5 $\mu$ M MG-132 for 6 hr and cell lysates were blotted the anti-FLAG M2 (left panel, top) or anti-caspase-3 antibody to detect endogenous caspase-3 (left panel, bottom). Expected processing intermediates detected by each antibody are shown to the right of the immunoblots. The expected size of full-length Casp6-TevS-2a' is 36.2 kD.

(B) The Casp6-TevS-2 line was treated with 10nM rapamycin for 0, 4 or 8 hr and blotted for critical apoptotic pathway components: Bid, caspase-9, the engineered Casp7 allele (FLAG epitope tag), PARP and GAPDH.



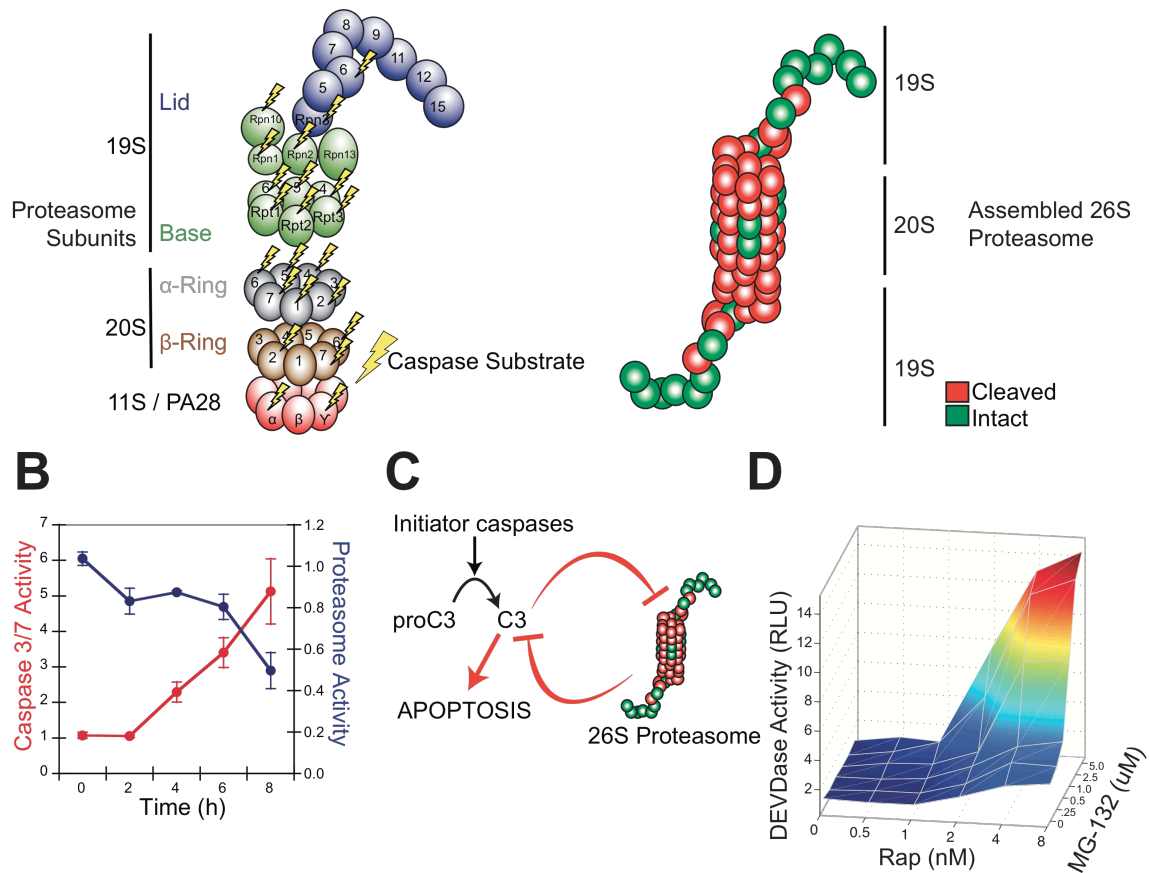


**Figure 2.11. Reciprocal Negative Regulation between the 26S Proteasome and Executioner Caspases**

**(A)** Novel and published proteasome subunits identified as caspase substrates are mapped to an inventory of 20S core, 19S lid/base and 11S activator subunits (left). Cleaved subunits (red) are also mapped onto a model of the fully assembled, multimeric 26S proteasome (right). **(B)** The Casp3-TevS-2 line was treated with 10nM Rap over a course of 8 hr and assayed for caspase activity with Caspase-Glo-3/-7 and protease activity with Proteasome-Glo (Chymotrypsin-Like). Data are presented as the average from an experiment performed in triplicate (Error Bars $\pm$ SD; note different scales). **(C)** A model for reciprocal negative regulation between activated executioner caspases and the 26S proteasome-ubiquitin system predicts synergy between caspase activation and proteasome inhibition. **(D)** The Casp3-TevS-2 line was co-treated with the indicated concentrations of Rap (0-8nM) and MG-132 (0-5 $\mu$ M) for 4 hr and caspase activation was measured with Caspase-Glo-3/-7 in triplicate.



## 2.7 REFERENCES

- Adrain, C., E. M. Creagh, et al. (2004). Caspase-dependent inactivation of proteasome function during programmed cell death in *Drosophila* and man. J Biol Chem. **279**: 36923-36930.
- Albeck, J. G., J. M. Burke, et al. (2008). Quantitative analysis of pathways controlling extrinsic apoptosis in single cells. Mol Cell. **30**: 11-25.
- Bedford, L., D. Hay, et al. (2008). Depletion of 26S Proteasomes in Mouse Brain Neurons Causes Neurodegeneration and Lewy-Like Inclusions Resembling Human Pale Bodies. Journal of Neuroscience. **28**: 8189.
- Casciola-Rosen, L., M. Garcia-Calvo, et al. (2007). Mouse and Human Granzyme B Have Distinct Tetrapeptide Specificities and Abilities to Recruit the Bid Pathway. Journal of Biological Chemistry. **282**: 4545.
- Choi, Y. E., M. Butterworth, et al. (2009). The E3 Ubiquitin Ligase cIAP1 Binds and Ubiquitinates Caspase-3 and -7 via Unique Mechanisms at Distinct Steps in Their Processing. J Biol Chem. **284**: 12772-12782.
- Dix, M. M., G. M. Simon, et al. (2008). Global mapping of the topography and magnitude of proteolytic events in apoptosis. Cell. **134**: 679-691.
- Earnshaw, W. C., L. M. Martins, et al. (1999). Mammalian caspases: structure, activation, substrates, and functions during apoptosis. Annu Rev Biochem. **68**: 383-424.
- Feeney, B., C. Pop, et al. (2006). Role of loop bundle hydrogen bonds in the maturation and activity of (Pro)caspase-3. Biochemistry. **45**: 13249-13263.
- Fuentes-Prior, P. and G. S. Salvesen (2004). The protein structures that shape caspase activity, specificity, activation and inhibition. Biochem J. **384**: 201-232.
- Graham, R. K., Y. Deng, et al. (2006). Cleavage at the caspase-6 site is required for neuronal dysfunction and degeneration due to mutant huntingtin. Cell. **125**: 1179-1191.
- Green, D. R. (2005). Apoptotic pathways: ten minutes to dead. Cell. **121**: 671-674.

- Hell, K., M. Saleh, et al. (2003). Substrate cleavage by caspases generates protein fragments with Smac/Diablo-like activities. Cell Death Differ. **10**: 1234-1239.
- Klaiman, G., N. Champagne, et al. (2009). Self-activation of Caspase-6 in vitro and in vivo: Caspase-6 activation does not induce cell death in HEK293T cells. Biochim Biophys Acta. **1793**: 592-601.
- Lakhani, S. A., A. Masud, et al. (2006). Caspases 3 and 7: key mediators of mitochondrial events of apoptosis. Science. **311**: 847-851.
- Mahrus, S., J. C. Trinidad, et al. (2008). Global sequencing of proteolytic cleavage sites in apoptosis by specific labeling of protein N termini. Cell. **134**: 866-876.
- Parks, T. D., K. K. Leuther, et al. (1994). Release of proteins and peptides from fusion proteins using a recombinant plant virus proteinase. Anal Biochem. **216**: 413-417.
- Pauli, A., F. Althoff, et al. (2008). Cell-Type-Specific TEV Protease Cleavage Reveals Cohesin Functions in Drosophila Neurons. Dev Cell. **14**: 239-251.
- Pop, C. and G. S. Salvesen (2009). Human caspases: activation, specificity, and regulation. J Biol Chem. **284**: 21777-21781.
- Rosenfeld, N., M. B. Elowitz, et al. (2002). Negative autoregulation speeds the response times of transcription networks. Journal of Molecular Biology. **323**: 785-793.
- Roy, S., C. I. Bayly, et al. (2001). Maintenance of caspase-3 proenzyme dormancy by an intrinsic "safety catch" regulatory tripeptide. Proc Natl Acad Sci USA. **98**: 6132-6137.
- Sun, X.-M., M. Butterworth, et al. (2004). Caspase activation inhibits proteasome function during apoptosis. Mol Cell. **14**: 81-93.
- Suzuki, Y., Y. Nakabayashi, et al. (2001). Ubiquitin-protein ligase activity of X-linked inhibitor of apoptosis protein promotes proteasomal degradation of caspase-3 and enhances its anti-apoptotic effect in Fas-induced cell death. Proc Natl Acad Sci USA. **98**: 8662-8667.

Taylor, R. C., S. P. Cullen, et al. (2008). Apoptosis: controlled demolition at the cellular level. Nat Rev Mol Cell Biol. **9**: 231-241.

Thornberry, N. A., T. A. Rano, et al. (1997). A combinatorial approach defines specificities of members of the caspase family and granzyme B. Functional relationships established for key mediators of apoptosis. J Biol Chem. **272**: 17907-17911.

Uhlmann, F., D. Wernic, et al. (2000). Cleavage of cohesin by the CD clan protease separin triggers anaphase in yeast. Cell. **103**: 375-386.

Wang, J., C.-E. Wang, et al. (2008). Impaired ubiquitin-proteasome system activity in the synapses of Huntington's disease mice. J Cell Biol. **180**: 1177-1189.

Wehr, M. C., R. Laage, et al. (2006). Monitoring regulated protein-protein interactions using split TEV. Nat Methods. **3**: 985-993.

Wehr, M. C., L. Reinecke, et al. (2008). Analysis of transient phosphorylation-dependent protein-protein interactions in living mammalian cells using split-TEV. BMC Biotechnol. **8**: 55.

Williams, D. J., H. L. Puhl, et al. (2009). Rapid modification of proteins using a rapamycin-inducible tobacco etch virus protease system. PLoS ONE. **4**: e7474.

Wolan, D. W., J. A. Zorn, et al. (2009). Small-molecule activators of a proenzyme. Science. **326**: 853-858.

Yi, C. H. and J. Yuan (2009). The Jekyll and Hyde functions of caspases. Dev Cell. **16**: 21-34.

## **Chapter 3: Vector Systems for Targeted Gene Replacement in Cells**

### 3.1 Introduction

Apoptosis, or programmed cell death, is a conserved cellular pathway required for development, immune cell maturation and as a primary defense against cancer (Taylor, Cullen et al. 2008). Apoptosis is triggered by signaling events that converge upon the activation of specific proteases called the caspases (Earnshaw, Martins et al. 1999). Intrinsic or extrinsic death signals are first integrated by the initiator caspase-8 or -9 by a self-cleavage mechanism driven by induced proximity. Initiator caspases cleave and activate the executioner caspase-3, -6 and -7. The executioner caspases then cleave a set of vital proteins or death substrates to produce characteristic apoptotic phenotypes such membrane blebbing (p160ROCK), nuclear condensation (PKC $\delta$ , MST1), and cleavage of chromatin-associated genomic DNA (ICAD) (Coleman, Sahai et al. 2001; Sebbagh, Renvoizé et al. 2001; Ura, Masuyama et al. 2001; Samejima and Earnshaw 2005). Apoptotic pathways, therefore, are defined by a hierarchical cascade of proteases resulting in the targeted destruction of the cell. In contrast to apoptosis, restrained caspase activity is implicated in diverse phenotypes such as red blood cell enucleation, T-cell anergy and long-term depression in post-synaptic neurons (Yi and Yuan 2009).

Utilizing an unbiased and global proteomics technique to identify caspase substrates, or degradomics, the Wells lab has recently identified ~1100 human caspase substrates that are cleaved during apoptosis (Mahrus, Trinidad et al. 2008). A key question, therefore, is which caspase targets are necessary and/or sufficient to demolish the cell? Can we functionally enumerate the role of single

caspase substrates and assign specific apoptotic phenotypes to individual substrates? Are there single substrates that are sufficient by themselves to induce apoptosis -- and would these make good drug targets?

There are several potential outcomes of caspase-mediated proteolysis. First, caspases may *inactivate* the protein by cleaving apart two or more domains required for catalysis or for other essential functions; by destabilizing protein structure resulting in degradation; or by preferentially attacking and disabling protein complexes. Such *loss of function* proteolytic events include the destruction of the cytoskeleton during apoptosis. Second, caspase-mediated cleavage of proteins could *activate* the substrate, e.g., by removing an inhibitory domain and lead to an increase in substrate activity or by re-localization to a new cellular compartment. These *gain of function* cleavage include the activation of the caspases themselves as well as several kinases (PKC $\delta$ , PAK2)(Vilas, Corvi et al. 2006; Hu, Liu et al. 2007). Third, caspase proteolysis of substrates may have *no apparent function* -- these are bystander substrates, and new technology is required to efficiently define which substrates are functional targets of caspases and which substrates are bystanders.

We have developed an inducible protease system to recapitulate caspase proteolysis *in cells*. An orthogonal protease, based on TEV protease (TevP), has been engineered to dimerize, fold, and activate in the presence of a small molecule rapalog (Gray, Mahrus et al. 2010). This split-TEV design implements protein complementation assay (or PCA) technology in which a small monomeric protein is strategically 'split' and expressed as individual protein fragments fused



to FRAP and FKBP domains that heterodimerize upon rapamycin treatment (Michnick, Ear et al. 2007). TevP is a highly specific protease used in many biotechnology applications due its 7-residue preferred cleavage site, and we have previously shown that we can replace the endogenous processing sites in the executioner caspases with the TEV substrate sequence. Cleavage of these engineered caspase isoforms is sufficient to activate each of the executioner caspases, and for caspase-3 and -7, orthogonal activation is sufficient to induce apoptosis in HEK293 and HeLa cells. Since TEV protease has no known substrates in the human proteome, we call our split-TEV design *the SNIPer* for “Single-Nick in Proteome” and only substrates with genetically-encoded TEV sites are cleaved. In this context, we have recapitulated “gain-of-function” proteolysis.

However, to study *loss of function* proteolysis, the endogenous protein must be depleted in order to measure the phenotypic effects of proteolyzing TEV-encoded alleles. We have developed a novel bicistronic viral vector system to knock-in engineered substrates, thus enabling *loss of function* analysis in the cellular context. The targeting vector comprises a microRNA (miRNA) expression cassette directed against the endogenous substrate locus. In contrast to siRNA, miRNA are expressed as single-stranded RNAs that fold as hairpins with stem-loop architecture (Chang, Elledge et al. 2006). Genomic analysis of miRNA loci reveals that miRNAs are often expressed within introns or other untranslated sequence of protein-coding messenger RNA (Morlando, Ballarino et al. 2008). miRNAs are released by the nuclear endonuclease Drosha, and the resulting

'pre-miRNA' hairpin is actively exported to the cytosol. Pre-miRNAs are further processed by Dicer and enter the RISC complex, which directs the targeted degradation of cognate mRNA and knockdown at the protein level. Several groups have successfully applied these observations to develop bicistronic miRNA expression vectors for the co-expression of both a miRNA and a fluorescent protein (Chung, Hart et al. 2006; Qiu, Wang et al. 2008). In this case, we express an engineered caspase substrate with a miRNA directed against the endogenous copy of the substrate of interest. Therefore, co-expression of both cassettes on the same transcript results in **(A)** the miRNA-mediated knockdown of the endogenous caspase substrate and **(B)** knock-in of an engineered variant that is susceptible to cleavage by split-TEV, which enables functional analysis of site-specific caspase proteolysis one substrate at a time. This rapid, cell-based engineering of protein alleles we call "Post-Transcriptional Gene Replacement" or *PTGR*.

ICAD (*Inhibitor of Caspase-Activated DNase*) is processed by caspase-3 at a key control point of apoptosis (Samejima and Earnshaw 2005). Cleavage leads to the destruction of genomic DNA by releasing CAD (*Caspase-Activated DNase*), the primary DNA endonuclease responsible for DNA laddering during apoptosis. ICAD is thought to bind to CAD as the nascent CAD peptide is translated at the ribosome. Cleavage of ICAD by caspase-3 releases CAD, which homodimerizes as an active endonuclease (**Figure 3.1**). ICAD is required for proper CAD folding in mammalian cells, and ICAD must be co-expressed with CAD to recover catalytically active CAD in *E. coli*. These data imply a dual role

for ICAD as both a negative regulator of CAD and as an obligate folding chaperone for CAD. Additionally, there are two isoforms of ICAD-L (DFF45) and ICAD-S (DFF35) that are generated by alternative splicing, and DFF35 lacks the nuclear localization signal encoded on the COOH-terminus of DFF45 (Widlak and Garrard 2005). Therefore, ICAD-L/DFF45 yields a nuclear ICAD:CAD complex and a ICAD-S/DFF35:CAD complex in the cytoplasm. The complexity of the ICAD:CAD regulatory mechanisms implies that conventional genetic approaches, e.g., RNAi, are unsuitable to model ICAD:CAD processing and activation during apoptosis. RNAi-mediated depletion of ICAD is predicted to result in misfolded CAD, not the active CAD homodimer. In this case, RNAi *would not recapitulate* loss of function proteolysis of ICAD by the caspases.

To faithfully recapitulate ICAD cleavage and CAD activation, PTGR vector technology is applied to replace endogenous ICAD with a TEV-cleavable allele, ICAD-TevS. In principle, this strategy preserves the chaperone function of ICAD, and CAD activation in cells can then be controlled by the SNIPer in a temporal and dose-dependent fashion. Importantly, we induce CAD activity in the absence of caspase activation using conventional apoptotic inducers. We identified a potent miRNA, ICAD-mir-3, that robustly depletes both endogenous ICAD-L/-S isoforms, and we express either ICAD-L or ICAD-S TEV-cleavable alleles. We also demonstrate cytoplasmic- and nuclear-specific SNIPer activity (NLS-SNIPer).

## 3.2 Results

### 3.2.1 PTGR Vector Design

To enable the replacement of endogenous proteins with engineered variants, we applied the following design principles: **(1)** the final vector must be a single construct capable of co-expressing both engineered proteins *and* RNAi targeting the endogenous locus **(2)** we envisioned a modular design for rapid construction of targeting vectors, and the system should leverage recombination technology (MultiSite Gateway) (Hartley, Temple et al. 2000; Cheo, Titus et al. 2004) **(3)** the vector should harbor a potent RNAi trigger, e.g. a miRNA framework, to ensure knockdown over a wide range expression levels and **(5)** expression of the system should be tunable either by FACS or by optimizing antibiotic concentrations.

The PTGR system comprises three MultiSite Gateway-compatible vectors: pDONR-CMV-EGFP-P4-P1r, pENTR-CMV-miR-GW-L1-L2 and pQCXI-EGFP/NeoR-R4-R2. **Figure 3.2** shows the vector maps and workflow for each construct. The PTGR workflow proceeds as follows: a caspase substrate, e.g. ICAD-TEV, is PCR amplified with attB4/B1 oligonucleotide primers and BP cloned into pDONR-CMV-EGFP-P4-P1r (**Figure 3.2A**). The miR-155 framework was BP cloned into pDONR-CMV-P1-P2 to yield pENTR-CMV-miR-GW-L1-L2, and ICAD or control miRNAs were cloned by directly ligating 65-mer dsDNA oligonucleotides to this vector (**Figure 3.2A**). Importantly, both vectors harbor a CMV promoter outside the sites of recombination, and thus each entry vector is competent for expression in transient transfection assays. Additionally, pDONR-CMV-EGFP-P4-P1r expresses EGFP *with* a stop codon (the ORF cloned into the

attP4-attP1r sites is present in the mRNA and can be targeted by RNAi, but *is not translated*) (**Figure 3.2B**). These vectors, therefore, can be transiently co-expressed in order to identify robust miRNA candidates against the substrate by monitoring GFP fluorescence.

### 3.2.2 miRNA Identification and Intron Characterization

A panel of 7 ICAD miRNAs were designed against ICAD in a region common to both ICAD-L/-S isoforms, and each ICAD miRNA was co-transfected against an EGFP-ICAD fusion construct to assess knockdown. A comparison of EGFP-ICAD fluorescence co-transfected with a negative control hairpin miR-EV (**Figure 3.3A**) and or a miR-ICAD#3 (**Figure 3.3B**) shows little to no EGFP-ICAD fluorescence and indicates ICAD-miR#3 is a potent miRNA trigger. The target sequence of the engineered allele in pENTR-CMV-EGFP-L4-R1-ICAD was mutated to prevent knockdown without altering the final peptide sequence (**Figure 3.4B and 3.4C**).

The first step in miRNA biogenesis is the excision of the pri-miRNA from mRNA by the nuclear endonuclease Drosha. Processing of mRNA by Drosha can result in removal of key mRNA stability / translation determinants such as the 5'-methyl guanosine (m<sup>7</sup>g) cap or the 3' retroviral long-terminal repeat (LTR). Numerous studies have shown that miRNAs are often found in introns in mammalian genomes, and miRNAs are often enriched in the first or second intron of protein-coding genes. We reasoned, therefore, that placing the miRNA within a strong intron would maintain strong knockdown while preserving transcript stability *and* physiologically-relevant ICAD-TevS expression. pENTR-

CMV-miR-GW-L1-L2 was recloned with a strong hybrid intron (Huang and Gorman 1990) containing a 5' splice donor derived from an Ad5 leader and 3' IgG splice acceptor to yield pCMV-miR-EV-IVS-GW-L1-L2 (**Figure 3.5A**). Four pCMV-miR-GW vectors were Gateway-cloned into a PTGR-IRES-mCherry acceptor vector: miR-Neg, miR-Neg-IVS, miR-ICAD, miR-ICAD-IVS. As an initial comparison, co-transfection of EGFP-ICAD and miR-ICAD or miR-ICAD-IVS indicated that placement of the miR framework within an intron did not affect knockdown efficiency (**Figure 3.6B and 3.6D**) as EGFP-ICAD fluorescence was undetectable in both cases. mCherry expression from the PTGR backbone, however, was increased by more than four-fold in the presence of miR-ICAD-Intron (**Figure 3.5C, 3.5D and 3.5F**), demonstrating that miRNA processing within an intronic context results in stabilized mRNA and increased translational efficiency of protein-coding sequence from the bicistronic transcript. In order to faithfully package finalized PTGR vectors harboring miR-155-IVS cassettes, the retroviral 'payload,' i.e., the sequence in the acceptor vector from the CMV promoter to IRES-EGFP/NeoR, was inverted (**Figure 3.5B**). Therefore, the intronic miR scaffold *is not spliced out* during viral RNA transcription for packaging of recombinant retrovirus. However, upon integration in target cell lines, expression of the bicistronic transcript is driven from the internal CMV promoter, and this transcript *is subject* to splicing, miR biogenesis, *et cetera*.

### 3.2.3 ICAD TevS-Substrate Engineering and Characterization of PTGR Cell Lines

Both wild-type ICAD-L and -S isoforms were cloned with a NH<sub>2</sub>-terminal FLAG-epitope tag into pDONR-P4-P1r by Gateway BP cloning to yield pENTR-ICAD-L4-R1. For the engineered ICAD alleles, TevS insertions were introduced via overlapping PCR at the following sites, D117 and D224 (**Figure 3.7A**). A previous group had engineered TevS sites into ICAD for expression in *Saccharomyces cerevisiae* (Xiao, Widlak et al. 2007), and we employed their TevS insertion strategy (**Figure 3.7B**). *Renilla luciferase* was BP cloned into pDONR-P4-P1r as an expression control, and a negative control miRNA was generated.

To ensure robust cleavage of ICAD-L / DFF45 (the long ICAD isoform localized to the nucleus), both N-TEV and C-TEV SNIPer constructs were cloned with a strong NH<sub>2</sub>-terminal nuclear localization signal (3xNLS) from the SV40 virus (Kalderon, Roberts et al. 1984). To confirm cleavage of ICAD-L or ICAD-S (nuclear and cytoplasmic isoforms) by NLS-SNIPer or the SNIPer, transient transfection experiments were performed  $\pm$ rapamycin. Western blot analysis using an antibody that reacts to both long and short ICAD isoforms (**Figure 3.8A, lane 1**) confirmed robust cleavage of ICAD-L by NLS-SNIPer (**lanes 2 and 3**) and cleavage of ICAD-S by the original SNIPer (**lanes 4 and 5**). Cytoplasmic and NLS-SNIPer expressing stable HEK293 cell lines were prepared by retroviral transduction, PTGR vectors were prepared by a Multisite Gateway LR reaction, and SNIPer cell lines were further transduced with PTGR retroviruses. Using the same ICAD antibody, significant knockdown was observed with cell line PTGR-

ICAD#2 (**Figure 3.8B, lane 2**) as compared to the miR-Neg control line (**lane 1**), which harbors the control RL cassette and ICAD-miR. The expression level of WT-ICAD in the PTGR-ICAD#3 line (**lanes 3 and 4**) closely match the levels of endogenous ICAD, and no cleavage of the ICAD-L-WT allele was observed  $\pm$ rapamycin as expected. In contrast, robust cleavage of both ICAD-L-TEV or ICAD-S-TEV (**lanes 5 & 6 and 7 & 8**) was achieved in a rapamycin-dependent fashion with NLS-SNIPer or the cytoplasmid SNIPer. In total, these data confirm the targeted replacement of endogenous ICAD with TEV-engineered alleles for both ICAD-L or ICAD-S alleles and cleavage by the SNIPer in a rapamycin- and compartment-dependent fashion.

### 3.3 Discussion

Several elegant 'chemical genetic' tools been recently developed. These technologies simultaneously exploit the rapid kinetics of small molecule pharmacology and the exquisite specificity of conventional genetic technology. Orthogonal enzyme and substrate systems, e.g. analog-sensitive kinases and the SNIPer, are based on the parallel engineering of both enzyme and substrate. In the case of analog-sensitive kinases, a 'bump and hole' strategy is employed in which a bulky residue within the kinase active site is mutated to an **Ala** or **Gly** residue to generate a 'hole,' and a chemical substituent is appended to the N<sup>7</sup> position of ATP or an inhibitor (e.g. PP1) as the 'bump' (Knight and Shokat 2007). For the SNIPer, an orthogonal protease and substrate system was developed by engineering a ligand-inducible small molecule protease, based on



TEV protease, with no known substrates in the human or mouse proteomes. Substrates of interest, therefore, are engineered with a TEV site, which renders a specific substrate susceptible to site-specific cleavage. Both approaches offer a rapid approach to induce or modulate post-translational modifications (PTMs) in cells, and PTMs represent a central mechanism by which cells control protein function, stability and information flow in cellular pathways (Deribe, Pawson et al. 2010). These approaches, however, are only effective for *gain of function* analysis in mammalian systems, which are generally less tractable to genetic manipulation than *S. cerevisiae* or *E. coli*. Thus, a *key crux of chemical biology* is the ability to apply chemical genetic tools for *loss of function* phenotypic analysis in mammalian cells. In most contexts, *loss of function* analysis requires the endogenous enzyme or substrate to be replaced by an engineered variant.

At present, several robust technologies comprise the 'genetic toolbox' for gene replacement in cell culture systems and in the germline of mice. Gene-targeting via homologous recombination is regularly used to knock-out or modify loci in mice and cultured cells. This approach requires access to long 'arms of recombination' and only a single copy of each gene is targeted at a time. The efficiency of homologous recombination is low, and propagating and identifying clones harboring the transgene is time consuming. The generation of double knockouts (homozygous for the engineered allele) requires a second round of gene targeting. Alternatively, heterozygous founder mice can be generated and then crossed to generate mice that are homozygous for the orthogonal enzyme and substrate pair. The development of bacterial artificial chromosome

recombineering, e.g. BAC TransgeneOmics, has significantly decreased the time required to develop gene-targeting vectors (Poser, Sarov et al. 2008). Although gene-targeting via homologous recombination offers the advantage of maintaining authentic transcriptional regulation from the endogenous promoter, homologous recombination of both alleles in diploid cell culture systems or animals is extremely time consuming (6-12 months) and therefore ill-suited for the rapid interrogation of multiple caspase substrates. To address these concerns, we have developed a rapid gene-targeting strategy in which endogenous proteins are depleted via RNAi and co-incidentally replaced with Tev-cleavable alleles in ~14d.

The ICAD-CAD complex was originally discovered and characterized in 1997, but several key questions remain as to its function and regulation in apoptosis. First, the precise, non-redundant roles of each ICAD isoform remain unclear in cells. Biochemical studies with recombinant ICAD:CAD complexes indicate that ICAD-S is insufficient to properly chaperone CAD. However, neurons only express ICAD-S, and DNA laddering *is observed* in neurons undergoing apoptosis. Additional chaperones may assist in proper folding of CAD, and a second apoptotic DNA nuclease, EndoG, may partially account for the cleavage of genomic DNA (Samejima, Toné et al. 2001). In a cell-free extract, cleavage of ICAD-S did not result in active CAD, and it was hypothesized that ICAD-S may serve as a buffer preventing inappropriate CAD activation. Second, it is unclear whether ICAD cleavage via the SNIPer in the absence of full-blown apoptosis is sufficient to induce apoptosis, and several lines of

evidence suggest that CAD *may not* work alone (Samejima and Earnshaw 2005).  
*Are there additional caspase-mediated proteolytic events that cooperate with CAD activation to induce apoptotic DNA laddering?*

Active CAD cuts chromatin-associated genomic DNA in open linker regions between nucleosomes, and two recent reports suggest that CAD activity is potentially modulated by specific chromatin modifications. Phosphorylation of the histone  $\gamma$ H2AX at Ser139 has been shown to be required for DNA laddering by active CAD *in vitro* and in cells (Lu, Zhu et al. 2006).  $\gamma$ H2AX knockout MEFs were resistant to DNA laddering, and knockout MEFs expressing  $\gamma$ H2AX S139A were also resistant to DNA laddering. Ablation of JNK kinase activity by RNAi or by a kinase inhibitor blocked  $\gamma$ H2AX Ser139 phosphorylation. JNK kinase activity was stimulated by UV irradiation, which was also sufficient to induce caspase-3 activation. These data point to a JNK/ $\gamma$ H2AX/CAD pathway that requires multiple death inputs to achieve DNA laddering. In a second report, extensive caspase-mediated processing of the N-CoR/SMRT co-repressor complex was demonstrated, including the catalytic core HDAC7, a histone de-acetylase. Histone acetylation controls chromatin topology and increased histone acetylation is typically associated with 'open' chromatin, which is more permissive to transcription and, by inference, to CAD-mediated DNA laddering (Mahrus, Trinidad et al. 2008). Caspase-mediated processing of the N-CoR/SMRT co-repressor complex, therefore, may cooperate with active CAD.

A recent study identified a state of 'partial cell death' in which stimulation with TRAIL ligand activated caspase-3, but activation was not sufficient to induce

full-blown apoptosis (Albeck, Burke et al. 2008). This study employed both computational pathway analysis, single-cell fluorescent microscopy, and extensive genetic manipulation was required to achieve intermediate executioner caspase activity. A key question, therefore, is partial and/or non-apoptotic caspase activity sufficient to activate CAD? If so, can activated CAD induce double-stranded breaks in genomic DNA and potentially induce chromosomal rearrangements in cells that survive partial caspase activity. It is tempting to speculate that partial caspase activation and CAD activity could drive oncogene amplification and translocation or tumor suppressor deletion.

Rapid cell-based engineering via PTGR technology and the SNIPer should enable the dissection of ICAD:CAD regulatory mechanisms to address these outstanding questions. Furthermore, this preliminary work indicates that this approach should be portable to additional caspase substrates.

### 3.4 Materials and Methods

#### 3.4.1 Vector Construction (Basic Three-Component Vector System)

The basic MultiSite Vectors: pDONR-P4-P1r, pDNOR-P1-P2 (pDNOR221), and pKA452 were a kind gift of Brendan Mullaney and Dr. Kaveh Ashrafi (UCSF). To generate pDONR-CMV-EGFP-P4-P1r, 5' and 3' *Apal* restriction sites were added to the CMV-EGFP segment from pEGFP-N1 (Clontech) by PCR and then subcloned into the unique *Apal* site of pDNOR-P4-P1r. pENTR-CMV-miR-GW-L1-L2 was constructed by first cloning the miR-155 scaffold by a PCR-based synthetic gene construction approach, a second round of PCR to add *attB1* and *attB2* sites, and the resulting product was Gateway BP (Invitrogen) cloned into pDONR221 to generate pENTR-*attL1*-miR155-EV-*attL2*. An *Apal* and *PvuII* *attL1*-miR155-EV-*attL2* fragment was then subcloned into the *SmaI* and *HpaI* sites of a modified pIRES2-dsRED vector (Clontech; the *BsaI* site were precisely removed by site-directed mutagenesis) to yield pENTR-CMV-miR-GW-L1-L2. The acceptor vector, pQCXI-EGFP/NeoR-R4-R2, was generated by PCR amplifying the *attR4-attR2* Gateway acceptor cassette from pKA452. An additional 5' *AgeI* restriction site was added during PCR, and the PCR product was cloned into the unique *AgeI* site of pQCXI-mCherry. To accommodate miR-155-IVS, pQCXI-mCherry was propagated in INV110 (*dam*<sup>-</sup> *E. coli*), and the CMV-MCS-IRES-mCherry segment was then inverted by digestion with *ClaI* and re-ligated into the same *ClaI* sites (the inverted configuration configuration was confirmed by restriction digest). The *attR4-attR2* Gateway acceptor cassette was then subcloned into the *AgeI* site of the inverted backbone to yield pQCXI-mCherry-R4-R2 (rev). The EGFP-NeoR fusion protein was generated by a two-

round PCR ligation protocol, 5' *Bst*XI and 3' *Xho*I sites were added during PCR, and the resulting fusion was sub-cloned into pQCXIN to generate pQCXI-EGFP/NeoR. To generate pQCXI-EGFP/NeoR-R4-R2 (rev), an *Eco*RI-IRES-EGFP/EGFP-*Xho*I from pQCXI-EGFP/NeoR was ligated to pQCXI-mCherry-R4-R2 or pQCXI-mCherry-R4-R2 (rev) to yield the final PTGR acceptor constructs, pQCXI-EGFP/NeoR-R4-R2 and pQCXI-EGFP/NeoR-R4-R2 (rev). A modified, intron-containing pENTR-CMV-miR-IVS-GW-L1-L2 vector was generated by amplifying the IVS (intervening sequence) from pIRES2-Puro. The miR-155-EV framework was inserted in the middle of the synthetic intron during in two rounds by overlapping PCR and the resulting PCR product was sub-cloned into the *Pvu*II and *Xba*I sites pENTR-CMV-miR-GW-L1-L2 to generate pENTR-CMV-miR-IVS-GW-L1-L2.

Control or ICAD-targeting miRNAs were designed on Invitrogen's BLOCK-IT web-server (<https://rnaidesigner.invitrogen.com/rnaiexpress/setOption.do?designOption=mirna&pid=5012334802634511024>). miR vectors were constructed by linearizing pENTR-CMV-miR-GW-L1-L2 ( $\pm$ IVS) with *Bsa*I and directly ligating annealed 65-mer oligonucleotides. Resulting miR vectors were validated by DNA sequencing. Two TevS sites were added by a two round overlapping PCR protocol using human ICAD-L/DFF45 cDNA (Open Biosystems); *att*B4 and *att*B1 sites were added in the second round of PCR, and PCR products were BP cloned into pDONR-P4-P1r. Once a robust miR-ICAD was identified, the corresponding 21-nt region in the expressed ICAD alleles was subjected to site-directed

mutagenesis in which five silent mutations were made. The EGFP-ICAD fusion construct was prepared by two rounds of overlapping PCR and cloned into the *EcoRI* and *NotI* sites of pcDNA3.1-Myc/His (Invitrogen).

BP and LR cloning were performed by using BP Clonase II and LR Clonase II (Invitrogen) according to the manufacture's recommendations. Acceptor vectors were propagated in One Shot ccdB Survival *E. coli* and Gateway transformants were propagated in DH5 $\alpha$

### **3.4.2 Generation of Stable Cell Lines**

Retroviral supernatants were generated by transfecting SNIPer plasmids (Frb-N-TEV and FKBP-C-TEV-219 or NLS variants) or PTGR vectors into the GPG packaging cell line, a gift of Orion Weiner (UCSF), using the standard Lipofectamine 2000 protocol. GPG cells were cultured in DMEM supplemented with 10% FBS, 100ug/uL Normocin, 2ug/mL puromycin (Invivogen), 300ng/uL G418 (Invitrogen) and 1ug/mL Doxycycline (Dox) (Sigma) and, 24 hr prior to transfection, GPG cells were set in poly-*d*-lysine coated wells 1 x 10<sup>6</sup> per 6-well or 4 x 10<sup>6</sup> per 10cm dish. Retroviral supernatants were harvested 4-5 days after transfection without Dox, contaminating cellular debris was removed by centrifugation at 2000 rpm x 10 min or by filtration with a .4uM filter, and clarified media with retrovirus was added to HEK293 cells for 8-20 hrs with 8ug/mL polybrene (Sigma). Stable SNIPer-PTGR lines were propagated in media with 1.5ug/mL puromycin, 150ug/mL hygromycin and 1000ug/mL G418.

### **3.4.3 Transfection and Fluorescence Microscopy**

Transient transfection of plasmids was performed at the 6-well plate scale in HEK293 cells. Wells were coated with poly-*d*-lysine prior to plating target cells. Cells were plated

to reach ~90% confluence the following day, and transfection mixes were prepared according to the standard Lipofectamine 2000 protocol.

Fluorescent microscopy was performed on a Zeiss Axiovert 200 M microscope with Axiovision software using Endow GFP and Texas Red Filter sets. Fluorescent quantitation was performed with ImageJ software (NIH).

#### **3.4.4 Western Blotting**

HEK 293 SNIPER PTGR ICAD cells were plated on poly-d-lysine coated plates and were allowed to grow overnight before addition of rapamycin to the medium for 24 hours. Cells were lysised in M-PER (Pierce) with the addition of Halt protease cocktail mix (Pierce). Protein concentration was normalized by BCA protein quantitation. 30ug of protein lysates were loaded into a 4-12% Bis Tris NuPAGE Novex Mini Gel (Invitrogen) and run at 200V with MES buffer. Protein was transferred to a PVDF membrane at 30V for 1 hour. Membranes were blocked in 5% nonfat milk and incubated overnight at 4 C in the primary antibody. The ICAD/DFF45 mouse antibody (cat. 611036, BD Transduction Laboratories) was used at 1:1000 dilution in 2.5% nonfat milk and TBS with .1% tween. Blots were washed 3X in TBST and then incubated for 1 hr at Rm temperature with a goat anti-mouse HRP conjugated secondary antibody, 1:1000(Pierce). Blots were imaged using a SuperSignal ELISA Pico chemiluminescent substrate (Pierce).



**Table 3.1 PTGR DNA Oligonucleotides**

<b>pDONR-CMV-EGFP-P4-P1r</b>	<b>DNA Sequence (5'-3')</b>
CMV_EGFP_Apal_Fwd	AAAGGGAAAGGGCCCCGATGTACGGGCCAGATATACGCGTTGACATT
CMV_EGFP_Apal_Rev	AAAGGGAAAGGGCCCTTTGCTAGCTCACTTGTACAGCTCGTCCAT
<b>GW Acceptor Cassette (R4-R2)</b>	
F-Agel-GW-attR4_2	AAAGGGAAAACCGGTCGCCAAGCTCGAAATTAACCCCTCACTAAA
R-Agel-GW-attR4_2	CCTTGAAGCGCATGAACTCCTTGATGATGGCCATGTT
<b>miR-155 (no Intron)</b>	
AttB1-miR-F	GGGGACAAGTTTGTACAAAAAAGCAGGCTGCTAAGCACTTCGTGGCCGTCGATCGTTAAAGGGAGGTAGTGAGT CGA
AttB2-miR-R	GGGGACCACTTTGTACAAGAAAGCTGGGTCTAGACTCGAGTGC GGCCAGATCTGGGCCA
miR-155-1	CTTTTTATAATGCCAAGTTTGTATACAAAAGTTGTTAAAGGGAGGTAGTGA
miR-155-2	CCAGGATCCACTGGTCGACTCACTACCTCCCTTTAACCACTT
miR-155-3	GTCGACCAGTGGATCCTGGAGGCTTGTGAAGGCTGTATG
miR-155-4	CCTTTCCCTTTGGTCTCCAGCATACAGCCTTCAGCAAGCC
miR-155-5	CTGGAGACCAAAGGGAAAGGTCTCTCAGGACACAAGGCCT
miR-155-6	GTTCCATGTGAGTGCTAGTAACAGGCCTTGTCTCTGAGAG
miR-155-7	GTTACTAGCACTCACATGGAACAAATGGCCAGATCTGGC
miR-155-8	AAGCTGTCTAGACTCGAGTGC GGCCAGATCTGGGCCATT
<b>miR-155 + Intron</b>	
Fwd_IVS_Outer_PvuI	AAAGGGAAACGATCGGAATTAATTCGCTGTCTGCGAGGGCCAGCTGTT CCTGAGAGACCTTTCCCTTTGGTCTCCAGCATACAGCCTTCAGCAAGCCTCCAGGATCCACTGGTCGACTC ACCGCGGGCCAGGTGAATA
rev_inner	TGCTGGAGACCAAAGGGAAAGGTCTCTCAGGACACAAGGCCTGTTACTAGCACTCACATGGAACAAATGGCC CAGATCTGGCCGCACTCGAGTGCCCTTTGAGGGTGGCCGCTCCATCTGGTCAGAA
fwd_inner	TGCTGGAGACCAAAGGGAAAGGTCTCTCAGGACACAAGGCCTGTTACTAGCACTCACATGGAACAAATGGCC CAGATCTGGCCGCACTCGAGTGCCCTTTGAGGGTGGCCGCTCCATCTGGTCAGAA
Rev_IVS_Outer_XbaI	AAAGGGAAATCTAGACGACCTGCAGTTGGACCTGGGAGTGGACACCTGTGGAGAGAAA
<b>EGFP-NeoR fusion</b>	
fwd_outer_bstXI	AAAGGGAAACCACAACCATGGTGAGCAAGGGCGAGGAGCTGTT
rev_inner	GCGCTCCGCCACCTCCCTTGTACAGCTCGTCCATGCCGAGAGT
fwd_inner	GGACGAGCTGTACAAGGGAGGTGGCGGAAGCGCTGAACAAGATGGATTGCACGCAGGTT
rev_outer_xhoI	AAAGGGAAACTCGAGTCAGAAGAACTCGTCAAGAAGGCGATAGAA
<b>miR-155-ICAD#3</b>	
ICAD-miR#3 Top	TGCTGAAAGTAATCGTCATCATCCACGTTTTGGCCACTGACTGACGTGGATGAACGATTACTTT
ICAD-miR#3 Bottom	CCTGAAAGTAATCGTTCATCCACGTCAGTCAGTGCCAAAACGTGGATGATGACGATTACTTTT
<b>miR-155-Neg</b>	
miR-Neg Top	TGCTGAAATGTAAGTGCAGTGGAGACGTTTTGGCCACTGACTGACGTCTCCACGCAGTACATTT
miR-Neg Bottom	CCTGAAATGTAAGTGCAGTGGAGACGTCAGTCAGTGCCAAAACGTCTCCACGCAGTACATTTT

<b>ICAD Alleles + QC</b>	
Fwd_N_FLAG_ICAD_att	GGGGACAACCTTTGTATAGAAAAGTTGCCACCATGGATTACAAGGATGACGACGATAAGGAGGTGACCGGGGACGC CGGG
Rev TEV 1	GCCCCGCTCTGGAAGTAGAGATTTTCGTCTGTTTCATCTACATCAAAGGACTCTT
Fwd TEV 1	CTACTTCCAGAGCGGGGCAGGATTAATAATGGAAAAACGTGGCCAGGCAGCTGAAAGAAGA
Rev TEV 2	ACCACTCTGGAAGTAGAGATTTTCGTCTACTGCATCCACCTCCTCACCAA
Fwd TEV 2	GACGAAAATCTACTTCCAGAGTGGTACGGGTATCAGCAGAGAGACCTCCTCGGA
Rev att ICAD Long	GGGGACTGCTTTTTTGTACAAACTTGTCTGTGGGATCCTGTCTGGCTCGCTTA
Rev att ICAD Short	GGGGACTGCTTTTTTGTACAAACTTGTCTGTGGGATCCTGTCTGGCTCGCTTA GCTC
ICAD_qc_miR3_top	CCATAGTCGACGACGATGACTACTTCTGTGTCTACCTTCCAATACTAAGTTTG
ICAD_qc_miR3_botto m	CACAGAAAGTAGTCATCGTCGACTATGGTGCCATCCTCTGCCAGGACC
<b>EGFP-ICAD fusions</b>	
F EcoRI EGFP	AAAGGGAAAAGAATCCACCATGGTGAGCAAGGGCGAGGAGCTGTT
Rev EGFP	GCCTCCCGGTCACCTCCCTTGTACAGCTCGTCCATGCCGAGAGTGAT
Fwd ICAD	GGACGAGCTGTACAAGGGGGAGGTGACCGGGGACGCCGGGTACCAGAA
Rev ICAD L NotI	AAAGGGAAAGCGGCCCTATGTGGGATCCTGTCTGGCTCGCTTA
Rev ICAD S NotI	AAAGGGAAAGCGGCCCTCAGTGACCCTGGTTTCGCCACCTCCAAA

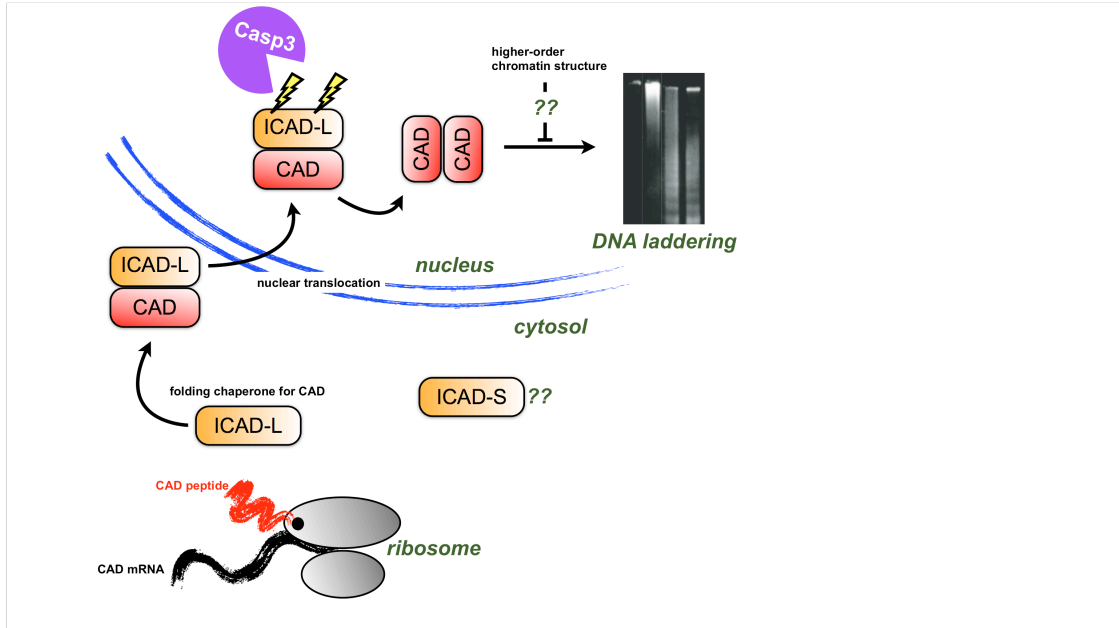


**Figure 3.1. ICAD:CAD Pathway in Apoptosis.**

ICAD-L or -S associates with the nascent CAD peptide during translation at the ribosome. The putative folded CAD resides in the nucleus in a complex with ICAD-L in healthy cells. Upon caspase-3 activation by either intrinsic or extrinsic apoptotic pathways, ICAD is cleaved twice, which releases CAD. The active CAD species is a homodimer, which cleaves chromatin-associated genomic DNA in the linker region between nucleosomes. The influence of chromatin topology on CAD activity is not fully defined.

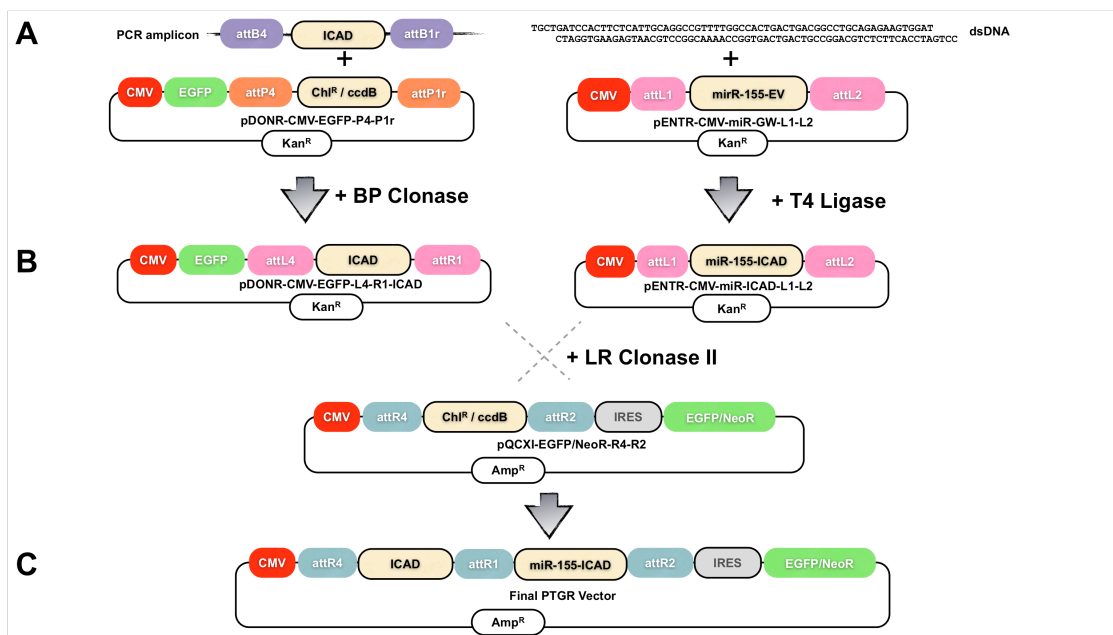


**Figure 3.2. Three-component PTGR system and Workflow**

(A) Entry vectors harboring ICAD are constructed by PCR amplifying wt-ICAD or TevS-alleles and BP-cloned into pDONR-CMV-EGFP-P4-P1r; ICAD-directed miRs are constructed by standard ligation of dsDNA into pENTR-CMV-miR-GW-L1-L2. (B) Since both vectors have CMV promoters, miRs can be validated by co-transfection experiments using EGFP fluorescence as a read-out. pDONR-CMV-EGFP-L4-R1-ICAD, pENTR-CMV-miR-ICAD-L1-L2 and pQCXI-EGFP/NeoR-R4-R2 are recombined by LR Cloning to generate the final PTGR retroviral vector (C).

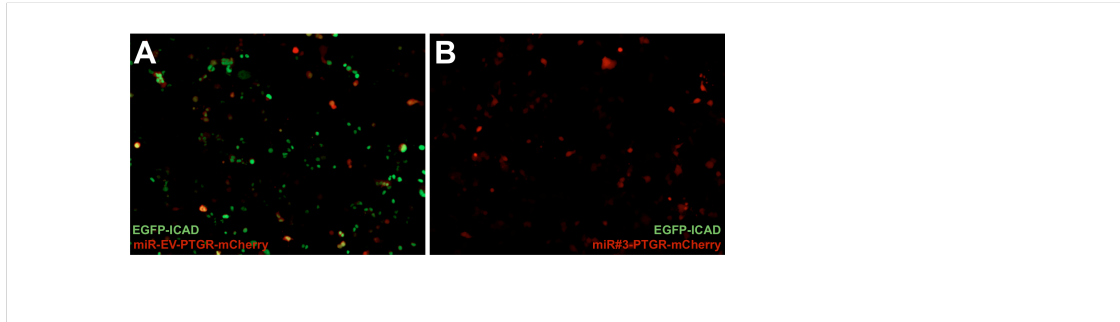


**Figure 3.3. Robust Knockdown of EGFP-ICAD by ICAD-mir#3**

Fluorescent microscopy indicates co-transfection of robust knockdown EGFP-ICAD by ICAD-mir#3 (B) as compared to a negative control miR (A). Equivalent mCherry expression from the backbone of both ICAD and control PTGR vectors is observed in both panels.

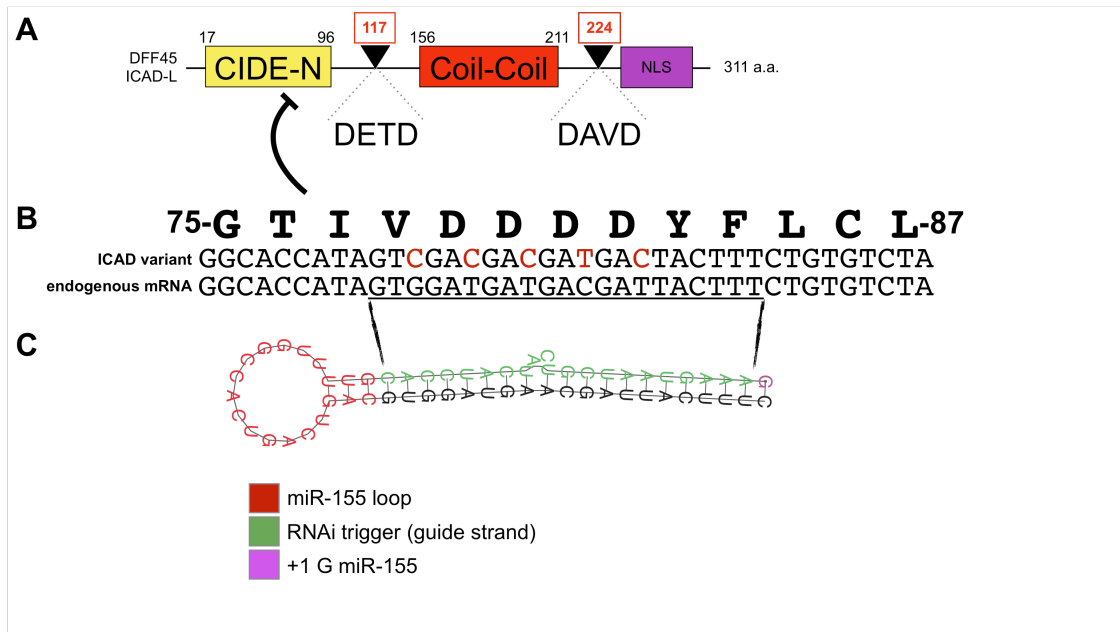


**Figure 3.4. ICAD-mir#3 structure and targeting region within ICAD**

- (A) Schematic representation of ICAD-L showing conserved domain structure and caspase cleavage sites.
- (B) 21-nt targeting region of wt-ICAD-L (endogenous allele) and the five silent mutations in the engineered ICAD variants to prevent knockdown.
- (C) ICAD-miR#3 RNA sequence and stem/loop architecture.

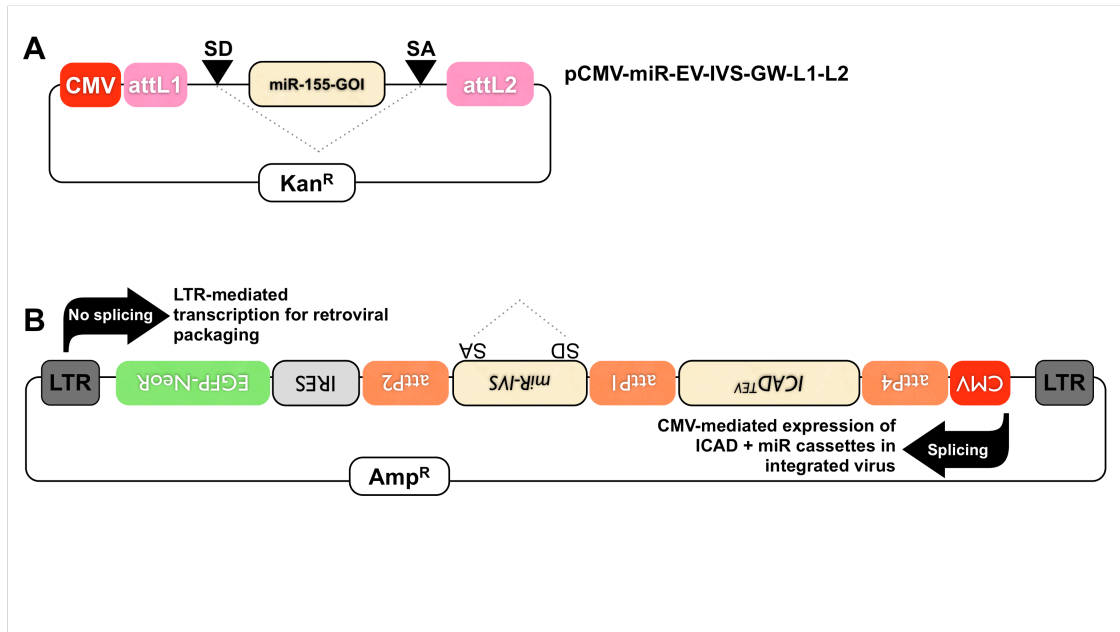


**Figure 3.5. Engineering Intron Sequence into pCMV-miR-EV-IVS-GW-L1-L2 and Reverse Configuration of a finalized PTGR Vector**

(A) Splicing Donor (SD) and Acceptor (SA) sites flank the miR scaffold sequence in pCMV-miR-EV-IVS-GW-L1-L2.

(B) Reversal of CMV-R4-R2-IRES-EGFP/NeoR cassette enables splicing-free transcription of recombinant viral RNA for packaging. Once integrated, CMV-driven expression of the PTGR transcript is in the proper orientation for splicing and miRNA biogenesis.

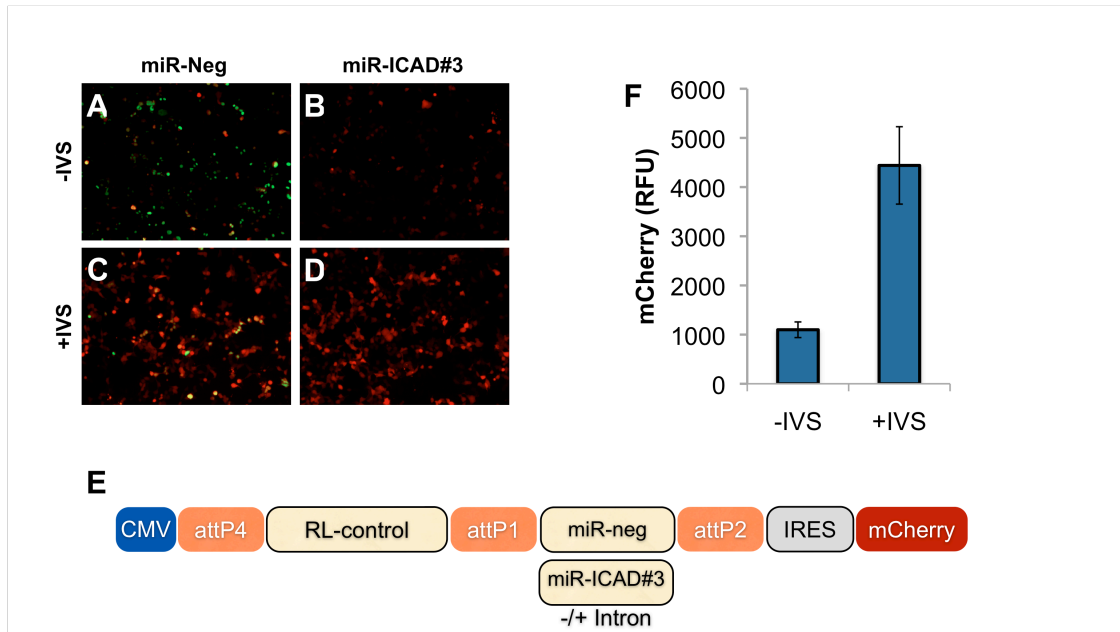


**Figure 3.6. Protein translation from IVS-PTGR vectors is enhanced.**

Inclusion of a synthetic intron sequence (IVS) maintains robust knockdown of an EGFP-ICAD reporter (6B and 6D compared to 6A and 6C). Vector backbone-derived mCherry translation (6E) is enhanced four-fold (6F) when the miR scaffold is flanked by an intron.



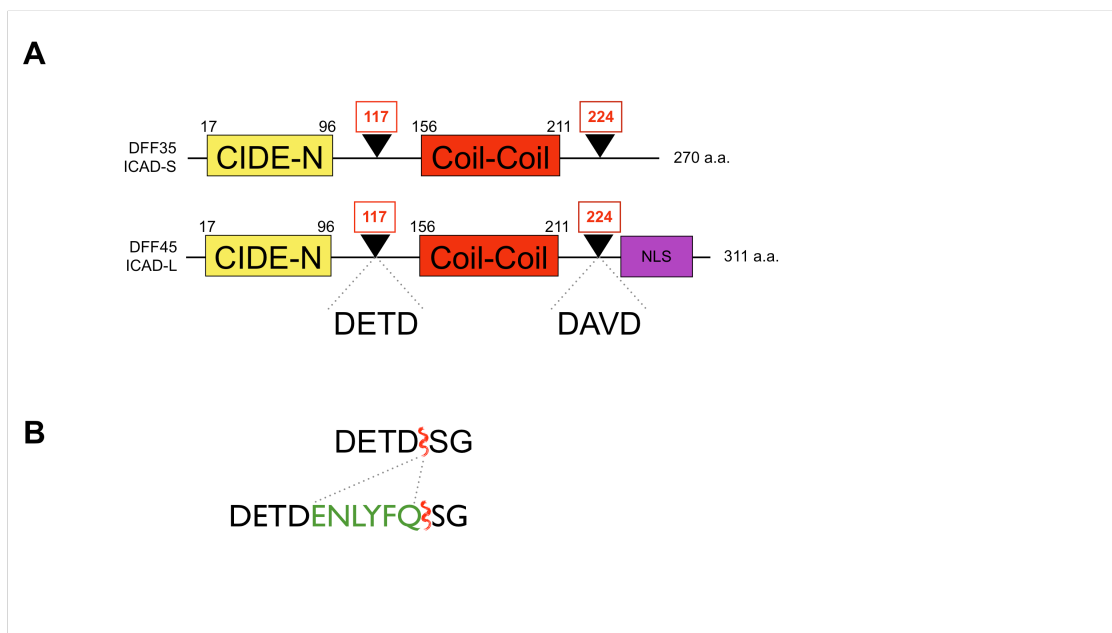


**Figure 3.7. ICAD-L and -S TevS Engineering.**

(A) Domain organization and caspase cleavage sites for ICAD-L and -S. ICAD-S lacks a COOH-terminal NLS sequence. (B) TevS Insertion strategy.

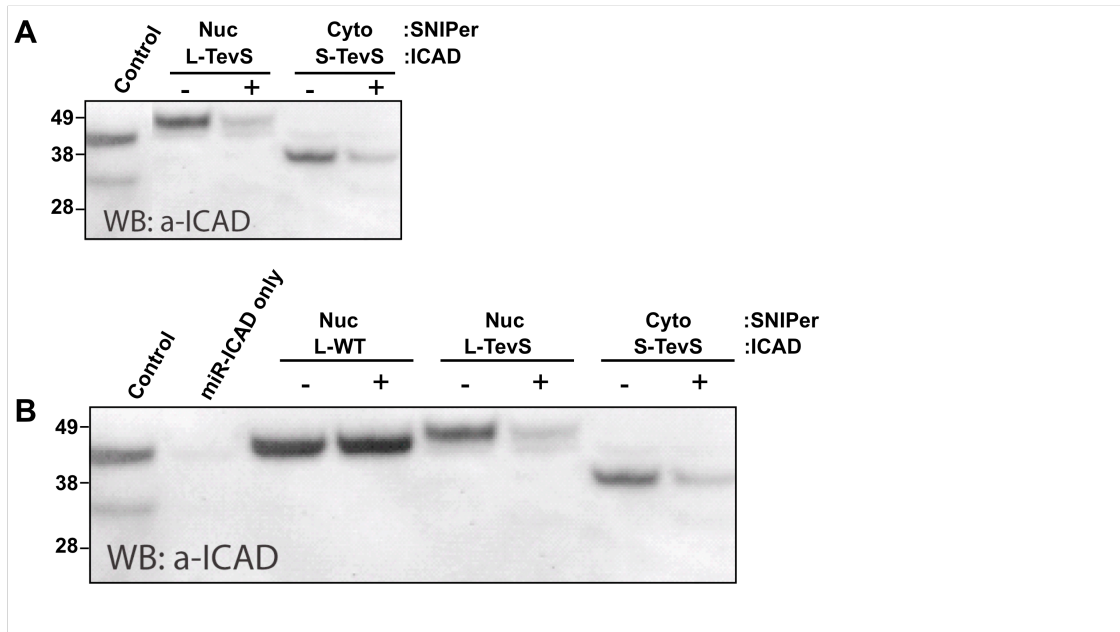


**Figure 3.8. ICAD processing by the SNIPer and PTGR-mediated replacement of ICAD in HEK293 cells.**

(A) Western blot analysis of a transient transfection of TevS-ICAD-L and NLS-SNIPer  $\pm 10$ nM Rap (8A, lanes 2 and 3) or TevS-ICAD-S and Cyto-SNIPer  $\pm 10$ nM Rap (8A, lanes 4 and 5) (B) Western blot analysis of stable PTGR HEK293 cells expressing the indicated ICAD alleles and compartment-targeted SNIPer constructs  $\pm 10$ nM Rap.

### 3.5 References

- Adrain, C., E. M. Creagh, et al. (2004). Caspase-dependent inactivation of proteasome function during programmed cell death in *Drosophila* and man. J Biol Chem. **279**: 36923-36930.
- Albeck, J. G., J. M. Burke, et al. (2008). Quantitative analysis of pathways controlling extrinsic apoptosis in single cells. Mol Cell. **30**: 11-25.
- Ashkenazi (2008). Directing cancer cells to self-destruct with pro-apoptotic receptor agonists. Nature reviews Drug discovery.
- Bedford, L., D. Hay, et al. (2008). Depletion of 26S Proteasomes in Mouse Brain Neurons Causes Neurodegeneration and Lewy-Like Inclusions Resembling Human Pale Bodies. Journal of Neuroscience. **28**: 8189.
- Bence, N. F., E. J. Bennett, et al. (2005). Application and analysis of the GFPu family of ubiquitin-proteasome system reporters. Meth Enzymol. **399**: 481-490.
- Bence, N. F., R. M. Sampat, et al. (2001). Impairment of the ubiquitin-proteasome system by protein aggregation. Science. **292**: 1552-1555.
- Brown, J. L. and W. K. Roberts (1976). Evidence that approximately eighty per cent of the soluble proteins from Ehrlich ascites cells are Nalpha-acetylated. J Biol Chem. **251**: 1009-1014.
- Casciola-Rosen, L., M. Garcia-Calvo, et al. (2007). Mouse and Human Granzyme B Have Distinct Tetrapeptide Specificities and Abilities to Recruit the Bid Pathway. Journal of Biological Chemistry. **282**: 4545.
- Chang, K., S. J. Elledge, et al. (2006). Lessons from Nature: microRNA-based shRNA libraries. Nat Methods. **3**: 707-714.
- Cheo, D. L., S. A. Titus, et al. (2004). Concerted assembly and cloning of multiple DNA segments using in vitro site-specific recombination: functional analysis of multi-segment expression clones. Genome Res. **14**: 2111-2120.
- Choi, Y. E., M. Butterworth, et al. (2009). The E3 Ubiquitin Ligase cIAP1 Binds and Ubiquitinates Caspase-3 and -7 via Unique Mechanisms at Distinct Steps in Their Processing. J Biol Chem. **284**: 12772-12782.

Chung, K.-H., C. C. Hart, et al. (2006). Polycistronic RNA polymerase II expression vectors for RNA interference based on BIC/miR-155. Nucleic Acids Res. **34**: e53.

Coleman, M. L., E. A. Sahai, et al. (2001). Membrane blebbing during apoptosis results from caspase-mediated activation of ROCK I. Nat Cell Biol. **3**: 339-345.

Datta, D., J. M. Scheer, et al. (2008). An allosteric circuit in caspase-1. J Mol Biol. **381**: 1157-1167.

Deribe, Y. L., T. Pawson, et al. (2010). Post-translational modifications in signal integration. Nat Struct Mol Biol. **17**: 666-672.

Dix, M. M., G. M. Simon, et al. (2008). Global mapping of the topography and magnitude of proteolytic events in apoptosis. Cell. **134**: 679-691.

Earnshaw, W. C., L. M. Martins, et al. (1999). Mammalian caspases: structure, activation, substrates, and functions during apoptosis. Annu Rev Biochem. **68**: 383-424.

Feeney, B., C. Pop, et al. (2006). Role of loop bundle hydrogen bonds in the maturation and activity of (Pro)caspase-3. Biochemistry. **45**: 13249-13263.

Fuentes-Prior, P. and G. S. Salvesen (2004). The protein structures that shape caspase activity, specificity, activation and inhibition. Biochem J. **384**: 201-232.

Gilon, T., O. Chomsky, et al. (1998). Degradation signals for ubiquitin system proteolysis in *Saccharomyces cerevisiae*. EMBO J. **17**: 2759-2766.

Graham, R. K., Y. Deng, et al. (2006). Cleavage at the caspase-6 site is required for neuronal dysfunction and degeneration due to mutant huntingtin. Cell. **125**: 1179-1191.

Gray, D. C., S. Mahrus, et al. (2010). Activation of specific apoptotic caspases with an engineered small-molecule-activated protease. Cell. **142**: 637-646.

Green, D. R. (2005). Apoptotic pathways: ten minutes to dead. Cell. **121**: 671-674.

Hardy, J. A., J. Lam, et al. (2004). Discovery of an allosteric site in the caspases. Proc Natl Acad Sci USA. **101**: 12461-12466.

Hartley, J. L., G. F. Temple, et al. (2000). DNA cloning using in vitro site-specific recombination. Genome Res. **10**: 1788-1795.

Hedstrom, L. (2002). Serine protease mechanism and specificity. Chem Rev. **102**: 4501-4524.

Hell, K., M. Saleh, et al. (2003). Substrate cleavage by caspases generates protein fragments with Smac/Diablo-like activities. Cell Death Differ. **10**: 1234-1239.

Hu, Y., Z. Liu, et al. (2007). Acinus-provoked protein kinase C delta isoform activation is essential for apoptotic chromatin condensation. Cell Death Differ. **14**: 2035-2046.

Huang, M. T. and C. M. Gorman (1990). Intervening sequences increase efficiency of RNA 3' processing and accumulation of cytoplasmic RNA. Nucleic Acids Res. **18**: 937-947.

Kalderon, D., B. L. Roberts, et al. (1984). A short amino acid sequence able to specify nuclear location. Cell. **39**: 499-509.

Kaufmann, S. H., T. J. Kottke, et al. (2001). Analysis of caspase activation during apoptosis. Curr Protoc Cell Biol. **Chapter 18**: Unit 18.12.

Kawane, K., H. Fukuyama, et al. (2003). Impaired thymic development in mouse embryos deficient in apoptotic DNA degradation. Nat Immunol. **4**: 138-144.

Klaiman, G., N. Champagne, et al. (2009). Self-activation of Caspase-6 in vitro and in vivo: Caspase-6 activation does not induce cell death in HEK293T cells. Biochim Biophys Acta. **1793**: 592-601.

Knight, Z. A. and K. M. Shokat (2007). Chemical genetics: where genetics and pharmacology meet. Cell. **128**: 425-430.

Lakhani, S. A., A. Masud, et al. (2006). Caspases 3 and 7: key mediators of mitochondrial events of apoptosis. Science. **311**: 847-851.

Lu, C., F. Zhu, et al. (2006). Cell apoptosis: requirement of H2AX in DNA ladder formation, but not for the activation of caspase-3. Mol Cell. **23**: 121-132.

Mahrus, S., J. C. Trinidad, et al. (2008). Global sequencing of proteolytic cleavage sites in apoptosis by specific labeling of protein N termini. Cell. **134**: 866-876.

Michnick, S. W., P. H. Ear, et al. (2007). Universal strategies in research and drug discovery based on protein-fragment complementation assays. Nature reviews Drug discovery. **6**: 569-582.

Morlando, M., M. Ballarino, et al. (2008). Primary microRNA transcripts are processed co-transcriptionally. Nat Struct Mol Biol.

Napirei, M., H. Karsunky, et al. (2000). Features of systemic lupus erythematosus in Dnase1-deficient mice. Nat Genet. **25**: 177-181.

Nguyen, A. W. and P. S. Daugherty (2005). Evolutionary optimization of fluorescent proteins for intracellular FRET. Nat Biotechnol. **23**: 355-360.

Ouyang, M., J. Sun, et al. (2008). Determination of hierarchical relationship of Src and Rac at subcellular locations with FRET biosensors. Proc Natl Acad Sci USA. **105**: 14353-14358.

Parks, T. D., K. K. Leuther, et al. (1994). Release of proteins and peptides from fusion proteins using a recombinant plant virus proteinase. Anal Biochem. **216**: 413-417.

Pauli, A., F. Althoff, et al. (2008). Cell-Type-Specific TEV Protease Cleavage Reveals Cohesin Functions in Drosophila Neurons. Dev Cell. **14**: 239-251.

Pop, C. and G. S. Salvesen (2009). Human caspases: activation, specificity, and regulation. J Biol Chem. **284**: 21777-21781.

Poser, I., M. Sarov, et al. (2008). BAC TransgeneOmics: a high-throughput method for exploration of protein function in mammals. Nat Methods. **5**: 409-415.

Qiu, L., H. Wang, et al. (2008). A construct with fluorescent indicators for conditional expression of miRNA. BMC Biotechnology 2008 8:77. **8**: 77.

Rano, T. A., T. Timkey, et al. (1997). A combinatorial approach for determining protease specificities: application to interleukin-1beta converting enzyme (ICE). Chem Biol. **4**: 149-155.

Reed, J. C., K. S. Doctor, et al. (2004). The domains of apoptosis: a genomics perspective. Sci STKE. **2004**: re9.

Ricci, J.-E., C. Muñoz-Pinedo, et al. (2004). Disruption of mitochondrial function during apoptosis is mediated by caspase cleavage of the p75 subunit of complex I of the electron transport chain. Cell. **117**: 773-786.

Riedl, S. J. and Y. Shi (2004). Molecular mechanisms of caspase regulation during apoptosis. Nat Rev Mol Cell Biol. **5**: 897-907.

Rosenfeld, N., M. B. Elowitz, et al. (2002). Negative autoregulation speeds the response times of transcription networks. Journal of Molecular Biology. **323**: 785-793.

Roy, S., C. I. Bayly, et al. (2001). Maintenance of caspase-3 proenzyme dormancy by an intrinsic "safety catch" regulatory tripeptide. Proc Natl Acad Sci USA. **98**: 6132-6137.

Ruchaud, S., N. Korfali, et al. (2002). Caspase-6 gene disruption reveals a requirement for lamin A cleavage in apoptotic chromatin condensation. EMBO J. **21**: 1967-1977.

Samejima, K. and W. C. Earnshaw (2005). Trashing the genome: the role of nucleases during apoptosis. Nat Rev Mol Cell Biol. **6**: 677-688.

Samejima, K., S. Toné, et al. (2001). CAD/DFF40 nuclease is dispensable for high molecular weight DNA cleavage and stage I chromatin condensation in apoptosis. J Biol Chem. **276**: 45427-45432.

Scheer, J. M., M. J. Romanowski, et al. (2006). A common allosteric site and mechanism in caspases. Proc Natl Acad Sci USA. **103**: 7595-7600.

Schröder, M. and R. J. Kaufman (2005). The mammalian unfolded protein response. Annu Rev Biochem. **74**: 739-789.

Schulze-Osthoff, K., H. Walczak, et al. (1994). Cell nucleus and DNA fragmentation are not required for apoptosis. J Cell Biol. **127**: 15-20.

Sebbagh, M., C. Renvoizé, et al. (2001). Caspase-3-mediated cleavage of ROCK I induces MLC phosphorylation and apoptotic membrane blebbing. Nat Cell Biol. **3**: 346-352.

Subach, O. M., I. S. Gundorov, et al. (2008). Conversion of red fluorescent protein into a bright blue probe. Chem Biol. **15**: 1116-1124.

Sun, X.-M., M. Butterworth, et al. (2004). Caspase activation inhibits proteasome function during apoptosis. Mol Cell. **14**: 81-93.

Suzuki, Y., Y. Nakabayashi, et al. (2001). Ubiquitin-protein ligase activity of X-linked inhibitor of apoptosis protein promotes proteasomal degradation of

caspase-3 and enhances its anti-apoptotic effect in Fas-induced cell death. Proc Natl Acad Sci USA. **98**: 8662-8667.

Taylor, R. C., S. P. Cullen, et al. (2008). Apoptosis: controlled demolition at the cellular level. Nat Rev Mol Cell Biol. **9**: 231-241.

Thornberry, N. A., T. A. Rano, et al. (1997). A combinatorial approach defines specificities of members of the caspase family and granzyme B. Functional relationships established for key mediators of apoptosis. J Biol Chem. **272**: 17907-17911.

Uhlmann, F., D. Wernic, et al. (2000). Cleavage of cohesin by the CD clan protease separin triggers anaphase in yeast. Cell. **103**: 375-386.

Ura, S., N. Masuyama, et al. (2001). Caspase cleavage of MST1 promotes nuclear translocation and chromatin condensation. Proc Natl Acad Sci USA. **98**: 10148-10153.

Vilas, G. L., M. M. Corvi, et al. (2006). Posttranslational myristoylation of caspase-activated p21-activated protein kinase 2 (PAK2) potentiates late apoptotic events. Proc Natl Acad Sci USA. **103**: 6542-6547.

Wang, J., C.-E. Wang, et al. (2008). Impaired ubiquitin-proteasome system activity in the synapses of Huntington's disease mice. J Cell Biol. **180**: 1177-1189.

Wehr, M. C., R. Laage, et al. (2006). Monitoring regulated protein-protein interactions using split TEV. Nat Methods. **3**: 985-993.

Wehr, M. C., L. Reinecke, et al. (2008). Analysis of transient phosphorylation-dependent protein-protein interactions in living mammalian cells using split-TEV. BMC Biotechnol. **8**: 55.

Widlak, P. and W. T. Garrard (2005). Discovery, regulation, and action of the major apoptotic nucleases DFF40/CAD and endonuclease G. J Cell Biochem. **94**: 1078-1087.

Williams, D. J., H. L. Puhl, et al. (2009). Rapid modification of proteins using a rapamycin-inducible tobacco etch virus protease system. PLoS ONE. **4**: e7474.

Wolan, D. W., J. A. Zorn, et al. (2009). Small-molecule activators of a proenzyme. Science. **326**: 853-858.



Xiao, F., P. Widlak, et al. (2007). Engineered apoptotic nucleases for chromatin research. Nucleic Acids Res. **35**: e93.

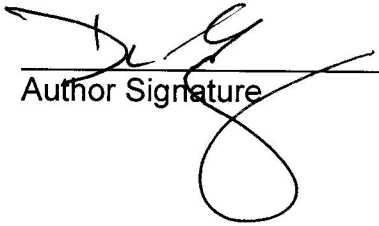
Yi, C. H. and J. Yuan (2009). The Jekyll and Hyde functions of caspases. Dev Cell. **16**: 21-34.

**Publishing Agreement**

*It is the policy of the University to encourage the distribution of all theses and dissertations. Copies of all UCSF theses and dissertations will be routed to the library via the Graduate Division. The library will make all theses and dissertations accessible to the public and will preserve these to the best of their abilities, in perpetuity.*

**Please sign the following statement:**

*I hereby grant permission to the Graduate Division of the University of California, San Francisco to release copies of my thesis or dissertation to the Campus Library to provide access and preservation, in whole or in part, in perpetuity.*

  
\_\_\_\_\_  
Author Signature

1/11/2011  
\_\_\_\_\_  
Date